MATERIALS CHEMISTRY FRONTIERS

REVIEW

View Article Online
View Journal | View Issue

Cite this: *Mater. Chem. Front.*, 2023, **7**, 2175

Stability improvements of metal halide perovskite nanocrystals and their optoelectrical applications

Yuhua Wang, * Jiejun Ren, Xiaopeng Zhou and Gangyi Zhang

Recently, metal halide perovskite (MHP) nanocrystals have emerged as luminescent star materials with excellent optical properties such as ultra-high photoluminescence quantum yields (PLQYs), narrow full width at half maximum (FWHM), tunable wavelength, *etc*. Their excellent photophysical properties make MHP nanocrystals attractive in various optoelectronic applications. However, the potential applications of MHP nanocrystals are seriously hindered by their poor stability against heat, oxygen, moisture, light illumination, *etc*. In this review, we provide a current progress survey on the fundamental structural properties, photophysical properties, and stability issues of MHP nanocrystals. Among various stability enhancing strategies, we paid particular attention to the integration and encapsulation of MHP nanocrystals in porous framework materials (PFMs). The PFMs possess the advantages of design flexibility, high porosity, environmental stability, and extensive functionality, which could effectively improve the stability of MHP nanocrystals with additional functions. Furthermore, the promising future applications of MHP hybrids are summarized and prospected.

Received 29th December 2022,
Accepted 20th February 2023

DOI: 10.1039/d2qm01355j

rsc.li/frontiers-materials

1. Introduction

Perovskites were named after a Russian mineralogist Lev Perovski over 180 years ago, referring to calcium titanium oxide ($CaTiO_3$) mineral species.[1] Generally, perovskites possess a similar crystal structure to $CaTiO_3$. The research history of perovskite materials could extend much further back in time. In the 20th and 21st centuries, perovskite materials have been extensively studied owing to their remarkable properties, including ferroelectricity, superconductivity, magnetoresistance, and optoelectronic properties. In 2014, Schmidt *et al.* synthesized $CH_3NH_3PbBr_3$ perovskite nanocrystals for the first time, which shows that perovskite nanocrystals have great potential in the field of luminescence.[2] And in 2015, Kovalenko *et al.* proposed the pioneering work of hot-injection synthesis of colloidal $CsPbX_3$ (X = Cl, Br and I) nanocrystals.[3] Since then, tremendous efforts have been devoted to the study of metal halide perovskite nanocrystals.

School of Materials and Energy, National and Local Joint Engineering Laboratory for Optical Conversion Materials, Lanzhou University, Tianshui South Road 222, Lanzhou, China. E-mail: wyh@lzu.edu.cn

Yuhua Wang

Yuhua Wang is a Professor of the School of Materials and Energy in Lanzhou University. He received his BS degree in chemistry from Shaanxi Normal University in 1989, MS degree in inorganic Chemistry from Lanzhou University in 1989, and PhD degree in Materials Chemistry from the Tohoku University in 2001. Prof. Yuhua Wang is mainly engaged in the discovery, development and application of novel functional materials, such as quantum dots, long-afterglow materials, LED phosphors, and photocatalysis materials and flame retardant materials.

Jiejun Ren

Jiejun Ren is currently a PhD candidate in the School of Materials and Energy at Lanzhou University. He received his B.S. degree from the School of Physical Science and Technology at Lanzhou University in 2017. Since then, he pursued a PhD degree at Lanzhou University under the guidance of Prof. Yuhua Wang. His current research interests focus on the optoelectronic properties of perovskite nanocrystals and their applications in lighting and displays.

The use of metal halide perovskite (MHP) nanocrystals, as a kind of semiconductor with outstanding photoelectric properties, has been increasing rapidly in a wide range of applications.[4] The MHP nanocrystals possess remarkable optoelectronic properties, including high photoluminescence quantum yield (PLQY), facilely tunable bandgaps, narrow full width at half maximum (FWHM), excellent carrier mobility, long charge-carrier diffusion length, high absorption coefficients, *etc.*, which make them attractive for optoelectronic applications, such as light-emitting diodes (LEDs),[5] micro/mini-LEDs,[6,7] backlight displays,[8] solar cells,[9] lasers[10] and photodetectors.[11] Nonetheless, the poor stability of MHP nanocrystals under environmental conditions is the main obstacle to its application. Due to the low energy of formation and intrinsic ion nature, they are very sensitive to environmental factors (such as water, air, light and temperature) and ease of ion-exchange and decomposition. The poor stability of MHP nanocrystals severely limits their commercial application, which urgently needs to be solved.

Research developments of MHP nanocrystals are very rapid; a large number of studies have been reported on their photophysical properties and application prospects in recent years.[12–14] In this review, we first summarize the fundamental structural properties, photophysical properties, and stability problems of MHP nanocrystals. The stability enhancing strategies of MHP nanocrystals including compositional engineering, surface modulation, and matrix encapsulation are further provided. The encapsulation of MHP nanocrystals in porous framework materials (PFMs) is particularly emphasized due to their high stability enhancement and additional functionalities for MHP nanocrystals. The fabrication of MHP@PFM composites could be realized through *in situ* growth, external coating, one-pot, and physical mixing strategies. Not merely the improved stability, but the MHP@PFM composites emerge with enhanced photoluminescence properties and new features also. Finally, we present a brief introduction of the potential optoelectronic applications of MHP@PFM composites. We believe that this review will provide some new perspectives for the development of MHP nanocrystals.

2. Metal halide perovskite (MHP) nanocrystals

2.1. Structural properties

2.1.1. Crystal structure. The three-dimensional (3D) MHP nanocrystals typically exhibit a cubic ($Pm\bar{3}m$) crystal structure, with a general chemical formula of ABX_3, where A is a monovalent cation such as Cs^+, Rb^+, methylammonium (MA^+), and formamidinium (FA^+), B is a divalent cation such as Pb^{2+} and Sn^{2+}, and X is a halide ion (Cl^-, Br^-, and I^-). The crystal structure of 3D metal halide perovskites of ABX_3 is shown in Fig. 1a, which is characterized by a corner-sharing $[BX_6]^{4-}$ octahedral array with B^{2+} surrounded by six X^-, and A^+ occupying the cavities of octahedra.[15] The most common 3D MHP nanocrystals are all-inorganic perovskites ($CsPbX_3$, $CsSnX_3$, *etc.*) and organic–inorganic hybrid perovskites ($MAPbX_3$, $FAPbX_3$, *etc.*). The difference between organic–inorganic hybrid perovskites and all-inorganic perovskites is that the inorganic A-site cations (Cs^+, Rb^+, *etc.*) are substituted with organic cations (MA^+, FA^+, *etc.*).

For the ideal $Pm\bar{3}m$ perovskite structure, the length of the X–A–X bond should be equal to $\sqrt{2}$ times the length of the X–B–X bond. Therefore, under ideal conditions, the ion radius should meet the formula $(R_A + R_B) = \sqrt{2} \times (R_X + R_B)$, where R_A, R_B, and R_X represent the ionic radii of the corresponding cations and anion, respectively. However, the radius of A^+, B^{2+} and X^- ions cannot perfectly satisfy the formula in the real perovskite structure materials. To quantitatively describe the difference between the actual perovskite crystal structure and the ideal situation for determining the structural stability, the Goldschmidt tolerance factor t was used to evaluate this relationship: $t = \frac{R_A + R_X}{\sqrt{2}(R_B + R_X)}$.[16] The value of Goldschmidt tolerance factor t is used to evaluate the suitability of A^+ within the cavities in the $[BX_6]^{4-}$ octahedra array. Generally, the closer t is to 1, the closer the compound is to the ideal $Pm\bar{3}m$ perovskite structure. Taking $SrTiO_3$ (R_{Sr} = 0.144 nm; R_{Ti} = 0.0605 nm; and R_O = 0.135 nm) as an example,[17] the Goldschmidt tolerance factor t is calculated to be 1.002, and the structure of $SrTiO_3$ is a standard $Pm\bar{3}m$ structure. Empirically, the Goldschmidt tolerance

Xiaopeng Zhou

Xiaopeng Zhou received his MS degree in materials science from Lanzhou University in 2020. He is currently a Ph.D. candidate in Prof. Yuhua Wang's group at Lanzhou University. Currently, he is involved in research on the synthesis and application of InP based quantum dot materials.

Gangyi Zhang

Gangyi Zhang is currently pursuing a PhD degree in the School of Materials and Energy at Lanzhou University. He received his MS degree in materials science from Lanzhou University in 2018. His research interests focused on the optical performance of low-dimensional perovskite materials.

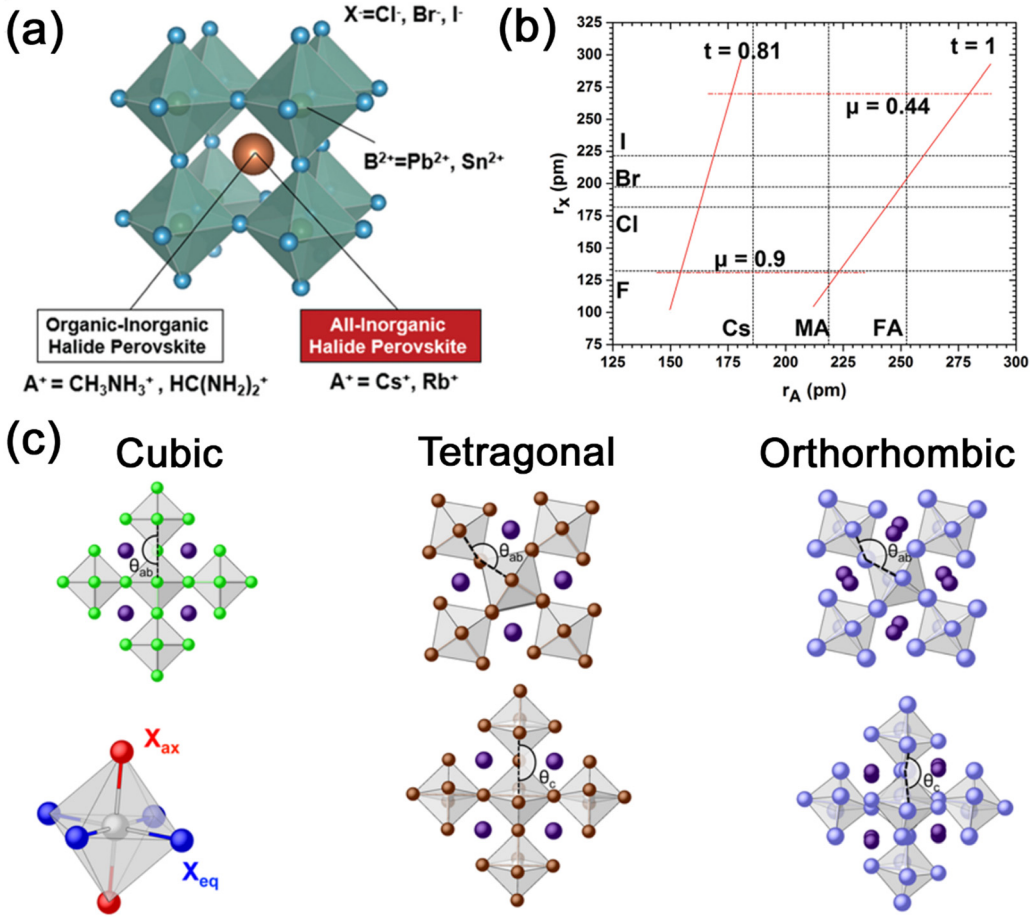

Fig. 1 (a) Schematic illustration of the typical ABX_3 structure of MHPs. Adapted from ref. 15 with permission. Copyright 2019, Royal Society of Chemistry. (b) Formability of 3D MHPs as a function of A-site cation and halide anion radii. Adapted from ref. 4 with permission. Copyright 2019, Royal Society of Chemistry. (c) Schematic illustration of the 3D arrangement of the $[BX_6]^{4-}$ octahedra in MHPs exhibiting a cubic, tetragonal, and orthorhombic structure. Adapted from ref. 18 with permission. Copyright 2017, American Chemical Society.

factor t of stable 3D perovskites should range from 0.81 to 1. If $t < 0.81$, A^+ is too small to support the $[BX_6]^{4-}$ octahedral array, which will lead to the tilting of the octahedra and result in a tetragonal or an orthorhombic structure. And if $t > 1$, this indicates that A^+ is too large and usually hinders the formation of perovskites. A semi-empirical octahedral factor, $\mu = \frac{R_B}{R_X}$, is introduced to evaluate the octahedral stability. Generally, the $[BX_6]^{4-}$ octahedra are stable when the octahedral factor μ lies in the range of 0.44–0.9. A combination of Goldschmidt tolerance factor t and octahedral factor μ provides a parameter space for 3D formability of perovskites (Fig. 1b). Taking $CsPbBr_3$ (R_{Cs} = 0.167 nm; R_{Pb} = 0.119 nm; and R_{Br} = 0.181 nm) as an example,[16] the Goldschmidt tolerance factor t could be calculated to be 0.82 and the octahedral factor μ could be calculated to be 0.66, which illustrate a relatively stable perovskite structure in $CsPbBr_3$. MA-Based MHP nanocrystals exhibit a nearly ideal cubic perovskite structure, while Cs and FA ions are slightly smaller or larger to perfectly accommodate A-sites. Both $MAPbCl_3$ and $MAPbBr_3$ have a cubic structure, and $MAPbI_3$ perovskites have a tetragonal structure at room temperature.

In addition to the common cubic structure (α phase), 3D metal halide perovskites also have a tetragonal structure (β phase) and an orthorhombic structure (γ phase). The presence of different structures of MHPs is mainly related to the deviation of the B–X–B bond angle, resulting in the tilting of the $[BX_6]^{4-}$ octahedra (Fig. 1c).[18] In cubic phase MHP, the B–X–B bond angle between octahedra is 180° in both the horizontal (θ_{ab}) and vertical (θ_c) planes. And in tetragonal phase MHP, the bond angle in the horizontal plane is less than 180°, while the bond angles in horizontal and vertical planes are both less than 180° in orthorhombic phase MHP. It is noteworthy that the α phase is a high-temperature stable phase. As the temperature decreases, the cubic phase could transform to the tetragonal phase and eventually to the orthorhombic phase. MHP nanocrystals can also maintain the cubic phase structure at room temperature because of the nanosize and protection of surface ligands. Ascribed to the ionic structure and large surface energy, colloidal MHP nanocrystals are usually stabilized by surface ligands such as oleic acid (OA) and oleyl amine (OAm). The surface ligands work as a capping layer to protect the nanocrystals from aggregation, yet the surface ligands are

usually not tightly bonded to nanocrystals. The surface ligands are highly dynamic and easy to lose, which also leads to the stability problems in MHP nanocrystals.

Variable shaped MHP nanocrystals, such as 3D nanocubes, 2D nanoplates and nanosheets, 1D nanowires, and 0D nanospheres, could be prepared by using different synthetic methods or tuning reaction parameters. The dimensionality is related to the connectivity of corner-sharing $[BX_6]^{4-}$ octahedrons in the perovskite structure. And lower-dimensional perovskites originate from separation of the $[BX_6]^{4-}$ octahedra from a 3D perovskite structure. Different from 3D perovskite structures, where $[BX_6]^{4-}$ octahedrons are connected three dimensionally, $[BX_6]^{4-}$ octahedrons are connected along crystallographic planes in 2D perovskites, connected in one dimension in 1D perovskites, and completely decoupled in 0D perovskites.

2.1.2. Band structure. In the electronic band structure of traditional III–V and II–VI semiconductor quantum dots (QDs), the valence band (VB) is formed by bonding orbitals and the conduction band (CB) is formed by antibonding orbitals.[19] In lead halide perovskites, the formal electronic configuration of Pb^{2+} is $6s^26p^0$, and the formal electronic configuration of halides is np^6 (n = 3, 4, and 5 for Cl, Br, and I, respectively).[20] As shown in Fig. 2a and b, the valence band of lead halide perovskites is formed by the halide (np) orbitals and Pb (6s) orbitals, while the conduction band consists of Pb (6p) and the halide (np) orbitals.[21] It is noted that A-site atoms do not contribute directly to the band structure, but the A-site atom indirectly affects the band structure by influencing the bond length between the B-site and X-site atoms. The electronic band structures of MHPs composed of different halides have common features, differing only in the band gap (Fig. 2c). The halide elements significantly influence the band structure of the MHPs as they determine the valence band transition. The energy of the halogen (np) orbitals increases from Cl to I, while the Pb 6p orbitals that form the CB show no obvious fluctuation (Fig. 2d).

2.2. Photophysical properties

2.2.1. Optical properties. The optical properties are one of the most attractive physical properties of MHP nanocrystals, which endow them with great potential in many optoelectronic applications. Compared with traditional semiconductor quantum dots and rare earth doped fluorescent materials, MHP nanocrystals possess fascinating optical properties, such as wide absorption spectrum, ultra-high PLQY, high color purity, *etc.*

Wide excitation spectrum. Conventional organic fluorescent dyes and rare earth elements doped fluorescent materials have relatively narrow excitation spectra, which leads to difficulties

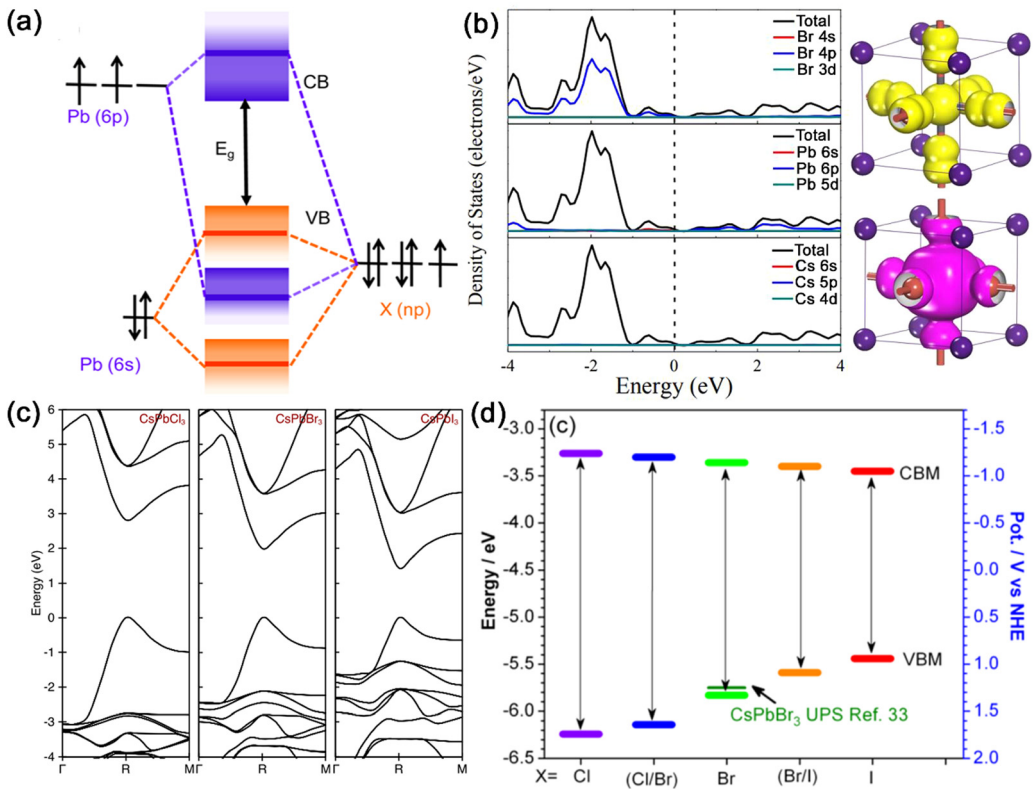

Fig. 2 (a) Schematic illustration of the VB and CB of $APbX_3$ MHPs formed by bonding and antibonding orbitals. Adapted from ref. 19 with permission. Copyright 2016, American Chemical Society. (b) Density of states of cubic $CsPbBr_3$ with corresponding contributions of elements to energy bands and electronic profiles of the valence band maximum (VBM) and conduction band minimum (CBM) for $CsPbBr_3$. Adapted from ref. 21 with permission. Copyright 2016, Wiley-VCH. (c) The calculated band structures of cubic $CsPbX_3$ (X = Cl, Br, and I) MHPs. Adapted from ref. 3 with permission. Copyright 2015, American Chemical Society. (d) Band edge energies of a series of $CsPbX_3$ MHPs with halogen modification. Adapted from ref. 19 with permission. Copyright 2016, American Chemical Society.

in multi-component excitation. In contrast, MHP nanocrystals exhibit strong and wide light absorption properties with high extinction coefficients. The excitation spectrum of MHP nanocrystals is wide and continuous. As long as the energy of excitation light is greater than its band gap energy, the MHP nanocrystals could be excited and emit strong light. Therefore, the MHP nanocrystals with different band gaps could be excited with one excitation source, which ensures their potential in LED applications.

Ultra-high PLQY. Due to a large surface-to-volume ratio in nanocrystals, shell layers are indispensable to passivate the highly active surface in conventional semiconductor nanocrystals (CdSe, InP, *etc.*). In contrast, MHP nanocrystals possess ultra-high PLQY, which could easily reach above 90% even without external shells. The surface defect energy levels in MHP nanocrystals can be eliminated by surface modification, which inhibits nonradiative recombination and leads to high PLQY.

High color purity. The high color purity of MHP nanocrystals is attributed to their symmetrical and narrow PL peaks. In MHP nanocrystals, the recombination rate of electrons and holes in the band gap is much higher than that of the thermal excitons, and the recombination of electrons and holes at higher energy levels is almost impossible. Therefore, the luminescence spectra of the obtained MHP nanocrystals are often symmetric. The FWHM of the emission peak of MHP nanocrystals is around 20 nm (Fig. 3a), which is ascribed to the narrow size distribution of MHP nanocrystals. The high monochromaticity of MHP nanocrystals is even better than the conventional Cd-based and InP-based QDs, which shows their great potential in display and lighting applications.

Wide color gamut. Ascribed to the flexible band gap tunability and high color purity, the MHP nanocrystals possess a wide color gamut. As shown in the Commision Internationale de l'Eclairage (CIE) chromaticity diagram in Fig. 3b, the color gamut of $CsPbX_3$ MHP nanocrystals reached ~140% of the National Television System Committee (NTSC) standard, which is much better than that of conventional semiconductor quantum dots (Cd-based QDs, ~110% NTSC). Compared with other semiconductor quantum dots, MHP nanocrystals possess a wider color gamut and excellent color rendering properties, which makes them a promising luminescent material for display applications.

2.2.2. Defeat tolerance. The influence of defects in traditional semiconductor nanocrystals and MHP nanocrystals on electronic properties is obviously different (Fig. 4a). In traditional semiconductor Cd-based and InP-based nanocrystals, the band gap is formed between the bonding orbital and the antibonding orbital. Therefore, the defects state tends to appear in the deep level region of the band gap, leading to severe non-radiative recombination and greatly reducing the luminescence performance.[22] MHP nanocrystals possess high defect tolerance properties, which endow them with nearly unity PLQY, high carrier mobility and long carrier lifetime. In MHP nanocrystals, vacancies are the main defects due to their low formation energy, while interstitial and antisite defects that generate deep traps in the band gap are rarely formed.[22] As mentioned above, the band gap of MHP nanocrystals is formed between anti-bonding orbitals. The defects energy levels of MHP nanocrystals are located in the VB and CB or shallow traps, rather than in middle of the band gap. Therefore, the defects have little influence on the luminescence performance of MHP nanocrystals.

2.2.3. Quantum confinement. The quantum confinement effect is a very important phenomenon in nanocrystals. Generally, when the wavefunctions of electrons and holes are spatially confined to dimensions smaller than Bohr radius, quantization of energy will occur. And the electronic energy level near the Fermi level will split from a continuous state to a discrete state, which will induce increases in the band gap and blue-shift the emission. The MHP nanocrystals exhibit typical size-related quantum confinement effects. When the edge length of $CsPbBr_3$ nanocrystals is larger than the Bohr radius of 7 nm, the quantum confinement effect is weak, and the band gap is similar to that of the bulk materials (Fig. 4b). Only when the edge length is much

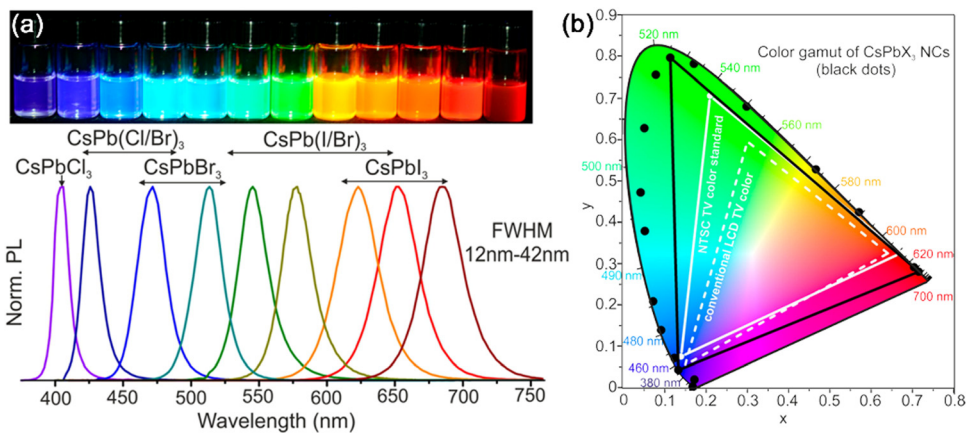

Fig. 3 (a) PL spectra and photographs of $CsPbX_3$ (X = Cl, Br, and I) MHP nanocrystals; (b) color coordinates of $CsPbX_3$ (X = Cl, Br, and I) MHP nanocrystals and the conventional LCD TV color and NTSC TV color standard. Adapted from ref. 3 with permission. Copyright 2015, American Chemical Society.

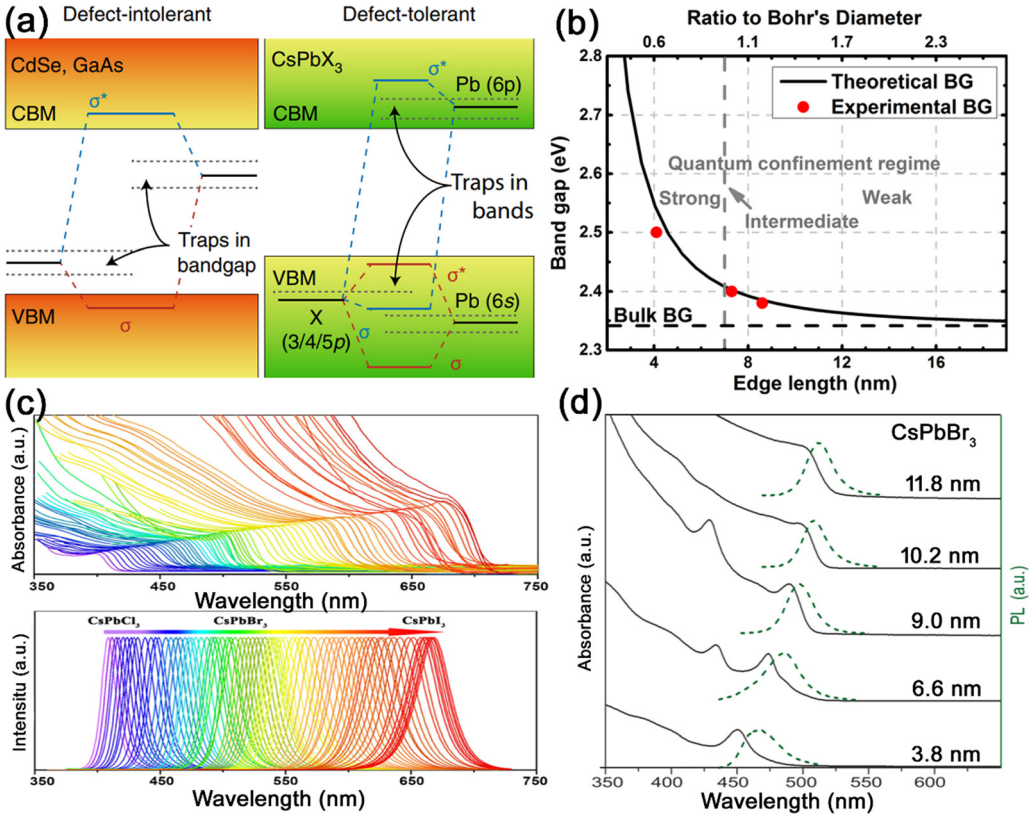

Fig. 4 (a) Schematic illustration of the band structure of defect-intolerant conventional semiconductors and defect-tolerant MHP nanocrystals. Adapted from ref. 22 with permission. Copyright 2018, Springer Nature. (b) Experimental *versus* theoretical size dependence of the band gap energy with quantum confinement regimes noted in relation to the Bohr diameter (d_b = 7 nm). Adapted from ref. 23 with permission. Copyright 2017, American Chemical Society. (c) Optical absorption and PL emission spectra of halide-exchanged $CsPbX_3$ nanocrystals, which demonstrate the composition-dependent band gap tunability over the entire visible range. Adapted from ref. 24 with permission. Copyright 2019, American Chemical Society. (d) Optical absorption and PL emission spectra of $CsPbBr_3$ nanocrystals with different sizes, demonstrating the size-dependent band gap tunability. Adapted from ref. 3 with permission. Copyright 2015, American Chemical Society.

smaller than exciton Bohr radius, the $CsPbBr_3$ nanocrystals will demonstrate a strong quantum confinement effect.[23] Usually, the average size distribution of MHP nanocrystals is about 10 nm, which belongs to a weak quantum confinement effect region, and the size has a rather little influence on the band gap.

2.2.4. Band modulation. Metal halide perovskites exhibit remarkable tunable band gaps and emission colors, which could be easily tuned from ultraviolet to near-infrared to cover the full visible spectra range. The emission spectra of MHPs nanocrystals could be tuned by controlling many factors, such as chemical composition and crystallite size. As mentioned above, the halide elements play a vital role in controlling the band gap of MHP nanocrystals. The band gap of MHP nanocrystals could be accurately controlled by modulating the ratio of halide precursors. Liu *et al.* reported that the emission of $CsPbX_3$ nanocrystals could be precisely tuned in the full visible range with an interval of 1 nm by an anion-exchange route.[24] As the halides are changed from Cl to Br and I, the emissions of fine-tuned $CsPbX_3$ nanocrystals gradually shift from 408 to 669 nm (Fig. 4c). The substitution of the A^+ cation is another possible strategy for tuning the band gap of MHP nanocrystals. The A^+ cation could tune the band gap of MHP nanocrystals through affecting the bond length between the B^{2+} and the X^-, the bandgap decreases as the size of A^+ increases. For instance, when the Cs^+ cation was replaced with a larger methylammonium cation (MA^+) or formamidinium cation (FA^+), the band gap energies decreased from 2.36 eV ($CsPbBr_3$) to 2.34 eV ($MAPbBr_3$) and 2.26 eV ($FAPbBr_3$), respectively.[25] Attributed to the quantum confinement effect, the band gap of MHP nanocrystals could also be tuned by adjusting crystal size. For instance, the emission of $CsPbBr_3$ nanocrystals blue-shifts from 520 to 460 nm as the size decreases from 11.8 to 3.8 nm (Fig. 4d).[3]

2.3. Stability problems

Despite the excellent photophysical properties of MHP nanocrystals, the stability problems severely hinder the further development of MHP nanocrystals. The outstanding photophysical properties of MHP nanocrystals could be easily changed or completely damaged by many factors, such as polar solvents, oxygen, light irradiation, high temperature, *etc*. As shown in Fig. 5, the instability of MHP nanocrystals was summarized into four aspects, including structural instability, surface instability, thermal stability, and environmental instability.

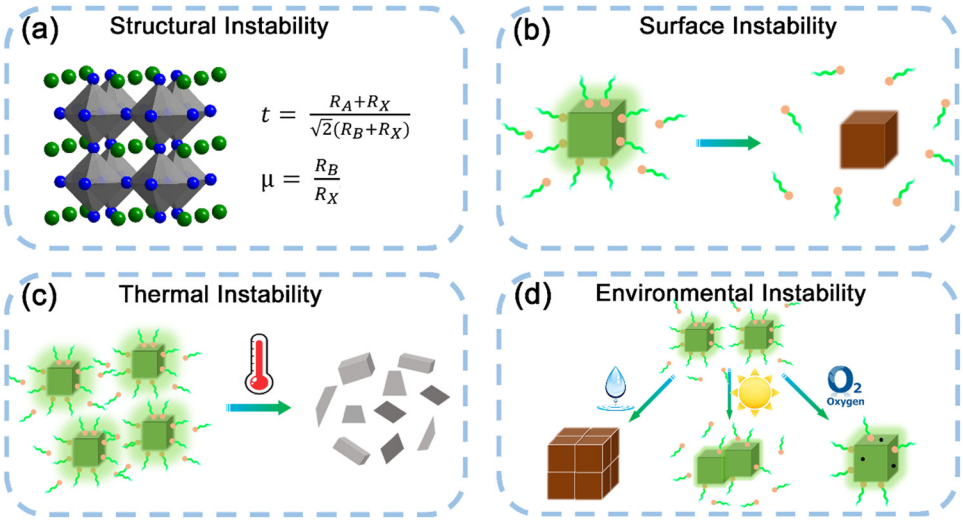

Fig. 5 Schematic illustration of the main stability problems of MHP nanocrystals, including (a) structure instability, (b) surface instability, (c) thermal instability, and (d) environmental instability.

2.3.1. Structural instability. The structural stability of MHP nanocrystals is mainly related to the Goldschmidt tolerance factor t and the octahedral factor μ (Fig. 5a). As mentioned above, the appropriate ionic radii are crucial in the formation of stable perovskite structures. In addition, the cubic phase of perovskites is a high-temperature stable phase, while tetragonal or orthorhombic phases are thermodynamically preferred at room temperature. Although MHP nanocrystals could maintain the cubic phase at room temperature due to the high surface energy, the cubic phase is still a sub-stable form at room temperature. Therefore, these two reasons lead to structural instability in MHP nanocrystals.

2.3.2. Surface instability. Due to the intrinsic ionic structure and large surface energy, MHP nanocrystals need to be stabilized by surface ligands such as OA and OAm. The organic ligands are not tightly bonded to the surface of MHP nanocrystals, but show a dynamic equilibrium between adsorption and desorption on the surface (Fig. 5b). The organic ligands are easily lost when they are stored for a long time or come in contact with polar solvents. When the organic ligands on the surface of nanocrystals are lost, the optical properties and colloidal stability of MHP nanocrystals will deteriorate, and even the crystal structure will be completely degraded. The intrinsic ionic properties and highly dynamic surface will also lead to a rapid anion exchange reaction in MHP nanocrystals. When MHP nanocrystals with different halide components are mixed together, rapid ion exchange occurs, resulting in severe spectral migration.

2.3.3. Thermal instability. The thermal stability of luminescent materials is always a crucial problem in the practical application of optoelectronic devices. The thermal-induced PL quenching seems to be a common phenomenon in all luminescent materials.[26] With an increase in temperature, lattice vibration is strengthened and more thermally active phonons are produced. The electrons in the excited state are coupled with the thermally active phonons. The excited electrons return to the ground state by a non-radiative transition, rather than a radiative transition, resulting in a reduction in PL intensity. In particular, the MHP nanocrystals show more severe response to external perturbations due to the intrinsic soft structure. The commercial Cd-based QDs show about 30% decrease in PL intensity when heated from room temperature (RT) to 373 K,[27] while the bare $CsPbBr_3$ nanocrystals show an almost 80% decrease in PL intensity from RT to 373 K.[28] Thermal treatment can induce a severe quenching of PL intensity and spectral redshift for MHP nanocrystals, which could predominantly arise from the thermally assisted traps in MHP nanocrystals. Upon further heating to high temperatures, the MHP nanocrystals exhibit an irreversible PL quenching, referred to as thermal degradation. The thermal degradation of MHP nanocrystals is mainly associated with the decomposition of the crystal structure and the loss of surface ligands. On one hand, due to the intrinsic ionic bonding of MHP nanocrystals, the average thermal energy calculated at 358 K is quite close to the formation energy per unit cells.[13] And it is expected that decomposition will occur with time after annealing to this temperature. The thermal decomposition is particularly severe in organic–inorganic hybrid perovskites, such as MA^+ based and FA^+ based perovskites. The organic–inorganic hybrid perovskites suffer from poor thermal stability due to the volatile nature of organic MA^+ and FA^+ cations. On the other hand, the organic ligand will undergo desorption and irreversible decomposition above 450 K, resulting in the aggregation of MHP nanocrystals and the loss of quantum confinement (Fig. 5c).[13]

Exciton binding energy (E_b) is an effective index to evaluate the thermal stability of materials, which is defined as the bond energy value of electron–hole pairs formed by the electrostatic Coulomb attraction. Electron–hole pairs with a large E_b value can resist thermal disturbance, leading to the excellent thermal stability of materials. The E_b value can be calculated using the following Arrhenius equation: $I(T) = \frac{I_0}{1 + Ae^{-E_b/KT}}$, where I_T and I_0 are the emission intensity at T and 0 K, respectively, and

K is the Boltzmann constant. Notably, a larger E_b value ensures the survival of excitons, which implies a higher possibility of radiative recombination.

2.3.4. Environmental instability. It is well known that the MHP nanocrystals degrade rapidly when exposed to an ambient environment. Even after capping with surface ligands, MHP nanocrystals are still sensitive to environmental factors such as oxygen, moisture, and light irradiation, which greatly hinders their actual applications (Fig. 5d).

Moisture instability. Ascribed to the intrinsic ion crystal properties, the MHP nanocrystals are sensitive to the polar solvents such as water, and even degrade in humid environments. The water-induced solvation and recrystallization produce large grains, which results in reduced luminescence properties. The poor moisture stability of MHP nanocrystals severely impedes their applications and degrades their performance in devices.

Irradiation instability. The MHP nanocrystals suffer from PL intensity loss with prolonged irradiation time. The irradiation instability of MHP nanocrystals is the major obstacle in application since continuous illumination is required in practical applications. The photo-induced deterioration of MHP nanocrystals is closely related to the diffusion of photo-generated carriers to the surface and capture by surface ligands, resulting in the desorption of ligands and aggregation of nanocrystals. Photo-induced phase segregation is also widely observed in mixed halide MHP nanocrystals such as $CsPb(Br/I)_3$, where halide ion migration results in altered emission properties.

Oxygen instability. The long-term oxygen stability is also a problem for MHP nanocrystals. The PL intensity of MHP nanocrystals gradually decreases with long-term storage in air. Oxygen works as an etching agent to etch unstable nuclei and enables formation of large crystals. The oxygen-induced PL quenching is closely related to the degradation of surface ligands, which leads to the failure of surface defect passivation and even agglomeration of MHP nanocrystals. Compared with other instability factors, oxygen instability is not a predominant issue, and has a little impact on the performance of MHP nanocrystals.

3. Strategies to improve the stability of MHP nanocrystals

3.1. Compositional engineering

As described above, the structural stability of MHP nanocrystals depends on the Goldschmidt tolerance factor t and the octahedral factor μ, which are mainly related to the radii of A-site, B-site and X-site ions. Due to the unique perovskite structure, the A^+, B^{2+} and X^- ions in the crystal lattice of MHP nanocrystals can be substituted or doped with other ions. The introduction of other ions in the crystal lattice of MHP nanocrystals could modulate the structure of nanocrystals and even provide new properties, leading to an improved PL performance, tunable band gaps and stable crystal structures. Therefore, the compositional engineering strategy is considered to be an effective method to optimize the structure of MHP nanocrystals and improve their stability. The proper compositional engineering not only improves the structural stability, but also expands the luminous properties of MHP nanocrystals. At present, ion doping in MHP nanocrystals is mainly concentrated in the A and B sites, and the doped ion types include organic ions, alkali metals, alkaline earth metals, transition metals, rare earth ions, *etc.*

3.1.1. A-Site doping. The A-site ions mainly dominate the structure of perovskite crystals, and further affect the stability of the MHP nanocrystals. Since the A-site cations occupy the interstices in $[BX_6]^{4-}$ octahedral arrays, there are limited cations suitable for the perovskite crystal lattice. The radii of organic cations FA^+ (2.53 Å) and MA^+ (2.17 Å) are larger than that of Cs^+ (1.67 Å),[15] which makes them advantageous in tuning and stabilizing the perovskite structure. Meng *et al.* reported that on substituting the A-site of MHPs with large FA^+ cations $FAPbBr_3$ nanocrystals were generated with the tolerance factor t close to 1, exhibiting better crystal stability.[29] Protesescu and co-workers synthesized monodisperse cubic $FAPbI_3$ and $FA_{0.1}Cs_{0.9}PbI_3$ nanocrystals, which possess better structural stability and chemical integrity than their MA-only or Cs-only based counterparts (Fig. 6a).[30] The alloying of FA^+ at the A site of the perovskite structure could stabilize the nanocrystals and help achieve a better balance between the structure and composition.[31] And yet, the organic FA^+ and MA^+ cations are volatile, making their thermal stability at high temperatures a problem. The inorganic A-site cations show higher thermal and chemical stability. Unfortunately, since Cs is the largest non-radioactive group I element, there are no better inorganic cations suitable for regulating the perovskite structure in MHP nanocrystals. The incorporation of inorganic Rb^+ ions in $CsPbX_3$ nanocrystals could produce high PL performance nanocrystals with a narrow FWHM of 31 nm and a high PLQY up to 91%.[32] However, the structural stability of $Rb_xCs_{1-x}PbX_3$ nanocrystals is poor due to the smaller ionic radius of the doped Rb^+ ion (1.61 Å) than Cs^+ ions. Even though the A-site doping strategy could effectively regulate and stabilize the perovskite structure, the suitable A-site ions are still limited, which restricts the further application of the A-site doping strategy.

3.1.2. B-Site doping. B-Site doping is also a widely explored strategy to stabilize the perovskite structure. Ascribed to the contributions of B-site ions to the band structure of MHP nanocrystals, the B-site doping strategy can not only regulate the structure of perovskites, but also improve the PL performance and endow novel functionalities to MHP nanocrystals. Pb^{2+} is the most common B-site ion in MHP nanocrystals with high PLQYs and stability. However, the content of toxic Pb^{2+} is restricted to less than 1000 ppm in devices, which greatly impedes its commercial application. The substitution or doping of B-site ions in MHP nanocrystals has proved its superiority in decreasing the toxic Pb^{2+} content, enhancing structural stability, and improving PL properties.

Sn is present in the same main group of the periodic table as Pb, and shows similar chemical properties as Pb. The radius of Sn^{2+} is only little smaller than that of Pb^{2+}, which could help

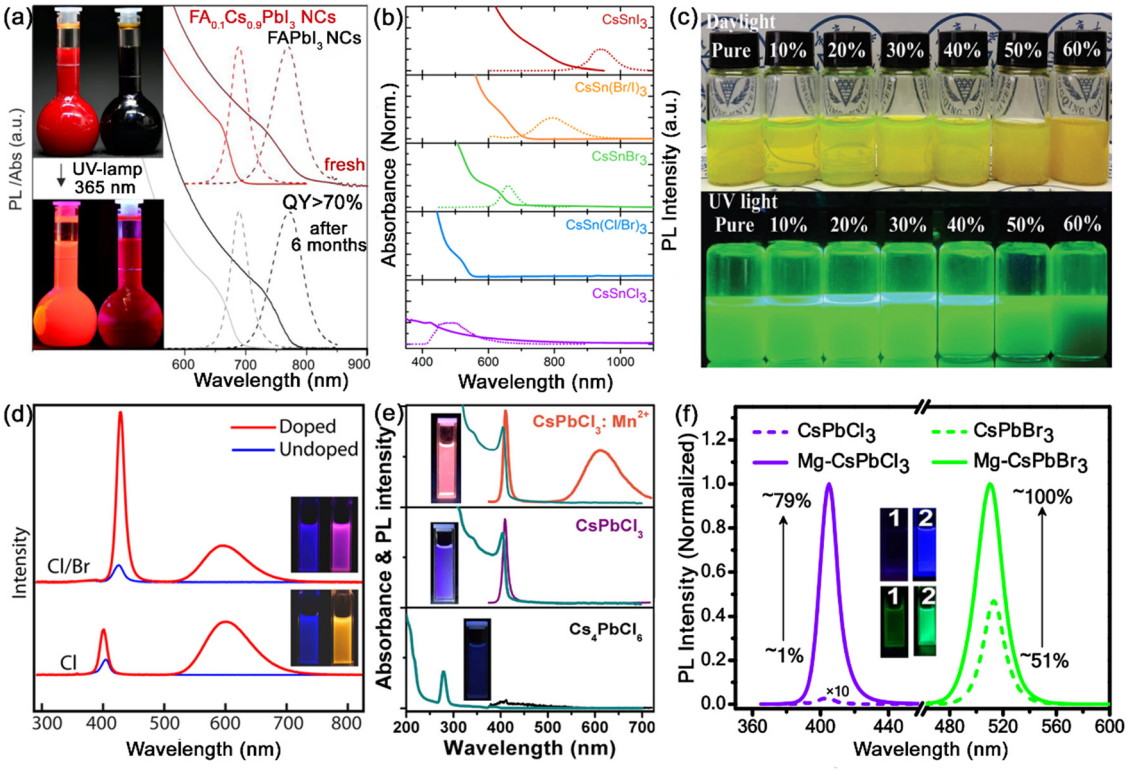

Fig. 6 (a) Optical absorption and PL emission spectra of $FAPbI_3$ nanocrystals and $FA_{0.1}Cs_{0.9}PbI_3$ nanocrystals before and after 6 months of storage. Adapted from ref. 30 with permission. Copyright 2017, American Chemical Society. (b) Optical absorption and PL emission spectra $CsSnX_3$ (X = Cl, Br, and I) nanocrystals. Adapted from ref. 33 with permission. Copyright 2016, American Chemical Society. (c) Photographs of $CsPbBr_3$:Sn^{2+} nanocrystals with different doping ratios. Adapted from ref. 34 with permission. Copyright 2021, Royal Society of Chemistry. (d) PL spectra of Mn-doped and undoped $CsPbCl_3$ and $CsPb(Cl/Br)_3$ nanocrystals. Adapted from ref. 35 with permission. Copyright 2016, American Chemical Society. (e) Optical absorption and PL emission spectra of pristine Cs_4PbCl_6, transformed $CsPbCl_3$ and $CsPbCl_3$:Mn^{2+} nanocrystals at water interfaces. Adapted from ref. 41 with permission. Copyright 2020, Springer Nature. (f) PL spectra and PLQYs of Mg-doped and un-doped $CsPbCl_3$ and $CsPbBr_3$ nanocrystals. Adapted from ref. 42 with permission. Copyright 2020, American Chemical Society.

effectively tune the tolerance factor of MHP nanocrystals. Jellicoe *et al.* reported the synthesis of lead-free $CsSnX_3$ nanocrystals with tunable emissions ranging from the near-infrared to visible spectral region (Fig. 6b).[33] Nevertheless, Sn^{2+} is vulnerable to oxidation and easily oxidizes to Sn^{4+}, resulting in the degradation of PL properties. Although $CsSnX_3$ does not seem promising in ambient air, partially Sn-doped $CsPbX_3$ ($CsPb_{1-x}Sn_xX_3$) exhibits higher structural stability and has reduced toxic Pb^{2+} content. Zang and co-workers proposed a facile room temperature method to synthesize Sn^{2+} doped $CsPbBr_3$ nanocrystals (Fig. 6c), which exhibit significantly improved thermal stability and a high PLQY of 82.7%.[34]

Mn^{2+} doping has received the maximum attention among the B-site doping strategies for MHP nanocrystals. Ascribed to the energy transfer from the MHP host to Mn^{2+} dopants and internal transition of Mn^{2+} dopants from T_1 to $^6A_1$, the Mn^{2+} doped MHP nanocrystals emit an additional Mn characteristic emission at ~600 nm. Parobek *et al.* reported the successful doping of Mn^{2+} ions into $CsPbCl_3$ and $CsPb(Cl/Br)_3$ nanocrystals.[35] Both $CsPbCl_3$:Mn^{2+} and $CsPb(Cl/Br)_3$:Mn^{2+} nanocrystals exhibited characteristic Mn^{2+} emissions, which result from exciton-to-Mn energy transfer (Fig. 6d). Zeng and Chen's group found that high-quality $CsPbX_3$:Mn^{2+} nanocrystals show much better thermal/air stability and optical performance than their pure counterparts. Since the dissociation energy of Mn–X bonds is higher than that of Pb–X bonds, the shrinkage of the $CsPbX_3$ lattice greatly increases the formation energy of $CsPbX_3$ nanocrystals, thus improving their stability.[36] Other Mn doping strategies such as the anion exchange strategy, one-pot synthesis strategy, *etc.* were also widely investigated for the synthesis of Mn doped MHP nanocrystals.[37–40] We also proposed a facile post-treatment doping method, which enables the preparation of highly luminescent $CsPbX_3$:Mn^{2+} nanocrystals at water interfaces (Fig. 6e).[41]

The incorporation of other bivalent cations in MHP nanocrystals has also been widely explored. Zeng and Chen *et al.* reported that Cd^{2+}, Sr^{2+}, Zn^{2+} and Co^{2+} ion-doped MHP nanocrystals possess enhanced excitonic luminescence, accompanied with increased formation energy.[36] The incorporation of Mg^{2+} into MHP nanocrystals also greatly enhances the PLQY and improves the stability under ambient conditions and in the presence of light and polar solvent (Fig. 6f).[42] In addition to these bivalent B-site doping ions, the substitution of aliovalent ions such as Bi^{3+}, Ti^{3+}, Ln^{3+}, *etc.* has also demonstrated their potential in regulating the optoelectronic properties and stability of MHP nanocrystals.[43–46]

Overall, the composition engineering strategy has been regarded as an effective strategy for tailoring the optical properties and improving the stability of MHP nanocrystals. The structural stability of MHP nanocrystals is mainly related to the Goldschmidt tolerance factor t and the octahedral factor μ. Through the composition engineering strategy, the Goldschmidt tolerance factor t and the octahedral factor μ could be tailed to fit the stable perovskite structure. The proper composition engineering strategy could modify the electronic band gap structure of MHP nanocrystals, and enhance the stability of MHP nanocrystals by affecting the formation energy. Exploring a multi-element co-doping strategy will be a challenging research direction, which may have synergistic and optimal effects in stabilizing MHP nanocrystals.

3.2. Surface modulation

Ascribed to the large surface-to-volume ratio, the surface plays an important role in dominating the optical properties and colloidal stability of MHP nanocrystals. The surface ligands of MHP nanocrystals are easily lost, which leads to the decomposition of nanocrystals. Appropriate surface modulation can not only inhibit the nonradioactive recombination by reducing the surface defects, but also increase stability against oxygen/moisture induced decomposition.

3.2.1. Ligand modification. Generally, MHP nanocrystals are capped by long chain ligands such as OA and OAm. OAm is usually used to control the growth of nanocrystals while OA is used as stabilizers. However, the weak interactions of OA/OAm ligands to MHP nanocrystals greatly limit the stability of MHP nanocrystals.

The ligands with strong interaction with nanocrystals are widely researched to stabilize the MHP nanocrystals. Octylphosphonic acid (OPA) with strong interaction to MHP nanocrystals was used to replace OA/OAm ligands, which dramatically enhanced the stability of $CsPbX_3$ nanocrystals.[47] Owing to robust bonding strength between OPA and $CsPbX_3$ nanocrystals, the OPA-capped $CsPbX_3$ nanocrystals not only preserved the high PLQY (>90%) but also maintained the colloidal stability after multiple purification processes (Fig. 7a). Trioctylphosphine oxide (TOPO),[48] bis-(2,2,4-trimethylpentyl) phosphinic acid (TMPPA),[49] di-dodecyl dimethyl ammonium bromide (DDAB)[50], *etc.* were also reported to passivate and stabilize the MHP nanocrystals due to their strong interaction.

Another strategy to strengthen the interactions between ligands and nanocrystals is to adopt cross-linking surface ligands. Sargent and Seferos *et al.* introduced the cross-linking and polymerization of 4-vinyl-benzyl-dimethyloctadecylammonium chloride (V18) ligands on the surface of $MAPbBr_3$ nanocrystals.[51] The cross-linking between MHP nanocrystals is achieved *via* heating with a radical initiator, which could effectively improve the stability of MHP nanocrystals (Fig. 7b). Light-initiated polymerizable molecule conjugated linoleic acid (CLA),[52] and light-induced 9-decenoic acid (DeA)[53], **etc.** were also reported to passivate and stabilize the MHP nanocrystals. Due to their

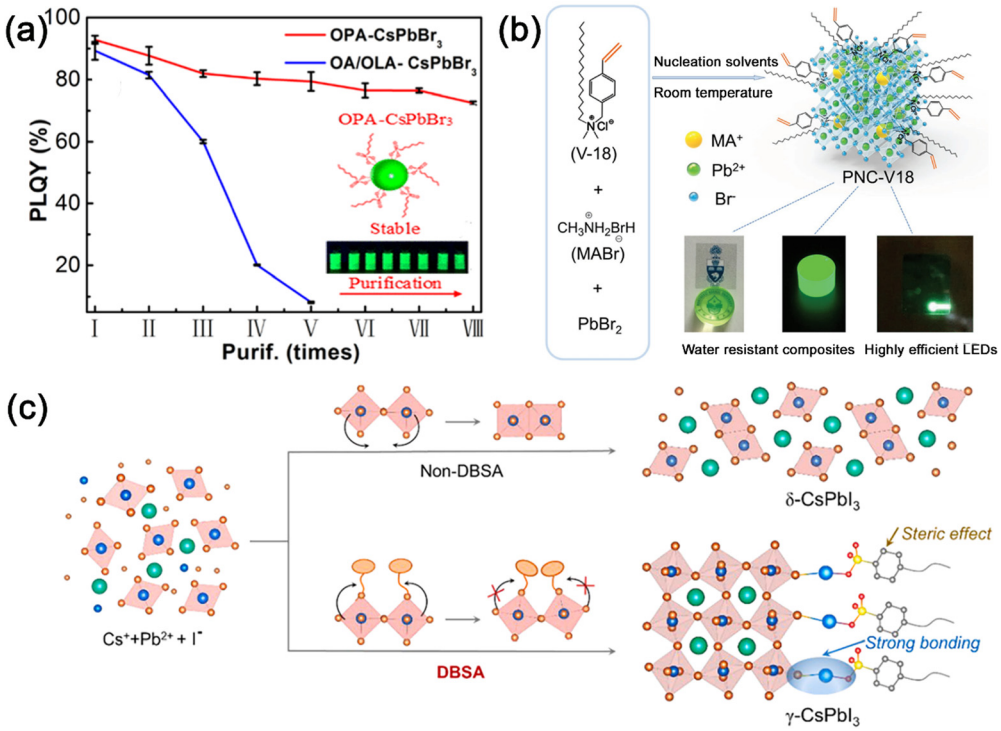

Fig. 7 (a) PLQY of OPA-$CsPbBr_3$ and OA/OLA-$CsPbBr_3$ nanocrystals with one to eight purification cycles. Reproduced from ref. 47 with permission. Copyright 2018, American Chemical Society. (b) Schematic illustration of the design of $MAPbBr_3$ nanocrystals modified with V18 ligands and their application in LEDs. Adapted from ref. 51 with permission. Copyright 2020, Wiley-VCH. (c) Schematic illustration of the synthesis of γ-$CsPbI_3$ nanocrystals assisted by DBSA. Adapted from ref. 54 with permission. Copyright 2021, Elsevier.

strengthened interactions, cross-linked surface ligands can passivate the surface of MHP nanocrystals and improve their stability.

The ligands with large steric hindrance could also improve the colloidal stability of MHP nanocrystals. The large steric hindrance of branched ligands not only prevents the nanocrystals from aggregation-induced degradation, but also prevents the protic solvent from penetrating the surface of MHP nanocrystals. Song and co-workers reported that the capping of the 4-dodecylben-zenesulfonic acid (DBSA) ligand could prevent the phase degradation of $CsPbI_3$ nanocrystals.[54] The strong bonding and steric hindrance of DBSA can suppress the distortion of the perovskite structure and improve the stability of $CsPbI_3$ nanocrystals (Fig. 7c). The resulting $CsPbI_3$ nanocrystals retained ~90% PL intensity after 36 h of storage in ambient air, and maintained ~85% PL intensity after 11 h of light illumination. Cage-like polyhedral oligomeric silsesquioxane (POSS),[55] poly(lactic acid) (PLA),[56] (3-aminopropyl)triethoxysilane (APTES),[57] *etc.* were also adopted to modify the surface of MHP nanocrystals with large steric hindrance.

The ligands play a vital role in passivating MHP nanocrystals. In the ligand modification strategy, the highly dynamic ligands could be replaced with strongly interacting ligands, cross-linked ligands, and large-steric hindrance ligands. The modified ligands are tightly bonded to the surface of MHP nanocrystals, protecting the MHP nanocrystals from aggregation-induced degradation and external environment factors.

3.2.2. Surface recovery. Even though the surface of MHP nanocrystals is passivated by the ligands, the dynamic and imperfect surface still affects the surface state. Therefore, surface recovery strategies were developed to modify the imperfect surface of MHP nanocrystals, which is usually achieved by filling vacancies or stripping redundant parts off the surface of MHP nanocrystals. Colvin and Yu *et al.* demonstrated that post-synthetic modification with trioctylphosphine (TOP) can help effectively and instantly recover the luminescent properties of aged $CsPbBr_{1.2}I_{1.8}$ nanocrystals.[58] The TOP treatment effectively promotes the repairing of surface defects on MHP nanocrystals (Fig. 8a). In addition to the increased PLQY, the TOP treatment also significantly enhances multiple stabilities of MHP nanocrystals. Alivisatos *et al.* reported that thiocyanate salts (NH_4SCN and NaSCN) could effectively modify the surface of $CsPbBr_3$ nanocrystals, improving the PLQY to nearly unity while maintaining the shape, size, and colloidal stability of $CsPbBr_3$ nanocrystals.[59] The thiocyanate-treatment effectively inhibits the non-radiative recombination by removing the uncoordinated Pb atoms from the MHP surface. Tetrafluoroborate salts ($NaBF_4$ and NH_4BF_4) were also reported to modify $CsPbX_3$ nanocrystals by stripping labile lead atoms off their surface.[60] The removal of these labile lead adatoms, which act

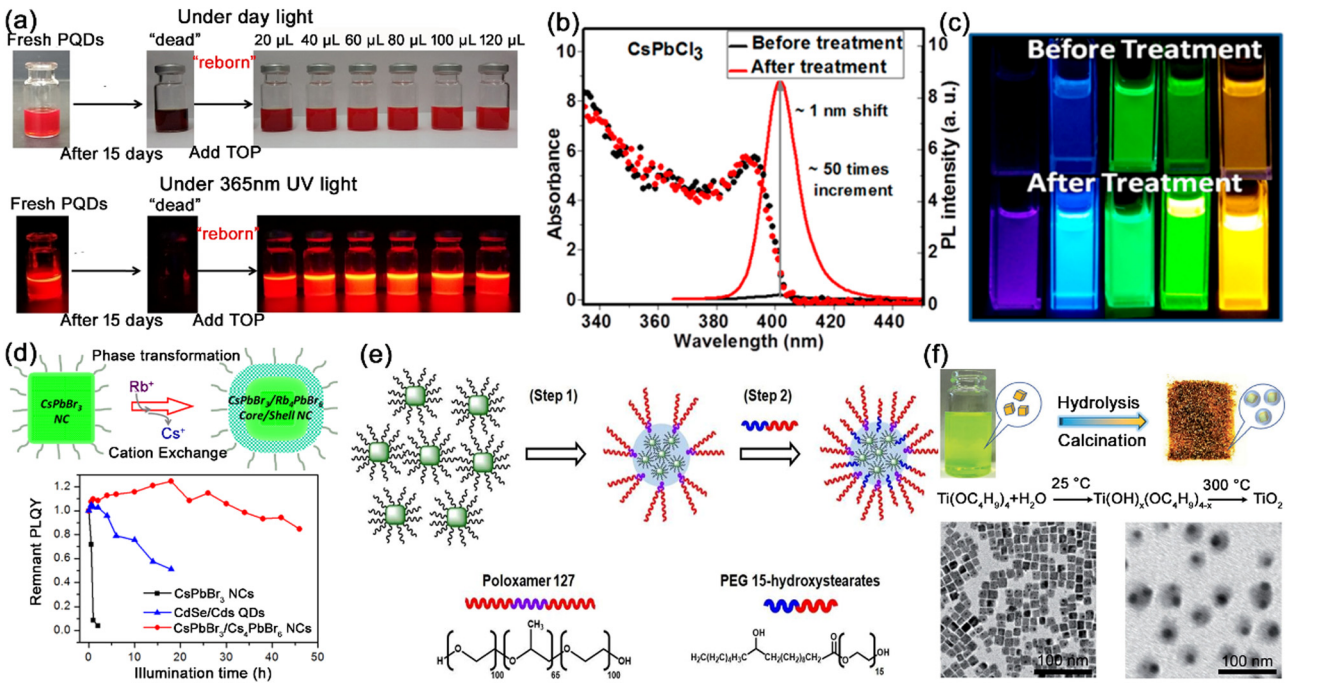

Fig. 8 (a) Photographs of fresh/aged $CsPbX_3$ nanocrystals and TOP treated $CsPbX_3$ nanocrystals. Adapted from ref. 58 with permission. Copyright 2018, American Chemical Society. (b) Absorption and PL emission spectra of $CsPbCl_3$ nanocrystals and (c) photographs of $CsPbX_3$ solution before and after tetrafluoroborate salt treatment. Adapted from ref. 60 with permission. Copyright 2018, American Chemical Society. (d) Schematic illustration of the synthesis of core/shell structured $CsPbBr_3/Rb_4PbBr_6$ nanocrystals, and the photostability tests of $CsPbBr_3$, CdSe/CdS, and $CsPbBr_3/Rb_4PbBr_6$ nanocrystals. Adapted from ref. 62 with permission. Copyright 2018, American Chemical Society. (e) Schematic illustration of the encapsulation of hydrophobic $CsPbBr_3$ nanocrystals in amphiphilic polymers. Adapted from ref. 65 with permission. Copyright 2018, Wiley-VCH. (f) Schematic illustration of the fabrication of the $CsPbBr_3$@TiO_2 core/shell nanocrystals, and TEM images of $CsPbBr_3$ and $CsPbBr_3$@TiO_2 core/shell nanocrystals. Adapted from ref. 72 with permission. Copyright 2017, Wiley-VCH.

as traps for charge carriers, results in the improvement of PLQY (Fig. 8b and c). The PLQY of tetrafluoroborate-treated MHP nanocrystals almost reach unity with a single-exponential PL decay. The surface recovery strategies could strip redundant atoms and modify the imperfect surface of MHP nanocrystals, which could help recover the PL properties of aged MHP nanocrystals and improve their long-term storage stability.

3.2.3. Core–shell structure. Traditional semiconductor nanocrystals (such as CdS@ZnS, CdSe@ZnS, and InP@ZnS) possess a monodisperse core–shell structure, which improves the stability by preventing environmental factors from permeating into the core and suppresses the nonradiative recombination by passivating surface defects. Moreover, the non-luminescent thin protective shell could minimize the light loss and maximize PL performance. Due to the inherent ionic bonding and vulnerable crystal lattice of perovskites, it is difficult to form an ideal core–shell structure of MHP nanocrystals through conventional methods. However, many valuable studies have been devoted to realize monodisperse core–shell MHP nanocrystals.[61]

Perovskite derivative shells are one of the mostly investigated shell materials for MHP nanocrystals. With higher exciton binding energy and wider band gaps, zero-dimensional perovskites possess higher structural stability than 3D perovskite nanocrystals in an ambient atmosphere, which makes them a good shell material for MHP nanocrystals. The $CsPbBr_3$@Rb_4PbBr_6 core–shell nanocrystals (Fig. 8d) and $CsPbBr_3$@Cs_4PbBr_6 core–shell nanocrystals were reported to possess better structural stability than bare $CsPbBr_3$ nanocrystals, which is attributed to the higher thermodynamic stability of the perovskite derivative shell.[62,63]

Polymer shells provide another route to synthesize highly stable MHP nanocrystals. Pramanik *et al.* utilized polystyrene triblock polymers (PS–PEB–PS and PEG–PPG–PEG) as shells to protect $CsPbBr_3$ nanocrystals. The hydrophobic parts strongly interact with MHP nanocrystals, and the water-soluble parts effectively prevent the degradation of MHP nanocrystals in water.[64] Bang *et al.* reported the non-ionic amphiphilic polymers (poloxamer 127 and PEG (15)-hydroxystearates) encapsulating $CsPbBr_3$ nanocrystals as thin shells. The polymeric shell of MHP–polymer nanospheres effectively prevents the diffusion of water into the nanospheres (Fig. 8e).[65]

Oxides have also been successfully used as shell materials for the core–shell MHP nanocrystals to enhance the stability. Silanes have been extensively explored to form thin silicon shells on the surface of MHP nanocrystals through hydrolysis reaction, such as (3-aminopropyl) triethoxysilane (APTES),[66,67] tetramethyl orthosilicate (TMOS),[68,69] tetraethoxysilane (TEOS),[70] di-*sec*-butoxyaluminoxytriethoxysilane (DBATES),[71] *etc.* The protective silica shell endows MHP@SiO_2 core–shell nanocrystals with greatly improved humidity, thermal and photostability and excellent anion-exchange resistance. Similar to silicon shells, shells of other oxides such as TiO_2 and ZrO_2 were also used as shell material to improve the mechanical rigidity and chemical stability of MHP nanocrystals. Zheng *et al.* reported the coating of TiO_2 shells on $CsPbBr_3$ nanocrystals through the hydrolysis reaction of titanium butoxide (TBOT) at low moisture and the calcination process at high temperature (Fig. 8f).[72] The monodispersed $CsPbBr_3$@TiO_2 core–shell nanocrystals showed excellent chemical stability, water stability, and photostability. Sun and Zhang *et al.* also utilized the slow hydrolysis of zirconium *tert*-butoxide ($Zr(OC_4H_9)_4$) to form ZrO_2 shells on $CsPbX_3$ nanocrystals. The ZrO_2 shell endows $CsPbX_3$@ZrO_2 core–shell nanocrystals with higher stability against illumination, oxygen, and moisture.[73]

The surface of MHP nanocrystals plays a significant role in carrier recombination processes. Therefore, the surface modulation strategy not only modifies the optical performance of MHP nanocrystals by inhibiting the nonradioactive recombination, but also improves their stability against harsh environments. However, due to the fragility of the surface of MHP nanocrystals, the surface modulating procedure is challenging. The surface modulating process requires mild experimental conditions to avoid the additional damage to the MHP nanocrystals.

3.3. Matrix encapsulation

The MHP nanocrystals suffer from poor stability against external harsh environmental factors, such as moisture, oxygen, heat *etc.* The matrix encapsulation strategy could protect the MHP nanocrystals from coming in contact with harsh environments, which effectively protects them from environmental degradation. To provide strong protection to MHP nanocrystals, the matrix should be durable and chemically inert under ambient environmental conditions.

3.3.1. Organic polymer encapsulation. Organic polymers often show structural and mechanical advantages like easy processability, high flexibility, high transmittance, and robust stability against moisture/oxidation, *etc.* Therefore, organic polymer encapsulation is an attractive strategy to improve the stability of MHP nanocrystals. Dense polymer chains can not only passivate the surface of MHP nanocrystals, but also avoid the direct contact with harsh environments. Generally, the MHP nanocrystals are well-dispersed in the polymer matrix, which inhibits the aggregation-induced degradation. The other advantage of the polymer encapsulation strategy is the flexible processing of the polymer, which could be processed into any shape though a variety of methods such as thermal/photocuring, spin-coating, microfluidic spinning, *etc.*

Many works have reported the encapsulation of MHP nanocrystals by polymers to enhance their stability. The commonly used polymers include polymethyl methacrylate (PMMA),[3] polystyrene (PS),[74] polycarbonate (PC),[75] polyvinyl chloride (PVC),[75] polyethylene oxide (PEO),[76] *etc.* The prepared MHP@polymers displayed high luminescence and high stability in harsh environments. We also reported the encapsulation of $CsPbX_3$ nanocrystals in an ultra-violet (UV) light curing adhesive (Ergo 8500), and the $CsPbX_3$@Ergo films exhibited greatly improved water-resistance and air-stability.[77] Unlike other thermal curing polymers, the Ergo adhesive can be cured under UV light, which prevents the degradation of PL properties of the $CsPbX_3$ nanocrystals during film forming processes. Other techniques were also widely investigated for polymer encapsulation of MHP nanocrystals. Pathak *et al.* reported the encapsulation of

$MAPbX_3$ nanocrystals in PS/PMMA matrix by a spin-coating method, and the resulting MHP@PS/PMMA showed high stability under continuous illumination.[78] Chen and co-workers realized the encapsulation the $CsPbX_3$ nanocrystals in PMMA matrix at room temperature through a microfluidic spinning technique, which is applicable for scale-up fabrication of MHP nanocrystals in a green way (Fig. 9a).[79] Wang *et al.* embedded $CsPbX_3$ nanocrystals in polyvinylpyrrolidone (PVP) flexible films by using a one-step electrospinning strategy, followed by coating a strongly hydrophobic silicone resin on the surface of the films.[80] The formed flexible luminescent films showed high resistance to water and anion exchange, and significantly prolonged lifetime under ambient air.

3.3.2. Inorganic matrix encapsulation. Although polymer encapsulation provides superior moisture/oxygen resistance to MHP nanocrystals, the thermal stability problem still limits their further applications. Generally, most inorganic solids are mechanically robust and exhibit better thermal resistance properties than the majority of organic compounds, which makes inorganic matrix encapsulation an effective strategy to protect MHP nanocrystals.

Due to the low diffusion rates of ions or atoms and thermal stability, oxides are often used as encapsulation materials to protect MHP nanocrystals.[71,81] Li *et al.* reported a high temperature solid state synthetic strategy for encapsulating MHP nanocrystals in Al_2O_3 matrixes, generating $CsPbX_3$@Al_2O_3 powders with excellent optical properties and exceptional thermal stability (Fig. 9b).[82] Costa *et al.* encapsulated $CsPbBr_3$ nanocrystals in SiO_2/ZrO_2 matrix, and the resulting $CsPbBr_3$@SiO_2/ZrO_2 composites showed excellent PL properties with significantly enhanced storage, thermal, moisture, and irradiation stabilities (Fig. 9c).[83]

In particular, the inorganic salts have the advantage of transparent, eco-friendly and compact characters, which could have a good effect on protecting MHP nanocrystals from environmental damage. The dense and robust structure of salt matrix could provide a solid surrounding for MHP nanocrystals, which could greatly enhance the stability. Gaponik *et al.* reported the immobilization of $CsPbBr_3$ nanocrystals in potassium halide salts (KCl, KBr, and KI) under high pressure.[84] The $CsPbBr_3$ nanocrystals are completely embedded in transparent potassium halide salts, leading to high robustness and improved stability under ambient conditions. $NaNO_3$ and NH_4Br were also utilized as solid matrix for encapsulating MHP nanocrystals, strongly improving their stability.[85,86]

Inorganic polymers, such as ceramic and glass, are polymers composed of noncarbon atoms with a skeleton structure. Generally, inorganic polymers are thermally stable and can be

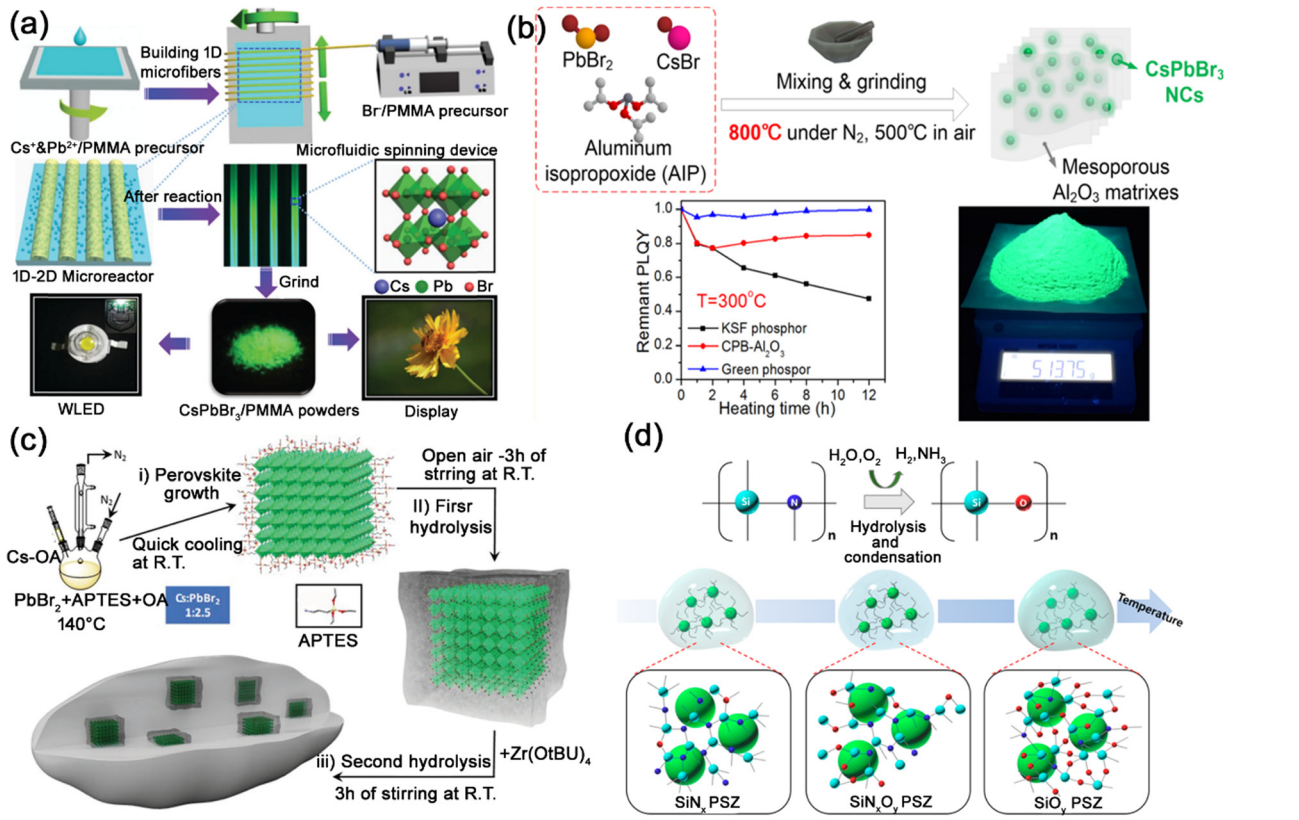

Fig. 9 (a) Schematic illustration of the preparation of $CsPbBr_3$@PMMA composites through microfluidic spinning and their applications in WLEDs. Adapted from ref. 79 with permission. Copyright 2017, Royal Society of Chemistry. (b) Schematic illustration of the high temperature solid-state synthesis procedure, and the thermal stability tests of $CsPbBr_3$@Al_2O_3 composites. Adapted from ref. 82 with permission. Copyright 2019, American Chemical Society. (c) Schematic illustration of the one-pot synthesis of the $CsPbBr_3$@SiO_2/ZrO_2 composites. Adapted from ref. 83 with permission. Copyright 2020, Wiley-VCH. (d) Schematic illustrations of the sol–gel synthesis process of $CsPbBr_3$@PSZ composites. Adapted from ref. 87 with permission. Copyright 2018, American Chemical Society.

used as thermal insulation materials. Transparent ceramics and glass ceramics are widely used as an encapsulation matrix for MHP nanocrystals, which could provide excellent resistance to heat/moisture for MHP nanocrystals. Yoon *et al.* reported the utilization of the polysilazane (PSZ) inorganic polymer to encapsulate $CsPbBr_3$ nanocrystals, generating $CsPbBr_3$@PSZ nanocomposites with high PLQY and improved environmental stability (Fig. 9d).[87] The strong PSZ inorganic ceramic matrix protects $CsPbBr_3$ nanocrystals from heat, moisture and polar solvents. Liang and Xiang *et al.* reported the encapsulation of $CsPb_2Br_5$ nanocrystals in borosilicate glasses through conventional melt-quenching and heat-treatment methods.[88] Other types of glass, such as phospho–silicate glass,[89] P_2O_5-based glass,[90] TeO_2-based glass,[10] GeO_2-based glass,[91] *etc.* were also utilized as matrix for the encapsulation of MHP nanocrystals. The glass matrixes show excellent thermal stability, mechanical stability and chemical stability, and endow the encapsulated MHP nanocrystals with greatly improved stability.

3.3.3. Porous matrix encapsulation. The above encapsulation strategies are used to grow protecting layers directly on MHP nanocrystals, which is challenging as the optical performance of MHP nanocrystals would be deteriorated in the harsh formation process of the protective layer. Accordingly, it is relatively feasible to introduce MHP nanocrystals into pre-synthesized porous materials. The pre-synthesized porous materials such as mesoporous inorganic materials, hierarchical inorganic materials, and hollow inorganic materials obtained through natural or artificial ways have been widely reported to encapsulate MHP nanocrystals.

The mesoporous inorganic materials possess a strong and abundant mesopore structure, which makes them a wonderful encapsulation matrix for MHP nanocrystals. Liu *et al.* reported the encapsulation of $CsPbX_3$ nanocrystals in mesoporous silica, which prevents ion exchange and increases stability (Fig. 10a).[8] Subsequently, various types of mesoporous silicon particles were reported to encapsulate MHP nanocrystals (Fig. 10b), including

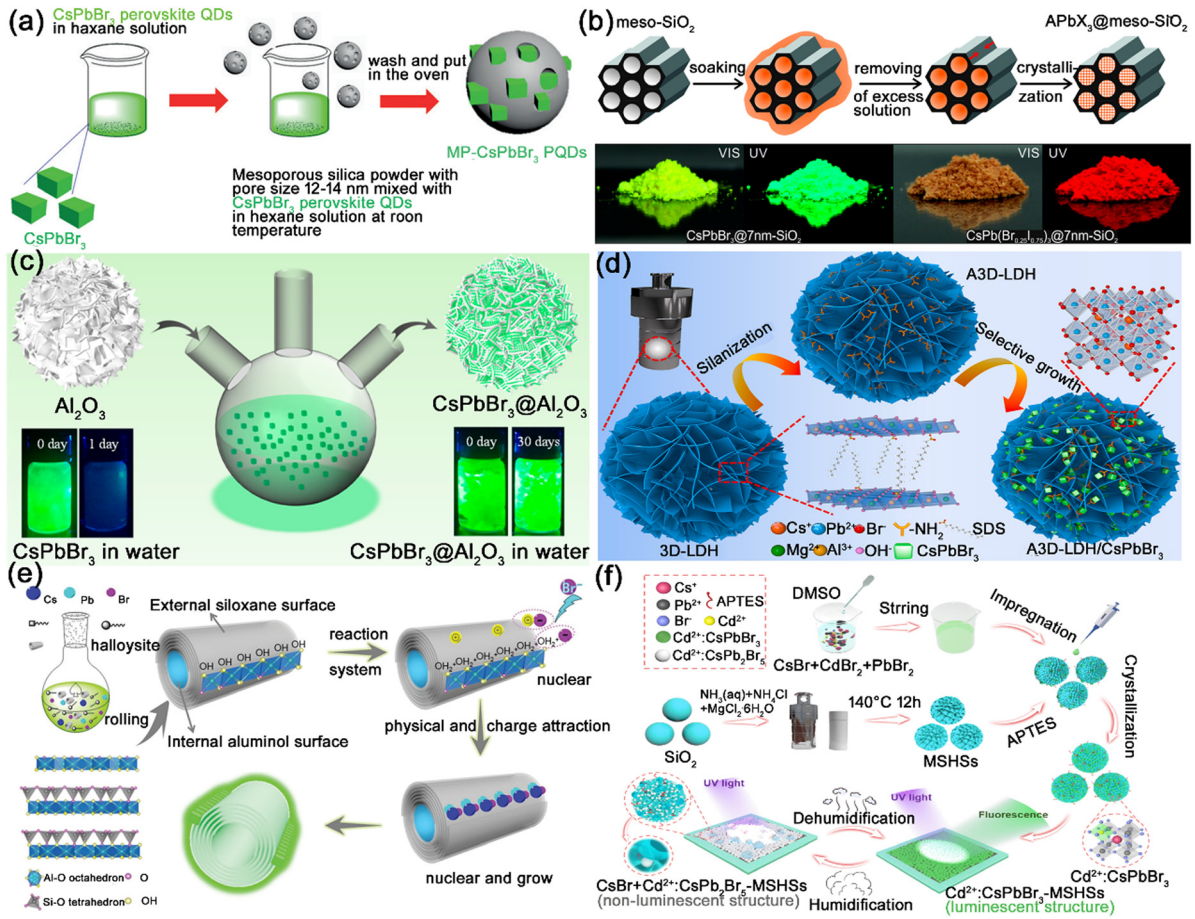

Fig. 10 (a) Schematic illustration of the synthesis of $CsPbBr_3$@SiO_2. Adapted from ref. 8 with permission. Copyright 2018, Wiley-VCH. (b) Schematic illustration of the template-assisted synthesis of $CsPbX_3$@meso-SiO_2 composites, and photographs of $CsPbX_3$@meso-SiO_2 composites under daylight and under UV illumination. Adapted from ref. 95 with permission. Copyright 2016, American Chemical Society. (c) Schematic illustration of the synthesis process of $CsPbBr_3$@h-Al_2O_3. Adapted from ref. 100 with permission. Copyright 2020, American Chemical Society. (d) Schematic illustration of the synthesis of $CsPbBr_3$@LDH composites through a selective growth strategy. Adapted from ref. 101 with permission. Copyright 2021, Elsevier. (e) Schematic illustration of the synthetic strategy and fabrication of the $CsPbBr_3$@HNTs composites. Adapted from ref. 102 with permission. Copyright 2018, Wiley-VCH. (f) Schematic illustration of the preparation of: $CsPbX_3$:Cd^{2+}@MSHSs composites. Adapted from ref. 103 with permission. Copyright 2022, Elsevier.

SBA-15,[92–95] MCM-41,[94–97] MCM-48,[95] *etc.* Mesoporous Y_2O_3 nanoparticles were also reported to encapsulate MHP nanocrystals, which inhibit the aggregation process of MHP nanocrystals, and show enhanced stability against heat-induced, irradiation-induced and humidity-induced decomposition.[98]

Hierarchical inorganic materials possess high surface areas and large pore volumes, which are also widely utilized in encapsulating MHP nanocrystals. Cheng and Lin *et al.* reported the integration of $CsPbX_3$ nanocrystals in CaF_2 hierarchical nanospheres, which preserved the PL performance of MHP nanocrystals and protected them from moisture, light exposure, and anion exchange.[99] Zhou and co-workers reported the anchoring of $CsPbBr_3$ nanocrystals on hierarchical alumina (h-Al_2O_3), and the hierarchical Al_2O_3 matrix produced a significant effect on the chemical stability of $CsPbBr_3$ nanocrystals (Fig. 10c).[100] As shown in Fig. 10d, Cao *et al.* proposed the anchoring of $CsPbBr_3$ nanocrystals on the aminated hierarchical layered double hydroxide (LDH). Attributed to the hierarchical isolated structure of LDH, the $CsPbBr_3$@LDH composites exhibit enhanced stability in adverse environments (humidity air, irradiation, and heat).[101]

The hollow inorganic materials possess large surface areas and strong hollow structures, which could provide large active nucleation and adsorption platforms for MHP nanocrystals. In addition, the large surface area and hollow structure could accelerate heat dissipation, and prevent the heat-induced damage to encapsulated MHP nanocrystals. Lin *et al.* reported the encapsulation of $CsPbX_3$ nanocrystals in natural mineral hollow halloysite nanotubes (HNTs), generating $CsPbX_3$@HNT nanocomposites with excellent thermal stability, irradiation stability, and moisture stability (Fig. 10e).[102] The excellent thermal stability is attributed to the synergistic effect of higher thermal conductivity and the increased heat dissipation area of hollow HNTs. Zhao *et al.* employed magnesium silicate hollow spheres (MSHSs) to encapsulate $CsPbBr_3$ nanocrystals, and the $CsPbBr_3$@MSHSs composites showed remarkedly improved photostability and thermal stability (Fig. 10f).[103] Liu and Li *et al.* reported the encapsulation of $CsPbBr_3$ nanocrystals in Gd_2O_3:Eu^{3+} hollow spheres, generating dual-emission $CsPbBr_3$@Gd_2O_3:Eu^{3+} composites with improved photostability and thermal stability.[104]

These porous inorganic matrices can effectively disperse MHP nanocrystals in their solid porous structure and effectively inhibit the aggregation-induce degradation. And the robust inorganic matrix has a physical barrier effect, and can act as a protective layer to prevent oxygen/moisture induced degradation, improving the stability of MHP nanocrystals. As an important kind of porous materials, porous framework materials (PFMs) show great potential in encapsulating MHP nanocrystals, which will be highlighted in the next chapter.

4. Design, synthesis, and properties of MHP@PFMs

Crystalline porous framework materials (PFMs) are widely used in industrial catalysis, crystalline separation and ion exchange due to the characteristics of diverse topological structures, regular framework structures, high specific surface areas, and ease of modification and regulation. Crystalline PFMs can be divided into inorganic materials represented by zeolites, inorganic–organic hybrid materials represented by metal–organic framework (MOFs), and organic materials represented by covalent–organic framework (COFs). Due to their structural regularity, inherent porosity, extensive functionality, and design flexibility, crystalline PFMs are attractive candidates for encapsulating MHP nanocrystals.

4.1. The category of MHP@PFMs

4.1.1. MHP@Zeolites. As an important family of PFMs, the zeolites are porous crystalline aluminosilicates with a framework structure of $[AlO_4]^{5-}$ and $[SiO_4]^{4-}$ tetrahedra, which is bridged with oxygen atoms to form a regular 3D structure of cages and channels.[13] The structural formula of zeolites can be represented as $A_{x/n}[(AlO_2)_x(SiO_2)_y]\cdot mH_2O$, where A is Ca, Na, K, Ba, and Sr, and the y/x ratio is usually between 1 to 5. Zeolites are materials composed of silicon and aluminum, in which Si atoms are replaced by Al atoms in the pure silicon skeleton. The substitution of Si^{4+} with Al^{3+} endows the whole skeleton with negative charges, while the A cations outside the skeleton play a role in balancing the charges. Due to the similar ionic radii of Si and Al, the ratio of Si to Al can be adjusted within a certain range while keeping the crystal structure of zeolites unchanged. The higher the Si/Al ratio of zeolites, the better the stability of zeolites. The 3D cages and channels of zeolites are in regular shape and structurally stable, which could act as matrix for diverse guests.[105]

Ye *et al.* first reported the encapsulation of MHP nanocrystals in zeolite-Y, where Cs^+ ions were infused into zeolite-Y by ion exchange and then reacted with PbX_2 to form $CsPbX_3$ nanocrystals in zeolite-Y matrix (Fig. 11a).[106] The zeolite-Y encapsulation reduces degradation of the MHP nanocrystals and improves the stability of the MHP nanocrystals under strong illumination. Zeolite-Y was further utilized to encapsulate $CsPbCl_3$:Mn^{2+} and Cs_4PbCl_6 MHP nanocrystals,[107,108] and the protective effect of zeolite-Y greatly improves the stability against moisture, heat, and illumination. Wang *et al.* reported the *in situ* growth of $MAPbBr_3$ nanocrystals in aluminophosphate AlPO-5 zeolite crystals, where the $MAPbBr_3$ nanocrystals were uniformly distributed within the AlPO-5 zeolite matrix (Fig. 11b).[109] The $MAPbBr_3$@AlPO-5 composites exhibited an obvious blue-shift of PL peaks, which should be due to the quantum confinement $MAPbBr_3$ nanocrystals in AlPO-5 zeolite. Meanwhile, the defects of $MAPbBr_3$ nanocrystals were passivated by the H-bonding interactions with AlPO-5 zeolite. The *in situ* passivation and shielding protection effect of AlPO-5 zeolite inhibit the heat, moisture, and oxygen-induced decomposition of $MAPbBr_3$ nanocrystals. Xia *et al.* encapsulated $CsPbBr_3$ nanocrystals in pure-silica zeolite Beta *via* a high temperature solid-state method, and the as-obtained composites exhibited high PLQY and ultra-stable PL performance.[110] The zeolite Beta matrix can effectively protect $CsPbBr_3$ nanocrystals against damage from oxygen, moisture, light irradiation, and heat. Hydrophobic zeolite SAPO-34,[111]

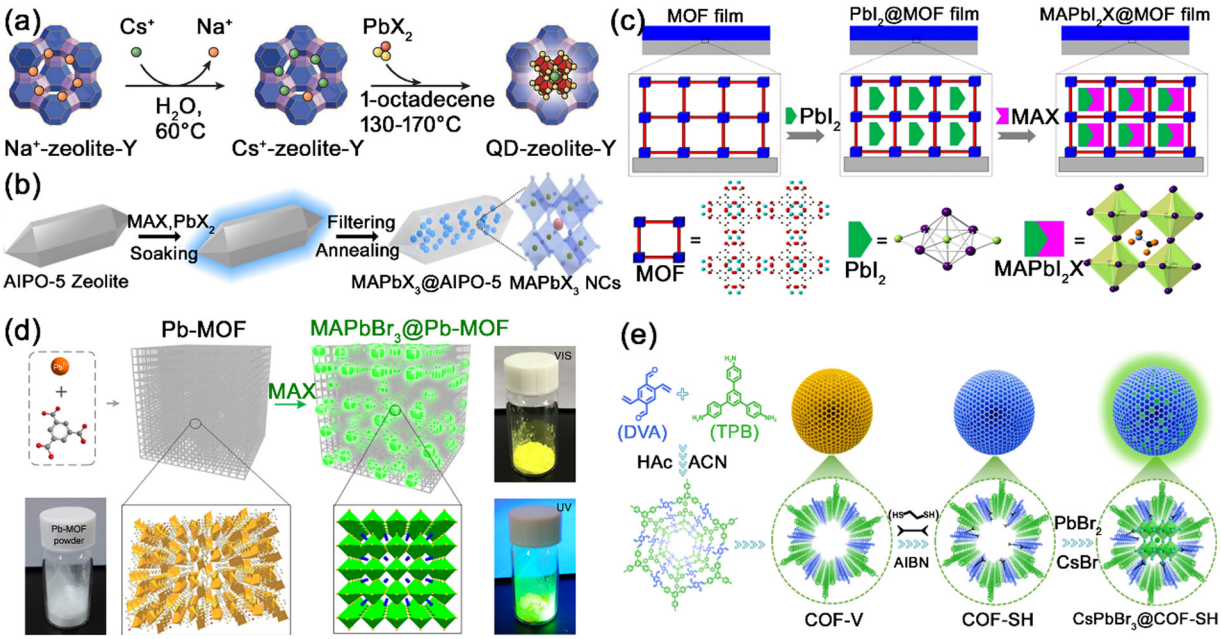

Fig. 11 (a) Schematic illustration of the two-step synthesis of $CsPbX_3$@zeolite-Y composites. Adapted from ref. 106 with permission. Copyright 2017, Wiley-VCH. (b) Schematic illustration of the synthesis of $MAPbX_3$@AlPO-5 composites. Adapted from ref. 109 with permission. Copyright 2020, Wiley-VCH. (c) Schematic Illustration of the confined synthesis of $MAPbX_3$@HKUST thin films. Adapted from ref. 126 with permission. Copyright 2016, American Chemical Society. (d) Schematic illustration of the conversion synthesis of $MAPbBr_3$@Pb–MOF. Adapted from ref. 128 with permission. Copyright 2017, Springer Nature. (e) Schematic illustration of the formation process of $CsPbBr_3$@COF–SH composites. Adapted from ref. 144 with permission. Copyright 2023, Elsevier.

hierarchical zeolite ZSM-5,[112] and other zeolites[113,114] were also reported to encapsulate MHP nanocrystals, which exhibit effective protective effects on the MHP nanocrystals.

4.1.2. MHP@MOFs. Metal–organic frameworks (MOFs) are porous framework materials composed of metal ions/metal clusters and organic ligands through strong coordination. MOFs are typically characterized by high crystallinity, large specific surface areas, ultra-high porosity, tunable pore/channel sizes, and tailorable functionality. Since the first report by Yaghi in 1995, MOFs have attracted enormous attention due to their excellent pore properties.[115,116] The MOFs can be synthesized by various methods, including solvothermal, mechanochemical, diffusion, electrochemical, ultrasonic and microwave methods. By adjusting the metal ions and organic ligands, MOFs with different topological structures, specific surface areas, pore structures, and functionalization can be easily designed and synthesized. Common MOF materials can be divided into the following categories: (1) IRMOFs. Yaghi's group synthesized a series of porous materials by utilizing reticulating metal ions and organic carboxylate, which were named isoreticular MOFs (IRMOFs).[117,118] (2) HKUSTs. Williams *et al.* from Hong Kong University of Science and Technology (HKUST) reported HKUST-1 with a typical "pocket-channel" structure.[119] (3) MILs. Ferey *et al.* reported MIL (Materials of Institute Lavoisier) series MOF materials. The crystal structure of the series of MIL contains trinuclear oxygen core secondary structure units, and each cluster is connected by the vertex angle to form a three-dimensional structure.[120] (4) ZIFs. Yaghi's group reported zeolitic imidazolate frameworks (ZIF) with a tetrahedral three-dimensional mesh structure.[121] (5) PCNs. Zhou's group developed a series of porous coordination network (PCN) materials with multiple cubic octahedral cages, which are composed of metal and porphyrin organic ligands.[122] (6) CPLs. Kitagawa's group designed and synthesized a series of coordination pillared-layer (CPL) MOFs, which show "gate opening" phenomenon.[123,124] (7) UiOs. Lillemd *et al.* discovered a series of ultra-stable MOF materials and named them UiO (University of Oslo). UiO series materials are obtained by interconnecting $[Zr_6O_4(OH)_4]$ clusters with 12 terephthalic acid ligands.[125]

Unlike traditional porous materials, MOFs exhibit tunable pore structures, high porosity, and tailorable functionalities, which make them attractive in catalysis, gas storage, molecular separation, and lighting. The high porosity and functionality of MOF materials endow them with great potential in encapsulating nanocrystals as host matrix. (1) Due to their tunable pores and strong interaction at specific sites, MOFs could provide better confinement for the nanocrystals. (2) MOF matrix could isolate nanocrystals from aggregation and protect them from harsh external environments. (3) Functional MOF matrix endows the nanocrystals with enhanced or new functions. Benefiting from these advantages, the MOFs have drawn enormous attention in encapsulating MHP nanocrystals.

Chen *et al.* utilized oriented microporous HKUST-1 thin films as a template for *in situ* synthesis of ultra-small $MAPbX_3$ nanocrystals by introducing PbI_2 and MAX stepwise (Fig. 11c).[126] The spectral blue-shifts of $MAPbX_3$@HKUST-1 should be attributed to the small size of $MAPbX_3$ confined by the micropores of HKUST-1. Under the protection of HKUST-1 matrix, the $MAPbX_3$@HKUST-1

thin film possesses high stability even under moist air with 70% humility. Xia's group also reported the encapsulation of $MAPbBr_3$ nanocrystals in MOF-5 microcrystals through stepwise adding precursors.[127] The resulting $MAPbBr_3$@MOF-5 composites featured excellent water resistance, pH resistance, and high thermal stability. Due to the intrinsic microporous structure (<2 nm) of common MOFs, the accessibility of MHP precursors in MOF matrix is hindered by the relatively large diffusion resistance. Li *et al.* developed a conversion strategy to grow $MAPbX_3$ nanocrystals in Pb–MOF matrix through a direct reaction between MAX halide salt and Pb–MOF (Fig. 11d).[128] Through the conversion strategy, highly luminescent $MAPbX_3$@Pb–MOF composites could be quickly and simply formed. Owing to the partial decomposition of Pb–MOF matrix, a large amount of MHP nanocrystals could be effectively and rapidly incorporated into MOF matrix. Meanwhile, the pores of common MOFs are mostly confined to a microporous regime (<2 nm), which makes it difficult for typical $CsPbX_3$ nanocrystals (~10 nm) to fit into the pore structure of MOFs. Alternatively, we first proposed the encapsulation of $CsPbX_3$ nanocrystals in the mesopores of mesostructured MOFs, where the pores of MOF-5 were expanded to mesopores by a templating strategy.[129] The generated $CsPbX_3$@MOF-5 composites possess improved stability (thermal-stability, photostability, long-term stability, and excellent anion exchange resistance) while maintaining excellent PL properties. Numerous series of MOFs, including UiO-66,[130,131] UiO-67,[132] Eu-BTC,[133] ZIF-8,[134] MIL-101,[135] ZJU-28,[136,137] *etc.*, have also been reported to encapsulate MHP nanocrystals, showing promising protective effects on the MHP nanocrystals.

4.1.3. MHP@COFs. Covalent organic frameworks (COFs) are crystalline porous framework materials formed by covalent bonding of organic monomers. After the first introduction of crystalline COFs (COF-1 and COF-5) by Yaghi's group in 2005,[138] COFs with various structural configurations have been reported. Connected by covalent bonds, the polymerization of COF monomers is guided by the topological structure, and the chains grow gradually in two-dimensional (2D) or three-dimensional (3D) directions, resulting in a clear, ordered and extended crystal structure of COFs. For 2D COFs, monomers are connected by covalent bonds, forming layered structures in the plane, and layers are conjugated by π–π interaction. And for 3D COFs, the monomers extend infinitely through covalent bonds, forming a framework with regular and periodic structures.[139] The crystalline COFs have the characteristics of high crystallinity, well-defined skeletons, high porosity, highly ordered periodic structures, coordinated topological structures, and convenient functional design. Due to the presence of covalent bonds between organic monomers, COFs possess better stability than MOFs and have more modified sites. Meanwhile, COFs have attracted much attention to confine nanoparticles owing to the following advantages: (a) the covalent bonds between the blocks ensure the physical and chemical stability of the nanoparticles in COFs; (b) the pore size of COF building blocks can be tuned to adapt to different nanoscale particles; (c) the unique pore structure of COFs provides efficient access to the active sites; and (d) the permanent pore structure of COFs can effectively constrain nanoparticles and prevent their agglomeration and decomposition.

Mukherjee and co-workers reported the encapsulation of $CsPbBr_3/Cs_4PbBr_6$ nanocrystals in Br containing COFs (EB-COF:Br), generating $CsPbBr_3/Cs_4PbBr_6$@EB-COF:Br composites with improved water stability, photostability and thermal stability.[140] The MHP nanocrystals were dispersed in the cavity of EB-COF:Br, and the COF encapsulation prevented the degradation of MHP nanocrystals. Zhu and Liu *et al.* reported the *in situ* growth of $MAPbBr_3$ nanocrystals in TAPT-DMTA COFs, and the $MAPbBr_3$@COF composites maintained the integrity of COFs and possessed enhanced stability under the protection of COF matrix.[141] Furthermore, they utilized TAPT-DMTA COFs to encapsulate $MA_3Bi_2Br_9$ nanocrystals, which exhibited strong stability in water and organic solvents.[142] Wang's group grew monodisperse $CsPbX_3$ nanocrystals in the thiol-functionalized COFs, which exhibited improved stability toward an artificial light-harvesting system and photocatalysis.[143] We further reported the *in situ* growth of $CsPbX_3$ nanocrystals in the ordered mesoporous channels of functionalized COFs (Fig. 11e).[144] Among the various functionalized COFs (–COOH modified, $-NH_2$ modified, –OH modified, and –SH modified COFs), the –SH modified COFs (COF–SH) possess the strongest connectivity to MHP nanocrystals. The –SH chains on COF–SH preferentially coordinate with the perovskite precursors to form nucleation sites, and then act as templates for the growth of $CsPbX_3$ nanocrystals in the channels of COF–SH. Meanwhile, the strong S–Pb coordination could passivate the surface defects of MHP nanocrystals, improving their stability against heat, water, and illumination.

4.2. The synthesis of MHP@PFMs

The synthesis process plays a vital role in determining the properties of MHP@PFM composites. Interfacial interactions and pore structures must be considered in the synthesis of high-quality MHP@PFM composites. To obtain high-quality MHP@PFM composites with excellent optical properties, several strategies for incorporating MHP nanocrystals into PFMs have been proposed. According to the formation sequence of MHP nanocrystals and PFM matrix, the synthetic strategies of MHP@PFM composites are divided into four categories as follows: (1) *in situ* growth; (2) external coating; (3) one-pot; and (4) physical mixing (Fig. 12).

4.2.1. *In situ* growth. In the *in situ* growth strategy, the preformed PFMs provide controllable pores for nucleation, leading to the confined growth of MHP nanocrystals. The pore structure of PFMs enables the fine control of the MHP nanocrystals by isolating the MHP nanocrystals and inhibiting their aggregation. This strategy usually involves two procedures, including the loading of the MHP precursors and confined growth of MHP nanocrystals. Due to the ionic crystal nature and confined pore space, MHP can be spontaneously formed in the PFMs once the constituents are mixed, or can be triggered by changing temperature or introducing anti-solvents.

The *in situ* growth strategy is the most common way to encapsulate MHP nanocrystals in PFMs. MHP can be spontaneously formed in the PFMs when mixed. Chen' group impregnated Pb^{2+} ions into the pores of UiO-66, and then soaked

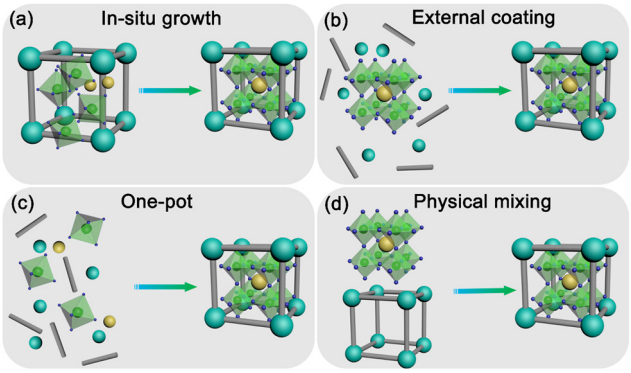

Fig. 12 Schematic illustration of the synthesis strategies of MHP@PFM composites. (a) *In situ* growth strategy; (b) external coating strategy; (c) one-pot strategy; and (d) physical mixing strategy.

Pb^{2+}@UiO-66 in a MABr solution to form $MAPbBr_3$@UiO-66 composites (Fig. 13a).[130] The $MAPbBr_3$ nanocrystals could be spontaneously formed when perovskite precursors were mixed in the pores of UiO-66 matrix. Ye' group also reported the synthesis of $CsPbX_3$@zeolite-Y composites by introducing Cs^+ and PbX_2 into the pores of zeolite-Y in a stepwise manner.[113] Cs^+ was first introduced into zeolite-Y through ion exchange, and then the PbX_2 precursor were injected to form $CsPbX_3$ nanocrystals in the zeolite-Y matrix. The $CsPbX_3$ nanocrystals were confined to a nanoscale by the pore structure of zeolite-Y matrix.

Apart from spontaneous growth, the formation of MHP nanocrystals in the PFMs can also be triggered by changing the temperature. Cao and Zhang *et al.* soaked mesoporous silica nanoparticles (MSNs) in CsBr and $PbBr_2$ solutions, and then heated to 150 °C in a vacuum oven to generate $CsPbBr_3$ nanocrystals in MSNs.[145] The $CsPbBr_3$@MSN composites could be obtained after thermal annealing, emitting bright green emission under UV light illumination. Zhou and co-workers also reported the *in situ* growth of $CsPbBr_3$ nanocrystals in hierarchically porous MOFs (HP-UiO-66) through heat treatment.[131] The CsBr and $PbBr_2$ precursors were infiltrated into the hierarchical structure of HP-UiO-66, and then the composites were heated at 150 °C to induce the confined growth of $CsPbBr_3$ in the pore structure of HP-UiO-66 (Fig. 13b).

Introducing anti-solvents can also trigger the formation of MHP nanocrystals in the PFMs. Kim and Jung *et al.* reported the *in situ* growth of $CsPbX_3$ nanocrystals in the pores of MIL-101 MOFs.[135] The PbX_2 precursor was impregnated into the pores of MIL-101, and then CsX/methanol solution was quickly injected into PbX_2@MIL-101 to induce the formation of $CsPbX_3$ nanocrystals. Methanol worked as an anti-solvent to trigger the formation of $CsPbX_3$ nanocrystals in the pores of MIL-101 (Fig. 13c). Egap' group also reported the anti-solvent triggered formation of $MAPbBr_3$ nanocrystals in TAPT-DMTA COFs.[141] $PbBr_2$ was first introduced into TAPT-DMTA COFs, and then the composites were soaked in a MABr alcoholic solution, leading to the *in situ* growth of $MAPbBr_3$ nanocrystals in TAPT-DMTA COFs.

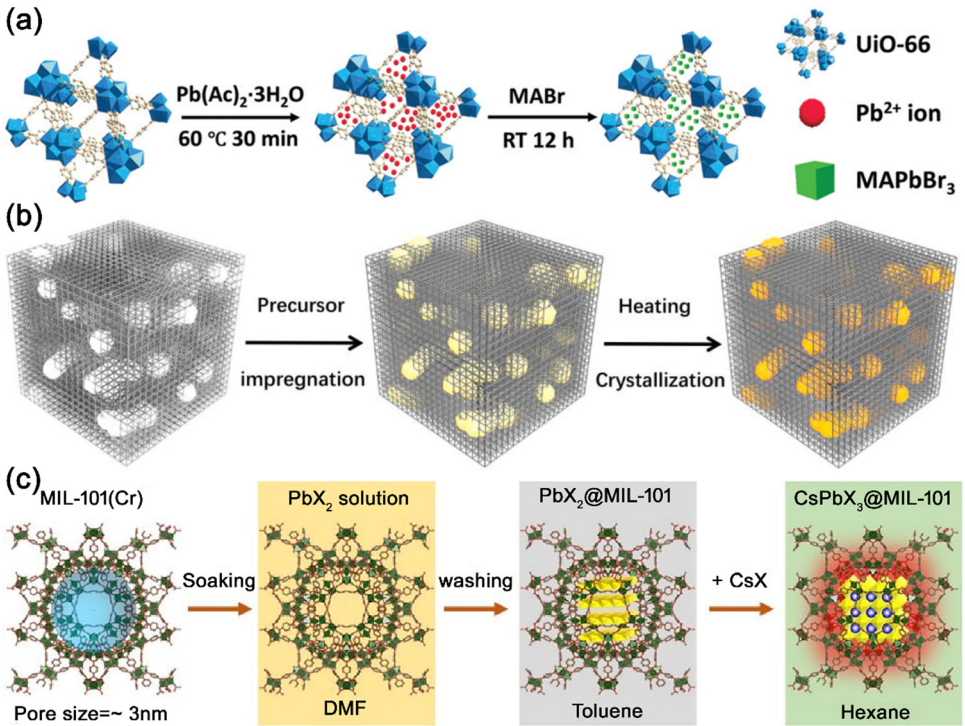

Fig. 13 (a) Schematic illustration of the *in situ* synthesis of $MAPbBr_3$@UiO-66 composites through spontaneous formation. Adapted from ref. 130 with permission. Copyright 2020, Royal Society of Chemistry. (b) Schematic illustration of the *in situ* synthesis of $CsPbX_3$@HP-UiO-66 composites triggered by changing the temperature. Adapted from ref. 131 with permission. Copyright 2021, Elsevier. (c) Schematic illustration of the *in situ* synthesis of $CsPbX_3$@MIL-101 composites triggered by anti-solvents. Adapted from ref. 135 with permission. Copyright 2019, American Chemical Society.

Basically, the *in situ* growth strategy has been proven to be effective in encapsulating MHP nanocrystals in PFMs. However, still there are some limitations of the *in situ* growth strategy, which need to be further considered. Due to the large diffusion resistance, only a small amount of perovskite precursors diffuses into the PFMs, which could lead to the low loading rate of MHP nanocrystals. And the morphology, size and distribution of MHP nanocrystals in PFMs are also difficult to control.

4.2.2. External coating. Apart from the large number of MHP@PFM composites based on the *in situ* growth strategy, the external coating strategy is also an effective method to encapsulate MHP nanocrystals in PFMs. In the external coating strategy, the MHP nanocrystals are pre-synthesized and then the precursors of PFMs are assembled on the MHP nanocrystals. Considering MHP nanocrystals of various sizes, the external coating strategy is expected to provide wide latitude in encapsulating MHP nanocrystals. The PFMs are constructed on the surface of pre-synthesized MHP nanocrystals, and the construction process could affect the crystallinity of MHP nanocrystals. Therefore, only the PFMs with mild synthesis conditions can be selected as host materials for the external coating strategy.

Kong *et al.* employed the external coating strategy to grow zeolitic imidazolate frameworks (ZIF) on the surface of $CsPbBr_3$ nanocrystals (Fig. 14a).[146] The ZIF materials, which could be prepared under relatively mild conditions (room temperature and moderate polarity solvents), were employed to encapsulate the $CsPbBr_3$ nanocrystals. The as-prepared $CsPbBr_3$ nanocrystals were dispersed into an ethyl acetate solution, and then zinc acetylacetonate and 2-methylimidazole were added and stirred for ZIF growth. The $CsPbBr_3$@ZIF composites show largely improved moisture stability due to the hydrophobicity of ZIF coating materials. Utilizing the same external coating strategy, Xu *et al.* also reported the coating of lanthanide metal–organic frameworks (Eu-BTC) on the surface of pre-synthesized $CsPbBr_3$ nanocrystals (Fig. 14b).[133] The precursors of Eu-BTC were mixed and stirred with pre-synthesized $CsPbBr_3$ nanocrystals, and then the mixtures were added to toluene to obtain $CsPbBr_3$@Eu-BTC composites.

4.2.3. One-pot. The one-pot synthesis strategy is also considered as an effective strategy for encapsulating MHP nanocrystals in PFMs since it is scalable time-saving, and cost-saving. The one-pot synthesis strategy involves premixing all building blocks of MHPs and PFMs. After controlling the reaction conditions, PFMs are constructed first and then MHP nanocrystals are generated in the PFMs.

Ghosh' group reported the encapsulation of $MAPbBr_3$ nanocrystals in zeolitic imidazolate frameworks (ZIF-8) through the

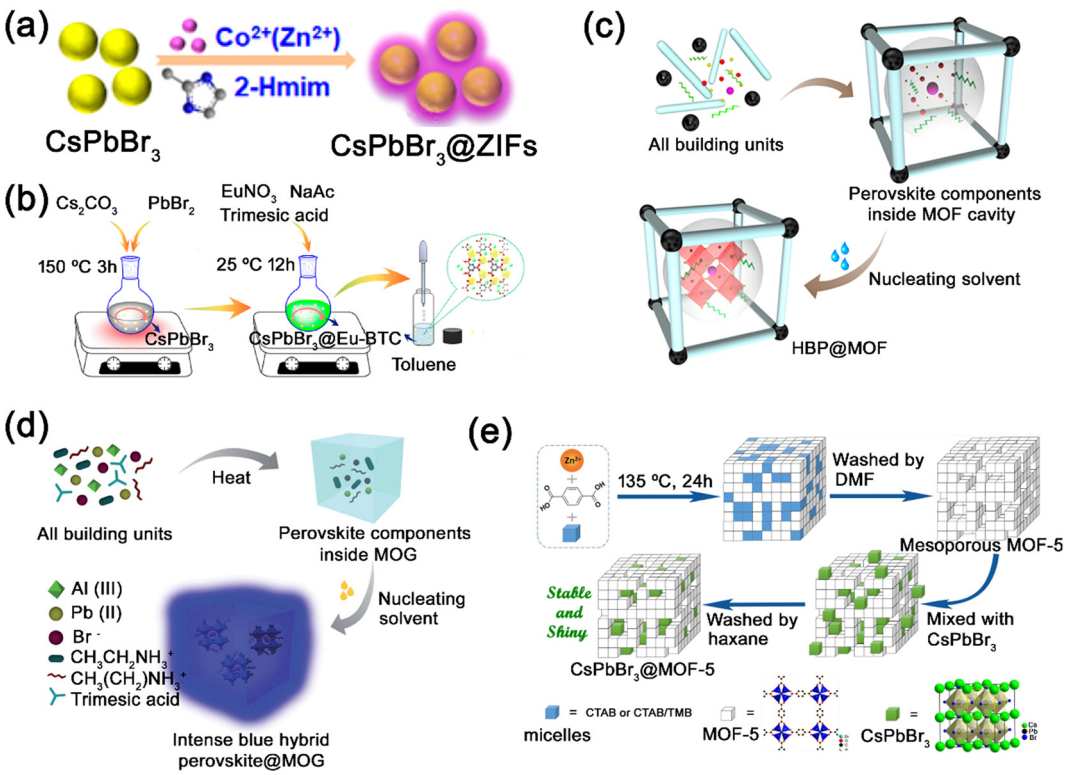

Fig. 14 (a) Schematic illustration of the fabrication process of $CsPbBr_3$@ZIF composites. Reproduced from ref. 146 with permission. Copyright 2018, American Chemical Society. (b) Schematic illustration of the external synthesis of $CsPbBr_3$@Eu-BTC composites. Reproduced from ref. 133 with permission. Copyright 2019, American Chemical Society. Schematic illustration of the one-pot synthesis of (c) $MAPbBr_3$@ZIF-8 composites. Adapted from ref. 134 with permission. Copyright 2019, American Chemical Society. (d) Schematic illustration of the one-pot synthesis of $EAPbBr_3$@MOG nanocomposites. Adapted from ref. 147 with permission. Copyright 2019, Royal Society of Chemistry. (e) Schematic illustration of the physical mixing synthesis of $CsPbX_3$@MOF-5 composites. Adapted from ref. 129 with permission. Copyright 2019, Elsevier.

one-pot strategy, where all building blocks of ZIF-8 and MHP are mixed in a mixture solution (Fig. 14c).[134] After stirring for few minutes, white precipitates (ZIF-8) started forming and the MHP precursors were encased in the pores of ZIF-8. Then, excessive anti-solvent toluene was added for the nucleation of $MAPbBr_3$ in ZIF-8. The $MAPbBr_3$@ZIF-8 composites were successfully synthesized through the one-pot strategy. By changing the MHP precursor MABr to EABr, $EAPbBr_3$@ZIF-8 composites could also be synthesized following the same method. Furthermore, Ghosh' group utilized the one-pot strategy to encapsulate $MAPbBr_3$/$EAPbBr_3$ nanocrystals in an Al-based hierarchical porous metal–organic gel (MOG) matrix (Fig. 14d).[147] All reacting components of MHP and MOG were mixed and heated at 110 °C, where MHP precursors were embedded in the constructed MOG matrix. And then, MHP nanocrystals were formed in the MOG matrix with the addition of anti-solvent (toluene).

4.2.4. Physical mixing. The above MHP@PFM composite synthesis strategies all involve the nucleation of MHP nanocrystals under complex environments, which might damage their PL performance. Alternatively, in the physical mixing strategy, the pre-synthesized MHP nanocrystals are directly mixed with PFMs, and subjected to ultrasonic or vacuum treatment to ensure the encapsulation of MHP nanocrystals in PFMs. The physical mixing strategy would maintain the excellent PL properties of MHP nanocrystals, and generate highly luminescent MHP@PFM composites. Since the size of pre-synthesized MHP nanocrystals is larger than that of the micropores of common PFMs, it is essential to expand the pore structure to the mesopore range.

Recently, we reported the successful encapsulation of $CsPbX_3$ nanocrystals in mesoporous MOF-5 matrix though the physical mixing strategy (Fig. 14e).[129] The mesoporous MOF-5 crystals with tailored porosity were first constructed by employing surfactants cetyltrimethylammonium bromide (CTAB) and 1,3,5-trimethylbenzene (TMB) as templating agents. And then, the mesoporous structured MOF-5 crystals were mixed with pre-synthesized $CsPbX_3$ nanocrystals under vacuum to obtain the $CsPbX_3$@MOF-5 composites. The $CsPbX_3$ nanocrystals were successfully encapsulated in mesoporous MOF-5 matrix though the physical mixing strategy, where the mesoporous MOF-5 crystals worked as an excellent dispersion matrix to protect $CsPbX_3$ nanocrystals from environmental factors.

4.3. Properties of MHP@PFMs

4.3.1. Stability improvements. The encapsulation of MHP nanocrystals into the pores of PFMs could yield greatly improved stabilities, including thermal stability, moisture stability, photostability, long-time storage stability, anion exchange resistance, *etc.* The mechanisms for the extended stability could be summarized as follows:

Physical barrier effect. Ascribed to the ionic nature and highly mobile surface ligands, the MHP nanocrystals suffer from the aggregation-induced degradation and poor stability against environmental factors. When encapsulated in PFMs, the stability of MHP nanocrystals is greatly improved. The MHP nanocrystals are well dispersed and encapsulated in the pore structure of PFMs, preventing the exposure and aggregation of PFMs. And the PFMs could work as a physical barrier to protect MHP nanocrystals from the invasion of environmental factors (heat, moisture, oxygen, and light illumination). The stability improvements for a series of MHP@PFM composites are collected and shown in Table 1, demonstrating the effective protection effect of PFMs on MHP nanocrystals.

Xiang and co-workers reported the encapsulation of $CsPbX_3$ nanocrystals in porous zeolite, generating $CsPbX_3$@zeolite with excellent thermal/photo/air stability under the surface passivation of zeolite.[113] The $CsPbBr_3$@zeolite retained 53% of the primary PL intensity at 120 °C (Fig. 15a), 93.6% of the primary PL intensity after being illuminated with UV light for 8 hours, and 86% of the primary PL intensity after 30 days of storage, respectively, revealing their excellent thermal/photo/air stability. These significant improvements in stability undoubtedly proved

Table 1 Summary of the methods, types, and stabilities of MHP@PFMs

Matrix	MHP	Synthesis method	PLQY	Thermal stability	Water stability	Photo stability	Storage stability	Ref.
Zeolite-Y	$CsPbX_3$	*In situ* growth	83%	100 °C, 40%	N/A	N/A	180 day	108
Zeolite AlPO-5	$MAPbBr_3$ $CsPbX_3$	*In situ* growth	18%	135 °C, 5%	12 day	N/A	450 day	109
Zeolite Beta	$CsPbBr_3$	*In situ* growth	61%	150 °C, 10%	30 day, 81%	20 day, 100%	N/A	110
Zeolite ZSM-5	$CsPbBr_3$	*In situ* growth	62%	N/A	100 day, 92%	N/A	100 day	112
Zeolite	$CsPbBr_3$	*In situ* growth	59%	120 °C, 53%	N/A	8 h, 94%	30 day, 86%	113
Zeolite/PMMA	$CsPbX_3$	*In situ* growth	54%	160 °C, 20%	20 day, 78%	N/A	60 day, 94.7%	114
MOF-5	$MAPbBr_3$	*In situ* growth	N/A	150 °C, 5%	30 day, ~5%	N/A	N/A	127
Meso-MOF-5	$CsPbX_3$	Physical mixing	52%	120 °C, 30%	N/A	80 h,72%	60 day, 79%	129
HP-UiO-66	$CsPbX_3$	*In situ* growth	45%	100 °C, 24%	15 day, 95%	2 h, 85%	15 day, 60%	131
UiO-67	$CsPbX_3$	*In situ* growth	N/A	150 °C, 10%	N/A	N/A	30 day,67%	132
Eu-BTC	$CsPbBr_3$	External coating	N/A	100 °C, 15%	N/A	N/A	N/A	133
ZIF-8	$MAPbBr_3$	One-pot	80%	140 °C, 70%	90 day, 75%	20 day, 90%	300 day	134
MOG	$EAPbBr_3$	One-pot	53%	N/A	12 h, 70%	300 h, 80%	120 day, 80%	147
ZJU-28	$CsPbX_3$	*In situ* growth	62%	160 °C, 10%	N/A	80 h, 85%	60 day, 84%	149
Ce-MOF@SiO_2	$CsPbX_3$	*In situ* growth	78%	140 °C, 10%	N/A	64 h, 65%	60 day, 76%	148
EB-COF:Br	$CsPbBr_3$/Cs_4PbBr_6	*In situ* growth	N/A	~200 °C	N/A	60 min	N/A	140
TAPT-DMTA COF	$MAPbBr_3$	*In situ* growth	N/A	N/A	7 day	N/A	60 day	141
COF–SH	$CsPbX_3$	*In situ* growth	82%	120 °C, 46%	7 day, 66%	96 h, 46%	N/A	144

that fully encapsulating the $CsPbBr_3$ nanocrystals into zeolite can effectively protect $CsPbBr_3$ nanocrystals against damage from heat, light irradiation, and oxygen. Zhou *et al.* utilized hierarchically porous MOFs (HP-UiO-66) as an encapsulation matrix for the confined growth of $CsPbX_3$ nanocrystals.[131] The $CsPbX_3$ nanocrystals were well dispersed in the hierarchical structure of HP-UiO-66, which protected them for harsh environments. The obtained $CsPbX_3$@HP-UiO-66 nanocomposites showed bright luminescence and greatly improved stability. The $CsPbX_3$@HP-UiO-66 nanocomposites could retain 24% of the PL intensity when heated from 25 to 100 °C (Fig. 15b), 85% of the PL intensity after 2 h of continuous illumination, and around 60% when stored in air for 15 days. These results prove that the MOF matrix can serve as a matrix to protect $CsPbX_3$ from various degradation factors. Recently, our group also reported a two-step encapsulation strategy for $CsPbX_3$ nanocrystals, including an *in situ* growth process and a silane hydrolysis–encapsulation process.[148] The $CsPbX_3$ nanocrystals were dispersed in the well-ordered mesopores of Ce-MOFs, and further coated with a thin SiO_2 shell to seal the open pores. The $CsPbBr_3$@Ce-MOF@SiO_2 composites exhibited greatly improved stability, which preserved 10% of its original PL intensity at 140 °C (Fig. 15c), 65% PL intensity under UV light illumination after 64 h, and 76% PL intensity after being stored for 60 days. The Ce-MOF@SiO_2 protecting shells effectively isolate the MHP nanocrystals, and protect them from the ambient atmosphere.

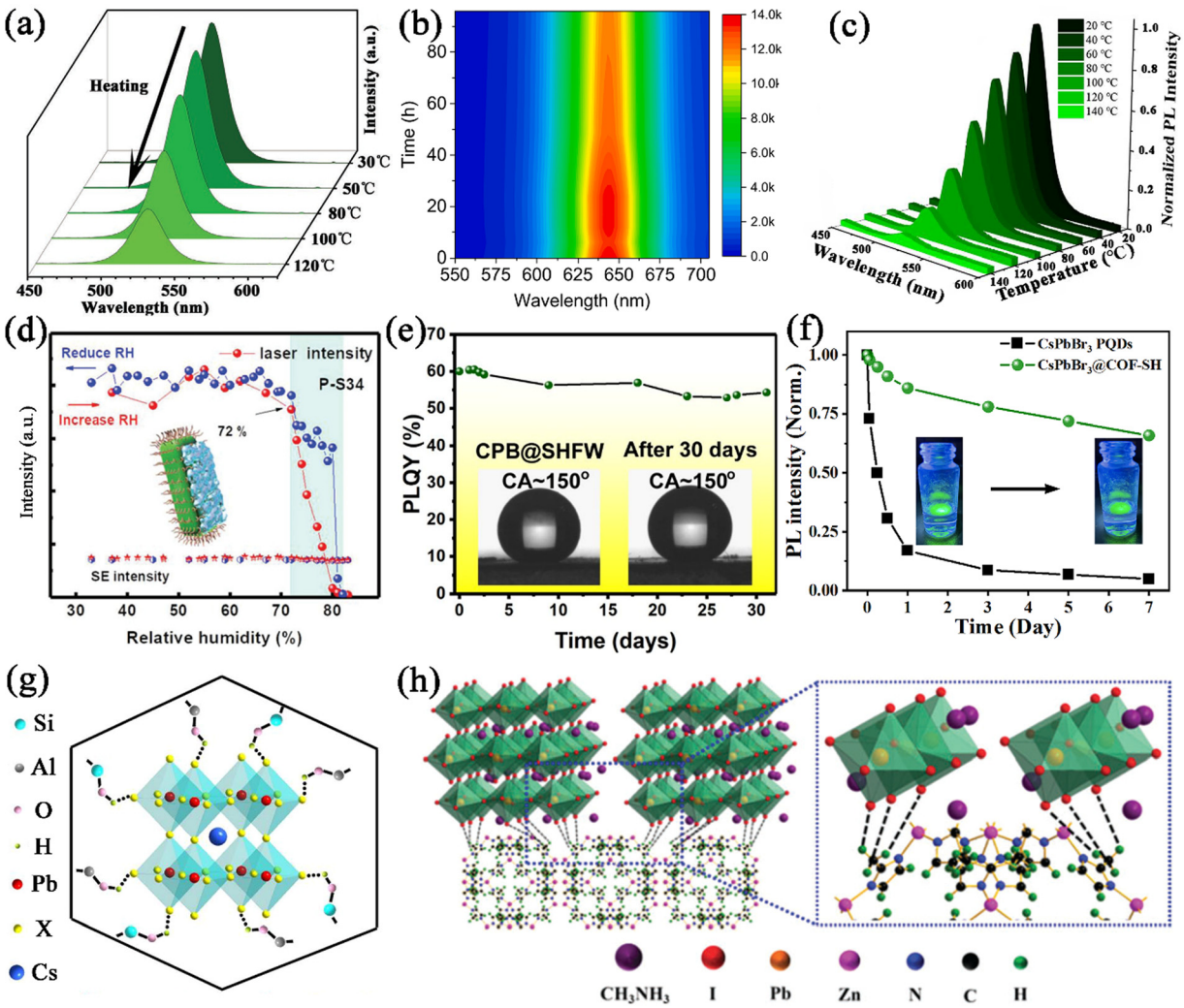

Fig. 15 (a) Temperature-dependent PL spectra for $CsPbBr_3$@zeolite. Adapted from ref. 113 with permission. Copyright 2021, Wiley-VCH. (b) Color-coded contour maps showing the time-dependent emission spectra of $CsPbI_3$@HP-UiO-66. Adapted from ref. 131 with permission. Copyright 2021, Elsevier. (c) Temperature-dependent PL spectra of $CsPbBr_3$@Ce-MOF@SiO_2 composites. Reproduced from ref. 148 with permission. Copyright 2022, Elsevier. (d) Lasing and spontaneous emission of $CsPbBr_3$@SAPO-34 as a function of relative humidity. Adapted from ref. 111 with permission. Copyright 2020, Royal Society of Chemistry. (e) Time-dependent PLQY of $CsPbBr_3$@SHFW composite powders in water. Adapted from ref. 150 with permission. Copyright 2019, American Chemical Society. (f) Time-dependent normalized PL intensity of $CsPbBr_3$ and $CsPbBr_3$@COF–SH in water. Adapted from ref. 144 with permission. Copyright 2023, Elsevier. (g) Schematic illustration of $CsPbX_3$ restricted in zeolite, showing H-bonding interactions between zeolite and $CsPbX_3$. Reproduced from ref. 113 with permission. Copyright 2021, Wiley-VCH. (h) Schematic illustration of the interaction between $MAPbI_3$ and ZIF-8. Adapted from ref. 151 with permission. Copyright 2018, Royal Society of Chemistry.

Thermal conductivity and hydrophobicity. The porous nature of the PFMs could result in a lower thermal conductivity, which could prevent the heat propagation from an external heat source to the embedded MHP nanocrystals. The lower thermal conductivity of the encapsulation matrix could reduce the temperature of the embedded MHP nanocrystals and significantly improve the thermal stability of MHP@PFM composites. Ye *et al.* reported the encapsulation of $CsPbCl_3$:Mn^{2+} MHP nanocrystals in zeolite-Y with low thermal conductivity, which could significantly improve the thermal quenching resistance of $CsPbCl_3$:Mn^{2+}@zeolite-Y composites.[107]

In addition, some certain PFMs possess special properties such as hydrophobicity, and could mitigate the diffusion of water into the framework, thereby enhancing the moisture stability of MHP@PFM composites. A series of hydrophobic PFMs were utilized to encapsulate MHP nanocrystals, which could enable the application of composites under humid conditions. For instance, hydrophobic zeolite SAPO-34 was reported to protect the $CsPbBr_3$ nanocrystals from humidity.[111] It should be noted that the emission from $CsPbBr_3$@SAPO-34 composites remained the same even when the relative humidity was increased from 30% to 72% (Fig. 15d). The strong moisture resistance of $CsPbBr_3$@SAPO-34 composites is ascribed to the hydrophobic surface of SAPO-34, which prevents the influence of water molecules. Similarly, Chen *et al.* employed ZIFs to coat the surface of $CsPbBr_3$ nanocrystals, generating $CsPbBr_3$@ZIF composites with greatly improved moisture stability.[146] The hydrophobic organic linker of ZIFs enables $CsPbBr_3$@ZIF composites to exhibit significantly improved moisture stability up to 10 days. Wang *et al.* reported the embedding of water-sensitive $CsPbBr_3$ nanocrystals in the super-hydrophobic porous organic polymer frameworks (SHFW).[150] The super hydrophobic structure of SHFW prevents water from coming in contact with $CsPbBr_3$ nanocrystals, avoiding the moisture-induced degradation (Fig. 15e). And the super-hydrophobic CPB@SHFW composites present good water-resistant properties even after being immersed in water for 6 months. Recently, our group also reported the encapsulation of $CsPbX_3$ nanocrystals in hydrophobic COF–SH.[144] The hydrophobic vinyl surface groups and the rough surface structure endowed COF–SH with hydrophobicity properties. Due to the hydrophobicity properties of COF–SH, the $CsPbBr_3$@COF–SH composites could maintain about 66% of their original PL intensity even after being immersed in water for 7 days (Fig. 15f). The hydrophobic surface of COF–SH prevents water intrusion, which endows it with excellent water stability.

Strong bonding effect. In the porous framework material encapsulation strategy, the MHP nanocrystals are confined in the pore structure of PFMs, where there are a large number of dangling functional groups. The functional groups of PFMs could bond with MHP nanocrystals, anchoring MHP nanocrystals tightly in the pore structure of PFMs. The strong bonding could isolate MHP nanocrystals and prevent the aggregation-induced degradation. For instance, the functional groups (Si–OH and Al–OH) in zeolite frameworks could form complex hydrogen bonds with the halide anion of $CsPbX_3$ nanocrystals.[113] The hydrogen bond interaction not only passivates the surface of $CsPbX_3$ nanocrystals, but also enables the strong connection between $CsPbX_3$ nanocrystals and zeolite (Fig. 15g). Similarly, the methyl groups in the crystal structure of ZIF-8 could form hydrogen bonds with the halide anions of the $MAPbI_3$ nanocrystals (Fig. 15h).[151] This hydrogen bond enhances the connection between $MAPbI_3$ nanocrystals and ZIF-8 matrix, which leads to the confined growth and improved stability of $MAPbI_3$ nanocrystals in the ZIF-8 matrix. Xia *et al.* also reported a strong connection between $MAPbBr_3$ nanocrystals and Eu-BTC matrix, where Pb^{2+} ions of $MAPbBr_3$ nanocrystals tend to bond with Eu-BTC.[152] The strong connection could provide active sites for the growth of $MAPbBr_3$ nanocrystals in Eu-BTC matrix. And recently, strong chemical bonding between the Pb^{2+} ions of $CsPbBr_3$ nanocrystals and the thiol groups (–SH) of COF–SH has also been reported in the $CsPbBr_3$@COF–SH composites.[144] The strong S–Pb bonding in $CsPbBr_3$@COF–SH composites anchors $CsPbBr_3$ nanocrystals tightly in the channels of COF–SH. Ascribed to the strong chemical bonding between $CsPbBr_3$ and COF–SH and the physical barrier effect of COF–SH, the $CsPbBr_3$@COF–SH composite exhibits comprehensive stability improvements.

4.3.2. Regulations on optical performance. In addition to the stability enhancement of the MHP@PFMs, some certain PFMs also possess special features (such as a unique pore structure, photoluminescence, circularly polarized luminescence, *etc.*), which could provide MHP@PFMs with additional photophysical properties.

Since MHP nanocrystals are confined in the pore structure of the PFMs in MHP@PFM composites, the pore structure of PFMs plays a vital role in regulating the PL properties of MHP@PFM composites. According to the quantum confinement effects, the emission peak could be tuned by adjusting the size of the embedded MHP nanocrystals. Chen *et al.* reported the obvious quantum confinement effect in $MAPbBr_3$@UiO-66 composites, where the confined $MAPbBr_3$ nanocrystals have tunable sizes.[130] The emission peaks of $MAPbBr_3$@UiO-66 composites blue-shifted from 521 nm to 486 nm, with the size of confined $MAPbBr_3$ nanocrystals being reduced from 6.4 to 3.3 nm (Fig. 16a). Some PFMs possess unique pore structures, which could also play a role in regulating the PL properties of the encapsulated nanocrystals.[153,154] The ordered pore structure of PFMs shows a unique waveguide effect, and shows great potential in reducing the reabsorption of MHP nanocrystals. In our previous studies, we revealed an internal waveguide effect in $CsPbX_3$@Ce-MOF@SiO_2 composites.[148] The ordered pore structure of Ce-MOFs shows an internal waveguide effect, which could interfere with the propagation of $CsPbX_3$ emission (Fig. 16b). Through this waveguide effect, the self-reabsorption losses of the $CsPbX_3$ emission could be reduced, thus increasing the light extraction efficiency. Similarly, the ordered pore structure of COF–SH also shows a strong waveguide effect on the embedded MHP nanocrystals and prevents the self-reabsorption losses.[144]

Additionally, some PFMs possess PL properties, and also show great potential in encapsulating MHP nanocrystals. The luminescent PFMs not only improve the stability of MHP

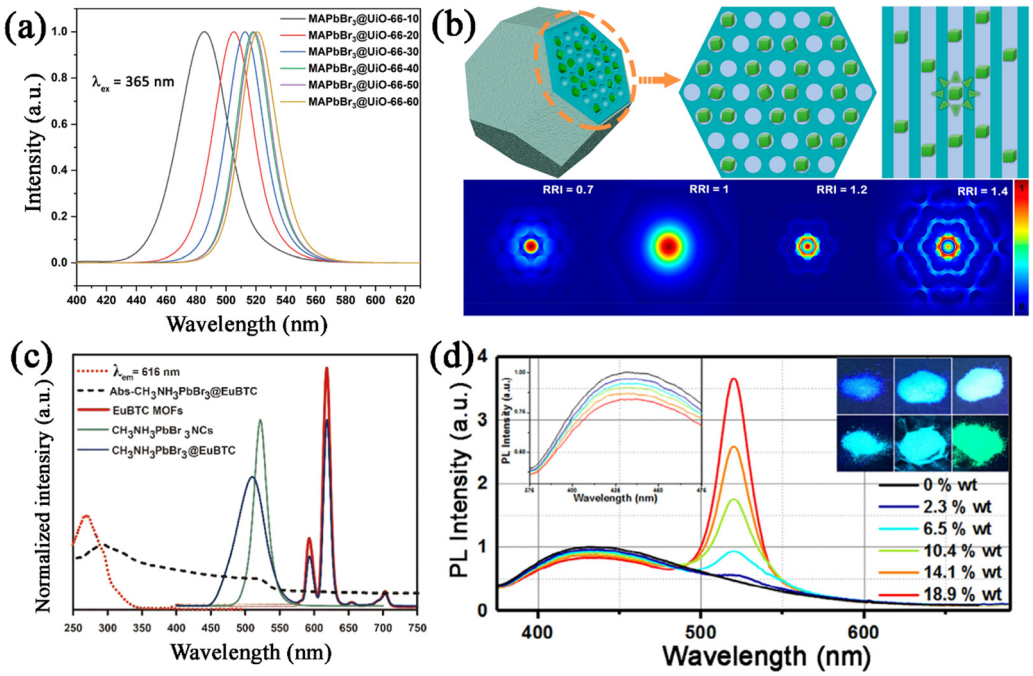

Fig. 16 (a) PL spectra of $MAPbBr_3$@UiO-66 composites with different sizes of confined $MAPbBr_3$ nanocrystals. Adapted from ref. 130 with permission. Copyright 2020, Royal Society of Chemistry. (b) Schematic illustration of the models of $CsPbBr_3$@Ce-MOF@SiO_2 in the FDTD simulation, and the simulated electric fields with different relative refractive index (RRI) values. Reproduced from ref. 148 with permission. Copyright 2022, American Chemical Society. (c) Absorption spectrum of the $MAPbBr_3$@EuBTC composite and the normalized PL spectra of EuBTC, $MAPbBr_3$, and $MAPbBr_3$@EuBTC. Adapted from ref. 152 with permission. Copyright 2018, American Chemical Society. (d) PL spectra of $CsPbBr_3$@ZJU-28 with different $CsPbBr_3$ contents. Adapted from ref. 149 with permission. Copyright 2020, Elsevier.

nanocrystals as an encapsulation matrix, but also provide extra emission for MHP@PFMs composites with more application potential. Taking luminescent MOFs as an example, the PL properties could originate from a variety of sources, such as ligand-based emission (conjugated organic ligands), metal-based emission (lanthanoid ions), and ligand-to-metal charge transfer (LMCT) and metal-to-ligand charge transfer (MLCT).[155] The PL properties of MHP@PFM could be greatly enhanced by employing luminescent PFMs as an encapsulation matrix. For instance, Xia *et al.* reported the encapsulation of $MAPbBr_3$ nanocrystals in europium-based luminescent MOFs (Eu-MOFs).[152] The $MAPbBr_3$@Eu-MOF possess dual-emission under UV excitation, with the green emission ascribed to the band-edge emission of $MAPbBr_3$ and the red emission attributed to the inherent Eu-MOFs emission (Fig. 16c). Benefiting from the unique dual-emission property, the $MAPbBr_3$@Eu-MOF composites exhibit excitation-wavelength-dependent and temperature-dependent color transformation. Blue-emission ZJU-28 MOFs were also utilized as a functional matrix to encapsulate MHP nanocrystals.[136,137,149] In our previous studies, we also reported the *in situ* growth of $CsPbX_3$ nanocrystals in blue-emitting ZJU-28 matrix, generating dual-emission $CsPbX_3$@ZJU-28 composites.[149] The broad blue emission could be attributed to the coordination-induced strong π–π* transition of ZJU-28, and the distinctive narrow emission could be attributed to $CsPbX_3$ nanocrystals. And the emission spectra of $CsPbX_3$@ZJU-28 could be easily tailored by changing the concentrations of $CsPbX_3$ or controlling the halide composition of $CsPbX_3$ (Fig. 16d). Furthermore, Dong and Zang *et al.* reported the *in situ* growth of $MAPbX_3$ nanocrystals in chiral MOFs ((P)-(+)/(M)-(−)-EuMOF), generating a pair of crystalline enantiomeric $MAPbX_3$@(P)-(+)/(M)-(−)-EuMOFs.[156] The emitted colors of the composites can be tuned by changing the halogen ions in the embedded MHP nanocrystals, and the handedness of the induced circularly polarized luminescence signals could be regulated by the chirality of the chiral MOFs.

5. Applications of MHP@PFM composites

Generally, composites can not only inherit advantages from each component, but also bring some new properties. Ascribed to the comprehensive advantages of MHP nanocrystals and PFMs, the formed MHP@PFM composites have emerged as a unique class of optoelectronic materials owing to their excellent optical properties and improved stability. This section provides an update on the potential applications of MHP@PFMs, including light emitting diodes, sensing and detection, information security, *etc.*

5.1. Light emitting diodes

Considering the outstanding PL properties and enhanced stability, the MHP@PFM composites were mainly utilized for LED applications. On the one hand, the luminescent MHP@PFM composites can be applied as a light converting layer for phosphor converted LEDs (pc-LEDs). On the other hand, the

luminescent MHP@PFM composites can be employed as an emission layer to accept electrons/holes injected from the electrodes for electroluminescent (EL) devices.

A typical pc-LED is generally composed of a high energy (UV or blue) LED coated with luminescent materials, where the high energy excitation light can be absorbed and down-converted to emit visible light. Generally, the MHP@PFM composites possessing high PLQYs, spectral tunability, and improved stability, are well suited for color conversion in pc-LEDs. Xiang *et al.* utilized highly luminescent and stable $CsPbX_3$@zeolite composites as color converters for constructing white LEDs.[113] The fabricated W-LEDs show white light coordinates of (0.3258, 0.3101) and a color temperature of 5837 K at a drive current of 20 mA (Fig. 17a). Attributed to the ultrapure color emission of $CsPbX_3$@zeolite, the color gamut of the fabricated WLEDs covers almost 134.2% of the NTSC standard, which is much higher than that of the previously reported quantum dot-based LEDs. The fabricated W-LEDs show no significant variation at a driving current of 40 mA for 48 h, demonstrating the long-term working stability of the W-LEDs. Recently, we also reported the application of $CsPbX_3$@Ce-MOF@SiO_2 in LEDs, where the $CsPbX_3$@Ce-MOF@SiO_2 composites were deposited on InGaN blue LED chips as a down-conversion layer.[148] The constructed W-LEDs emit warm white light with color coordinates of (0.42, 0.37), a color temperature of 2924 K, a high luminous efficiency of 87.8 l m W^{-1}, a color-rendering index of 84, and a color gamut of 125% NTSC, illustrating the excellent luminous performance of the constructed W-LED (Fig. 17b). The constructed W-LEDs also show no obvious variation after several hours of continuous operation. A series of MHP@PFM based pc-LEDs are summarized and shown in Table 2, demonstrating the great promise of the MHP@PFM composites in LED applications.

Typically, electroluminescent LEDs consist of electrodes, an electron transport layer, an emission layer and a hole transport layer. MHP@PFM composites could also work as an emission layer to accept the electrons/holes injected in electroluminescent LEDs. The injected electrons and holes are recombined in the MHP@PFM layer, leading to electroluminescence. Tsai and Nie *et al.* employed $MAPbBr_3$@Pb–MOFs as an emission layer for electroluminescent LED devices (Fig. 17c).[157] The fabricated LEDs emitted strong electroluminescence with high brightness of over 10^5 cd m^{-2} and maximum external quantum efficiency of 15% (Fig. 17d). The long-term operation stability of the $MAPbBr_3$@Pb–MOF based LED device is greatly enhanced, leading to a stable performance over 50 hours. Furthermore, they introduced $CsPbX_3$ nanocrystals into Pb–MOFs as an emission layer for stable blue LEDs.[158] By tuning the halide composition, deep blue and sky blue $CsPbX_3$@Pb–MOF LEDs are fabricated with external quantum efficiencies of 5.6% and 0.7% respectively. The EL intensity and spectral stability of $CsPbX_3$@Pb–MOF LEDs are improved using the MOF protected MHP nanocrystal layers.

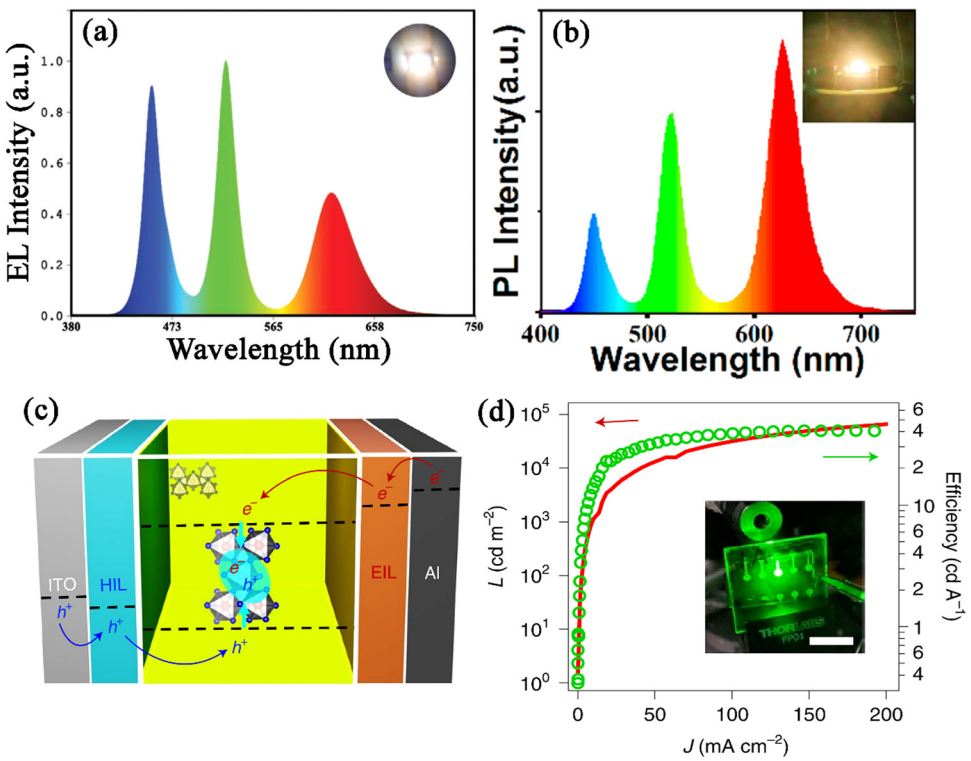

Fig. 17 (a) EL spectrum for the constructed $CsPbX_3$@zeolite white LED device. Reproduced from ref. 113 with permission. Copyright 2021, Wiley-VCH. (b) Emission spectrum and the corresponding photograph of the $CsPbX_3$@Ce-MOF@SiO_2 white LED device. Adapted from ref. 148 with permission. Copyright 2022, Elsevier. (c) Schematic illustration of the structure and (d) luminance and current efficiency as a function of the current density for a $MAPbBr_3$@Pb–MOF-based LED device. (c and d) Reproduced from ref. 157 with permission. Copyright 2021, Springer Nature.

Table 2 Summary of the MHP@PFMs based pc-LEDs

Color converters	Color coordinate	Color temperature (K)	Ra	Gamut (NTSC)	Luminous efficiency	Ref.
$CsPbX_3$@Zeolite-Y	(0.38, 0.37)	3876	N/A	114%	3.5 l m W^{-1}	106
$CsPbX_3$:Mn^{2+}@Zeolite Y	(0.34, 0.36)	5336	81	N/A	N/A	107
$CsPbX_3$@Zeolite-Y	(0.31, 0.31)	6824	60	N/A	20 l m W^{-1}	108
$CsPbBr_3$@Zeolite Beta + KSF	(0.288, 0.323)	8109	N/A	123.5%	95 l m W^{-1}	110
$CsPbX_3$@Zeolite	(0.3258, 0.3101)	5837	N/A	134.2%	N/A	113
$CsPbBrI_2$@zeolite/PMMA + YAG: Ce	(0.3359, 0.3455)	5354	94.5	N/A	77.2 l m W^{-1}	114
$CsPbX_3$@Meso-MOF-5	(0.375, 0.321)	3607	83	124%	21.6 l m W^{-1}	129
$CsPbX_3$@HP-UiO-66	(0.36, 0.32)	4184	N/A	125%	21 l m W^{-1}	131
$CsPbX_3$@UiO-67 + KSF	(0.3690, 0.3437)	4082	N/A	138%	N/A	132
$MAPbX_3$@MOG	(0.34, 0.32)	5245	N/A	144%	N/A	147
$CsPbX_3$@Ce-MOF@SiO_2	(0.42, 0.37)	2924	84	125%	87.8 l m W^{-1}	148
$CsPbX_3$@ZJU-28	(0.3812, 0.3527)	3748	84.2	N/A	N/A	149
$CsPbX_3$@COF–SH	(0.392, 0.318)	2989	84	128%	89.6 l m W^{-1}	144

5.2. Sensing and detection

Luminescent MHP@PFM composites are considered as reliable and promising candidates for sensing applications due to their advantages of high sensitivity and rapid responsivity. Due to the fast response of luminescence properties and reversible phase transitions of MHP@PFM composites under temperature/moisture change, the MHP@PFM composites have been employed as promising candidates for temperature/moisture sensing applications. Xu *et al.* designed a novel temperature-dependent dual-emissive $CsPbBr_3$@EuBTC composite, which served as a ratiometric thermometer for temperature sensing applications.[133] The thermo-response luminescence intensity ratio between $CsPbBr_3$ nanocrystals and Eu-MOFs is an exponential function with temperature in the range of 20–100 °C (Fig. 18a). And the $CsPbBr_3$@EuBTC composites exhibited a high relative sensitivity of 3.9% $°C^{-1}$ at 20 °C and excellent

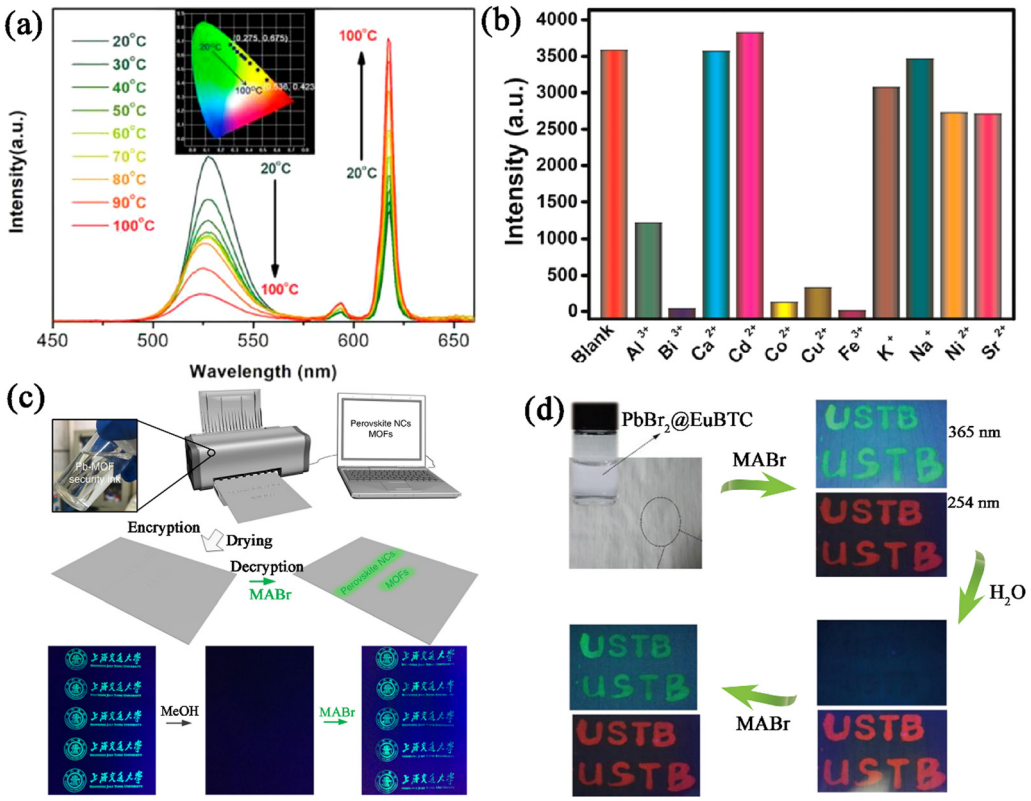

Fig. 18 (a) Temperature-dependent PL spectra of $CsPbBr_3$@EuBTC in the temperature range of 20–100 °C. Adapted from ref. 133 with permission. Copyright 2019, American Chemical Society. (b) Comparison of selectivity toward different metal ions for $MAPbBr_3$@MOF-5 composites in aqueous solutions. Adapted from ref. 127 with permission. Copyright 2018, American Chemical Society. (c) Schematic illustrations of the patterning, information encryption, and decryption process of the $MAPbBr_3$@Pb–MOF platform and reversible fluorescence switching of the $MAPbBr_3$@Pb–MOF pattern in one encryption–decryption cycle. Reproduced from ref. 128 with permission. Copyright 2017, Springer Nature. (d) Reversible fluorescence switching of the $MAPbBr_3$@EuBTC at different stages and different excitation wavelengths of 254 nm and 365 nm. Reproduced from ref. 152 with permission. Copyright 2018, American Chemical Society.

cyclic sensing stability, indicating their superiority as self-calibrating temperature sensors. Furthermore, we also reported the application of dual-emitting $CsPbX_3$@ZJU-28 composites as promising thermometers for monitoring temperature changes due to their temperature sensitivity and resolution.[149] In addition to the application in temperature sensing, the MHP@PFM composites also show promising application in humidity sensing. Li *et al.* utilized $CsPbBr_3$@SAPO-34 zeolite composites as sensitive laser humidity sensors, which exhibit high sensitivity and good reliability.[111] The lasing intensity of $CsPbBr_3$@SAPO-34 composites demonstrated high humidity sensitivity and reversible characteristics, indicating their good reliability as humidity sensors.

Besides, the luminescent MHP@PFM composites have also been utilized as fluorescent probes for metal ion detection. Xia *et al.* developed $MAPbBr_3$@MOF-5 composites with excellent tolerance for a wide range of pH values and significant selective luminescence response to several different metal ions in aqueous solution, making them attractive as aqueous heavy metal ion detectors.[127] Particularly, Al^{3+}, Cu^{2+}, Co^{2+}, Bi^{3+}, and Fe^{3+} metal ions exhibited a significant quenching effect on the fluorescence intensity of $MAPbBr_3$@MOF-5 composites, while Cd^{2+} metal ions enhanced the fluorescence intensity (Fig. 18b). And the PL intensities of $MAPbBr_3$@MOF-5 composites varied linearly with the concentration of metal ions, demonstrating their promising application in detecting metal ions in aqueous solutions.

5.3. Information security

Encryption and anti-counterfeiting technology play an important role in the field of information security. Benefiting from the stimuli-response photoluminescence properties of MHP nanocrystals and the encapsulation effects of PFM matrix, the MHP@PFM composites have advantages in information security applications, where the emission can be switched through reversible decomposition–generation or phase transition of MHP nanocrystals.

Li *et al.* employed $MAPbBr_3$@Pb–MOF composites to realize the information encryption and decryption with various inkjet-printed patterns.[128] The encrypted information can be decrypted from the luminescence of the generated $MAPbBr_3$ nanocrystals through MABr processing, and further encrypted through polar solvent treatment. The MABr processing and polar solvent treatment allow the luminescence on/off switch for multiple information encryption and decryption processes (Fig. 18c). Similarly, Xia and co-workers also reported the application of dual-emissive $MAPbBr_3$@Eu-BTC composites in anti-counterfeiting.[152] The $MAPbBr_3$@Eu-BTC composites possessed dual-emission, with the green emission attributed to $MAPbBr_3$ nanocrystals and the red emission ascribed to Eu-BTC. The green emission of $MAPbBr_3$@Eu-BTC composites (under an excitation of 365 nm UV light) was quenched by water immersion and recovered with the addition of MABr solution. In contrast, the red luminescence of $MAPbBr_3$@Eu-BTC composites (under the excitation of 254 nm UV light) remained the same even after water immersion (Fig. 18d). These switchable dual-emission properties of the $MAPbBr_3$@Eu-BTC composites demonstrated their great potential for anti-counterfeiting application.

6. Conclusion and perspective

MHP nanocrystals possess outstanding optical and electronic properties, and yet their potential applications are seriously hindered by the poor stability. Due to the low formation energy, intrinsic ion crystal properties, and mobile surface ligands, MHP nanocrystals are severely affected by moisture, heat, oxygen, UV illumination, *etc.* In light of the impressive achievements of MHP nanocrystals, the stability of MHP nanocrystals becomes an urgent issue which needs to be addressed. This review offers an all-inclusive summary of fundamental structural properties, photophysical properties, and stability problems of MHP nanocrystals, followed by three main routes to stabilize MHP nanocrystals: (a) compositional engineering, (b) surface modulation, and (c) matrix encapsulation. Among the various matrixes for encapsulating MHP nanocrystals, the porous framework materials (PFMs) possess the merits of high porosity, environmental stability, extensive functionality, and design flexibility, and are highly effective in improving the stability of MHP nanocrystals with additional functions. The MHP@PFM composites could be fabricated through *in situ* growth, external coating, one-pot, and physical mixing strategies. Ascribed to the physical barrier effect, low thermal conductivity and hydrophobicity, and strong bonding effects of PFMs, the formed MHP@PFM composites exhibit enhanced stability. In addition, the MHP@PFM composites could also exhibit new features and application possibilities due to the extensive functionality of PFMs. Overall, MHP@PFM composites are emerging perovskite materials that combine the excellent photophysical properties of MHP nanocrystals and the multifunctional properties of PFMs. Finally, we overviewed the main application of MHP@PFM composites in optoelectronic devices, especially in light emitting diodes.

Over the past few years, great efforts have been devoted in understanding the degradation mechanism and enhancing the stability of MHP nanocrystals. Although rapid progress has been made in recent years, the following research directions still need to be resolved:

(a) The toxicity of heavy metals (such as Pb) in MHP@PFM composites restricts their practical application. Therefore, seeking an appropriate element to replace Pb and developing lead-free and eco-friendly materials will be the focus of future research.

(b) The PL properties of MHP nanocrystals will be influenced more or less when growing in a PFM matrix, which could be related to the poor nucleation environment or insufficient surface passivation. Hence, more efforts should be devoted to realize the growth of MHP nanocrystals in PFM matrix while preserving the excellent PL performance in future research works.

(c) So far, the MHP@PFMs are still in their infancy of research field. More efforts are required to integrate these promising composites in optoelectronic devices to take advantage of their intriguing properties.

We hope that this review will provide reference to readers for understanding and developing perovskite-based composites for multifunctional applications in the future.

Conflicts of interest

There are no conflicts to declare.

Acknowledgements

The authors gratefully acknowledge the financial support from the National Natural Science Foundation of China (no. U1905213).

References

1 J. Hou, Z. Wang, P. Chen, V. Chen, A. K. Cheetham and L. Wang, Intermarriage of Halide Perovskites and Metal–Organic Framework Crystals, *Angew. Chem., Int. Ed.*, 2020, **59**(44), 19434–19449.

2 L. C. Schmidt, A. Pertegas, S. Gonzalez-Carrero, O. Malinkiewicz, S. Agouram, G. Minguez Espallargas, H. J. Bolink, R. E. Galian and J. Perez-Prieto, Nontemplate synthesis of $CH_3NH_3PbBr_3$ perovskite nanoparticles, *J. Am. Chem. Soc.*, 2014, **136**(3), 850–853.

3 L. Protesescu, S. Yakunin, M. I. Bodnarchuk, F. Krieg, R. Caputo, C. H. Hendon, R. X. Yang, A. Walsh and M. V. Kovalenko, Nanocrystals of Cesium Lead Halide Perovskites (CsPbX(3), X = Cl, Br, and I): Novel Optoelectronic Materials Showing Bright Emission with Wide Color Gamut, *Nano Lett.*, 2015, **15**(6), 3692–3696.

4 Y. Wei, Z. Cheng and J. Lin, An overview on enhancing the stability of lead halide perovskite quantum dots and their applications in phosphor-converted LEDs, *Chem. Soc. Rev.*, 2019, **48**(1), 310–350.

5 X. Mei, D. Jia, J. Chen, S. Zheng and X. Zhang, Approaching high-performance light-emitting devices upon perovskite quantum dots: advances and prospects, *Nano Today*, 2022, **43**, 101449.

6 Y. Liu, F. Li, L. Qiu, K. Yang, Q. Li, X. Zheng, H. Hu, T. Guo, C. Wu and T. W. Kim, Fluorescent Microarrays of in Situ Crystallized Perovskite Nanocomposites Fabricated for Patterned Applications by Using Inkjet Printing, *ACS Nano*, 2019, **13**(2), 2042–2049.

7 T. Xuan, S. Shi, L. Wang, H. C. Kuo and R. J. Xie, Inkjet-Printed Quantum Dot Color Conversion Films for High-Resolution and Full-Color Micro Light-Emitting Diode Displays, *J. Phys. Chem. Lett.*, 2020, **11**(13), 5184–5191.

8 H. C. Wang, S. Y. Lin, A. C. Tang, B. P. Singh, H. C. Tong, C. Y. Chen, Y. C. Lee, T. L. Tsai and R. S. Liu, Mesoporous Silica Particles Integrated with All-Inorganic $CsPbBr_3$ Perovskite Quantum-Dot Nanocomposites (MP-PQDs) with High Stability and Wide Color Gamut Used for Backlight Display, *Angew. Chem., Int. Ed.*, 2016, **55**(28), 7924–7929.

9 X. Ling, S. Zhou, J. Yuan, J. Shi, Y. Qian, B. W. Larson, Q. Zhao, C. Qin, F. Li, G. Shi, C. Stewart, J. Hu, X. Zhang, J. M. Luther, S. Duhm and W. Ma, 14.1% $CsPbI_3$ Perovskite Quantum Dot Solar Cells via Cesium Cation Passivation, *Adv. Energy Mater.*, 2019, **9**(28), 1900721.

10 S. Yuan, D. Chen, X. Li, J. Zhong and X. Xu, In Situ Crystallization Synthesis of $CsPbBr_3$ Perovskite Quantum Dot-Embedded Glasses with Improved Stability for Solid-State Lighting and Random Upconverted Lasing, *ACS Appl. Mater. Interfaces*, 2018, **10**(22), 18918–18926.

11 C. Bi, S. V. Kershaw, A. L. Rogach and J. Tian, Improved Stability and Photodetector Performance of CsPbI3 Perovskite Quantum Dots by Ligand Exchange with Aminoethanethiol, *Adv. Funct. Mater.*, 2019, **29**(29), 1902446.

12 X. Wang, Z. Bao, Y. Chang and R. Liu, Perovskite Quantum Dots for Application in High Color Gamut Backlighting Display of Light-Emitting Diodes, *ACS Energy Lett.*, 2020, **5**(11), 3374–3396.

13 W. Lv, L. Li, M. Xu, J. Hong, X. Tang, L. Xu, Y. Wu, R. Zhu, R. Chen and W. Huang, Improving the Stability of Metal Halide Perovskite Quantum Dots by Encapsulation, *Adv. Mater.*, 2019, **31**(28), 1900682.

14 G. Zhang, D. Wang, B. Lou, C. G. Ma, A. Meijerink and Y. Wang, Efficient Broadband Near-Infrared Emission from Lead-Free Halide Double Perovskite Single Crystal, *Angew. Chem., Int. Ed.*, 2022, **61**(33), 202207454.

15 Y. Zhou and Y. Zhao, Chemical stability and instability of inorganic halide perovskites, *Energy Environ. Sci.*, 2019, **12**(5), 1495–1511.

16 V. M. Goldschmidt, Die gesetze der krystallochemie, *Naturwissenschaften*, 1926, **14**(21), 477–485.

17 R. D. Shannon and C. T. Prewitt, Effective Ionic Radii in Oxides and Fluorides, *Acta Crystallogr., Sect. B: Struct. Crystallogr. Cryst. Chem.*, 1969, **25**(5), 925–946.

18 F. Bertolotti, L. Protesescu, M. V. Kovalenko, S. Yakunin, A. Cervellino, S. J. L. Billinge, M. W. Terban, J. S. Pedersen, N. Masciocchi and A. Guagliardi, Coherent Nanotwins and Dynamic Disorder in Cesium Lead Halide Perovskite Nanocrystals, *ACS Nano*, 2017, **11**(4), 3819–3831.

19 V. K. Ravi, G. B. Markad and A. Nag, Band Edge Energies and Excitonic Transition Probabilities of Colloidal $CsPbX_3$ (X = Cl, Br, I) Perovskite Nanocrystals, *ACS Energy Lett.*, 2016, **1**(4), 665–671.

20 K. T. Butler, J. M. Frost and A. Walsh, Band alignment of the hybrid halide perovskites $CH_3NH_3PbCl_3$, $CH_3NH_3PbBr_3$ and $CH_3NH_3PbI_3$, *Mater. Horiz.*, 2015, **2**(2), 228–231.

21 X. Li, Y. Wu, S. Zhang, B. Cai, Y. Gu, J. Song and H. Zeng, $CsPbX_3$ Quantum Dots for Lighting and Displays: Room-Temperature Synthesis, Photoluminescence Superiorities, Underlying Origins and White Light-Emitting Diodes, *Adv. Funct. Mater.*, 2016, **26**(15), 2435–2445.

22 Q. A. Akkerman, G. Raino, M. V. Kovalenko and L. Manna, Genesis, challenges and opportunities for colloidal lead halide perovskite nanocrystals, *Nat. Mater.*, 2018, **17**(5), 394–405.

23 J. Butkus, P. Vashishtha, K. Chen, J. K. Gallaher, S. K. K. Prasad, D. Z. Metin, G. Laufersky, N. Gaston, J. E. Halpert and J. M. Hodgkiss, The Evolution of Quantum Confinement in $CsPbBr_3$ Perovskite Nanocrystals, *Chem. Mater.*, 2017, **29**(8), 3644–3652.

24 H. Liu, Z. Liu, W. Xu, L. Yang, Y. Liu, D. Yao, D. Zhang, H. Zhang and B. Yang, Engineering the Photoluminescence of CsPbX(3) (X = Cl, Br, and I) Perovskite

Nanocrystals Across the Full Visible Spectra with the Interval of 1 nm, *ACS Appl. Mater. Interfaces*, 2019, **11**(15), 14256–14265.

25 J. He, W. H. Fang and R. Long, Unravelling the Effects of A-Site Cations on Nonradiative Electron–Hole Recombination in Lead Bromide Perovskites: Time-Domain ab Initio Analysis, *J. Phys. Chem. Lett.*, 2018, **9**(17), 4834–4840.

26 Y. Wang, J. Ding, Y. Wang, X. Zhou, Y. Cao, B. Ma, J. Li, X. Wang, T. Seto and Z. Zhao, Structural design of new Ce^{3+}/Eu^{2+}-doped or co-doped phosphors with excellent thermal stabilities for WLEDs, *J. Mater. Chem. C*, 2019, **7**(7), 1792–1820.

27 Y. Zhao, C. Riemersma, F. Pietra, R. Koole, C. D. M. Donega and A. Meijerink, High-Temperature Luminescence Quenching of Colloidal Quantum Dots, *ACS Nano*, 2012, **6**(10), 9058–9067.

28 S. Wei, Y. Yang, X. Kang, L. Wang, L. Huang and D. Pan, Room-temperature and gram-scale synthesis of $CsPbX_3$ (X = Cl, Br, I) perovskite nanocrystals with 50–85% photoluminescence quantum yields, *Chem. Commun.*, 2016, **52**(45), 7265–7268.

29 L. Meng, E. P. Yao, Z. Hong, H. Chen, P. Sun, Z. Yang, G. Li and Y. Yang, Pure Formamidinium-Based Perovskite Light-Emitting Diodes with High Efficiency and Low Driving Voltage, *Adv. Mater.*, 2017, **29**(4), 1603826.

30 L. Protesescu, S. Yakunin, S. Kumar, J. Bar, F. Bertolotti, N. Masciocchi, A. Guagliardi, M. Grotevent, I. Shorubalko, M. I. Bodnarchuk, C. J. Shih and M. V. Kovalenko, Dismantling the ''Red Wall'' of Colloidal Perovskites: Highly Luminescent Formamidinium and Formamidinium-Cesium Lead Iodide Nanocrystals, *ACS Nano*, 2017, **11**(3), 3119–3134.

31 C. Wang, Y. Zhang, A. Wang, Q. Wang, H. Tang, W. Shen, Z. Li and Z. Deng, Controlled Synthesis of Composition Tunable Formamidinium Cesium Double Cation Lead Halide Perovskite Nanowires and Nanosheets with Improved Stability, *Chem. Mater.*, 2017, **29**(5), 2157–2166.

32 F. Li, S. Huang, X. Liu, Z. Bai, Z. Wang, H. Xie, X. Bai and H. Zhong, Highly Stable and Spectrally Tunable Gamma Phase RbxCs1–xPbI3 Gradient-Alloyed Quantum Dots in PMMA Matrix through A Sites Engineering, *Adv. Funct. Mater.*, 2021, **31**(11), 100019.

33 T. C. Jellicoe, J. M. Richter, H. F. Glass, M. Tabachnyk, R. Brady, S. E. Dutton, A. Rao, R. H. Friend, D. Credgington, N. C. Greenham and M. L. Bohm, Synthesis and Optical Properties of Lead-Free Cesium Tin Halide Perovskite Nanocrystals, *J. Am. Chem. Soc.*, 2016, **138**(9), 2941–2944.

34 D. Yan, Q. Mo, S. Zhao, W. Cai and Z. Zang, Room temperature synthesis of Sn^{2+} doped highly luminescent $CsPbBr_3$ quantum dots for high CRI white light-emitting diodes, *Nanoscale*, 2021, **13**(21), 9740–9746.

35 D. Parobek, B. J. Roman, Y. Dong, H. Jin, E. Lee, M. Sheldon and D. H. Son, Exciton-to-Dopant Energy Transfer in Mn-Doped Cesium Lead Halide Perovskite Nanocrystals, *Nano Lett.*, 2016, **16**(12), 7376–7380.

36 S. Zou, Y. Liu, J. Li, C. Liu, R. Feng, F. Jiang, Y. Li, J. Song, H. Zeng, M. Hong and X. Chen, Stabilizing Cesium Lead Halide Perovskite Lattice through Mn(II) Substitution for Air-Stable Light-Emitting Diodes, *J. Am. Chem. Soc.*, 2017, **139**(33), 11443–11450.

37 J. Zhu, X. Yang, Y. Zhu, Y. Wang, J. Cai, J. Shen, L. Sun and C. Li, Room-Temperature Synthesis of Mn-Doped Cesium Lead Halide Quantum Dots with High Mn Substitution Ratio, *J. Phys. Chem. Lett.*, 2017, **8**(17), 4167–4171.

38 W. J. Mir, Y. Mahor, A. Lohar, M. Jagadeeswararao, S. Das, S. Mahamuni and A. Nag, Postsynthesis Doping of Mn and Yb into $CsPbX_3$ (X = Cl, Br, or I) Perovskite Nanocrystals for Downconversion Emission, *Chem. Mater.*, 2018, **30**(22), 8170–8178.

39 L. Wu, Y. Wang, M. Kurashvili, A. Dey, M. Cao, M. Doblinger, Q. Zhang, J. Feldmann, H. Huang and T. Debnath, Interfacial Manganese-Doping in $CsPbBr_3$ Nanoplatelets by Employing a Molecular Shuttle, *Angew. Chem., Int. Ed.*, 2022, **61**(15), 202115852.

40 M. C. De Siena, D. E. Sommer, S. E. Creutz, S. T. Dunham and D. R. Gamelin, Spinodal Decomposition During Anion Exchange in Colloidal Mn^{2+}-Doped $CsPbX_3$ (X = Cl, Br) Perovskite Nanocrystals, *Chem. Mater.*, 2019, **31**(18), 7711–7722.

41 J. Ren, X. Zhou and Y. Wang, Water triggered interfacial synthesis of highly luminescent $CsPbX_3$:Mn^{2+} quantum dots from nonluminescent quantum dots, *Nano Res.*, 2020, **13**(12), 3387–3395.

42 S. Das, A. De and A. Samanta, Ambient Condition Mg(2+) Doping Producing Highly Luminescent Green- and Violet-Emitting Perovskite Nanocrystals with Reduced Toxicity and Enhanced Stability, *J. Phys. Chem. Lett.*, 2020, **11**(3), 1178–1188.

43 Y. Kang, S. Kang and S. Han, Influence of Bi doping on physical properties of lead halide perovskites: a comparative first-principles study between $CsPbI_3$ and $CsPbBr_3$, *Mater. Today Adv.*, 2019, **3**, 100019.

44 S. Kachhap, S. Singh, A. K. Singh and S. K. Singh, Lanthanide-doped inorganic halide perovskites ($CsPbX_3$): novel properties and emerging applications, *J. Mater. Chem. C*, 2022, **10**(10), 3647–3676.

45 Y. Li, Q. Liu, X. Liu, J. Feng, L. He, H. Li, C. Li and H. Zhang, Simultaneous Enhancement of Photoluminescence and Stability of CsPbCl3 Perovskite Enabled by Titanium Ion Dopant, *J. Phys. Chem. Lett.*, 2021, **12**(44), 10746–10752.

46 G. Pan, X. Bai, D. Yang, X. Chen, P. Jing, S. Qu, L. Zhang, D. Zhou, J. Zhu, W. Xu, B. Dong and H. Song, Doping Lanthanide into Perovskite Nanocrystals: Highly Improved and Expanded Optical Properties, *Nano Lett.*, 2017, **17**(12), 8005–8011.

47 Y. Tan, Y. Zou, L. Wu, Q. Huang, D. Yang, M. Chen, M. Ban, C. Wu, T. Wu, S. Bai, T. Song, Q. Zhang and B. Sun, Highly Luminescent and Stable Perovskite Nanocrystals with Octylphosphonic Acid as a Ligand for Efficient Light-Emitting Diodes, *ACS Appl. Mater. Interfaces*, 2018, **10**(4), 3784–3792.

48 L. Wu, Q. Zhong, D. Yang, M. Chen, H. Hu, Q. Pan, H. Liu, M. Cao, Y. Xu, B. Sun and Q. Zhang, Improving the Stability and Size Tunability of Cesium Lead Halide Perovskite Nanocrystals Using Trioctylphosphine Oxide as the Capping Ligand, *Langmuir*, 2017, **33**(44), 12689–12696.

49 H. Liu, Z. Wu, H. Gao, J. Shao, H. Zou, D. Yao, Y. Liu, H. Zhang and B. Yang, One-Step Preparation of Cesium Lead Halide $CsPbX_3$ (X = Cl, Br, and I) Perovskite Nanocrystals by Microwave Irradiation, *ACS Appl. Mater. Interfaces*, 2017, **9**(49), 42919–42927.

50 X. Li, W. Cai, H. Guan, S. Zhao, S. Cao, C. Chen, M. Liu and Z. Zang, Highly stable $CsPbBr_3$ quantum dots by silica-coating and ligand modification for white light-emitting diodes and visible light communication, *Chem. Eng. J.*, 2021, **419**, 129551.

51 H. Sun, Z. Yang, M. Wei, W. Sun, X. Li, S. Ye, Y. Zhao, H. Tan, E. L. Kynaston, T. B. Schon, H. Yan, Z.-H. Lu, G. A. Ozin, E. H. Sargent and D. S. Seferos, Chemically Addressable Perovskite Nanocrystals for Light-Emitting Applications, *Adv. Mater.*, 2017, **29**(34), 1701153.

52 Y. Wei, X. Li, Y. Chen, Z. Cheng, H. Xiao, X. Li, J. Ding and J. Lin, In Situ Light-Initiated Ligands Cross-Linking Enables Efficient All-Solution-Processed Perovskite Light-Emitting Diodes, *J. Phys. Chem. Lett.*, 2020, **11**(3), 1154–1161.

53 S. Shin, Y. Kim, N. Gwak, I. Jeong, M. Lee, K. Kang, S. Yeon, S. Kim, T. A. Kim and N. Oh, Light-induced crosslinking of perovskite nanocrystals for all-solution-processed electroluminescent devices, *Appl. Surf. Sci.*, 2023, **608**, 155016.

54 T. Wang, X. Li, T. Fang, S. Wang and J. Song, Room-temperature synthesis of perovskite-phase $CsPbI_3$ nanocrystals for optoelectronics via a ligand-mediated strategy, *Chem. Eng. J.*, 2021, **418**, 129361.

55 H. Huang, B. Chen, Z. Wang, T. F. Hung, A. S. Susha, H. Zhong and A. L. Rogach, Water resistant $CsPbX_3$ nanocrystals coated with polyhedral oligomeric silsesquioxane and their use as solid state luminophores in all-perovskite white light-emitting devices, *Chem. Sci.*, 2016, **7**(9), 5699–5703.

56 L. Rao, Y. Tang, C. Yan, J. Li, G. Zhong, K. Tang, B. Yu, Z. Li and J. Z. Zhang, Tuning the emission spectrum of highly stable cesium lead halide perovskite nanocrystals through poly(lactic acid)-assisted anion-exchange reactions, *J. Mater. Chem. C*, 2018, **6**(20), 5375–5383.

57 V. González-Pedro, S. A. Veldhuis, R. Begum, M. J. Bañuls, A. Bruno, N. Mathews, S. Mhaisalkar and Á. Maquieira, Recovery of Shallow Charge-Trapping Defects in $CsPbX_3$ Nanocrystals through Specific Binding and Encapsulation with Amino-Functionalized Silanes, *ACS Energy Lett.*, 2018, **3**(6), 1409–1414.

58 H. Wang, N. Sui, X. Bai, Y. Zhang, Q. Rice, F. J. Seo, Q. Zhang, V. L. Colvin and W. W. Yu, Emission Recovery and Stability Enhancement of Inorganic Perovskite Quantum Dots, *J. Phys. Chem. Lett.*, 2018, **9**(15), 4166–4173.

59 B. A. Koscher, J. K. Swabeck, N. D. Bronstein and A. P. Alivisatos, Essentially Trap-Free $CsPbBr_3$ Colloidal Nanocrystals by Postsynthetic Thiocyanate Surface Treatment, *J. Am. Chem. Soc.*, 2017, **139**(19), 6566–6569.

60 T. Ahmed, S. Seth and A. Samanta, Boosting the Photoluminescence of $CsPbX_3$ (X = Cl, Br, I) Perovskite Nanocrystals Covering a Wide Wavelength Range by Postsynthetic Treatment with Tetrafluoroborate Salts, *Chem. Mater.*, 2018, **30**(11), 3633–3637.

61 C. Zhang, J. Chen, L. Kong, L. Wang, S. Wang, W. Chen, R. Mao, L. Turyanska, G. Jia and X. Yang, Core/Shell Metal Halide Perovskite Nanocrystals for Optoelectronic Applications, *Adv. Funct. Mater.*, 2021, **31**(19), 2100438.

62 B. Wang, C. Zhang, S. Huang, Z. Li, L. Kong, L. Jin, J. Wang, K. Wu and L. Li, Postsynthesis Phase Transformation for $CsPbBr_3/Rb_4PbBr_6$ Core/Shell Nanocrystals with Exceptional Photostability, *ACS Appl. Mater. Interfaces*, 2018, **10**(27), 23303–23310.

63 C. Jia, H. Li, X. Meng and H. Li, $CsPbX_3/Cs_4PbX_6$ core/shell perovskite nanocrystals, *Chem. Commun.*, 2018, **54**(49), 6300–6303.

64 A. Pramanik, K. Gates, S. Patibandla, D. Davis, S. Begum, R. Iftekhar, S. Alamgir, S. Paige, M. M. Porter and P. C. Ray, Water-Soluble and Bright Luminescent Cesium-Lead-Bromide Perovskite Quantum Dot-Polymer Composites for Tumor-Derived Exosome Imaging, *ACS Appl. Bio Mater.*, 2019, **2**(12), 5872–5879.

65 S. M. Lee, H. Jung, W. I. Park, Y. Lee, E. Koo and J. Bang, Preparation of Water-Soluble $CsPbBr_3$ Perovskite Quantum Dot Nanocomposites via Encapsulation into Amphiphilic Copolymers, *ChemistrySelect*, 2018, **3**(40), 11320–11325.

66 C. Sun, Y. Zhang, C. Ruan, C. Yin, X. Wang, Y. Wang and W. W. Yu, Efficient and Stable White LEDs with Silica-Coated Inorganic Perovskite Quantum Dots, *Adv. Mater.*, 2016, **28**(45), 10088–10094.

67 J. Cai, K. Gu, Y. Zhu, J. Zhu, Y. Wang, J. Shen, A. Trinchi, C. Li and G. Wei, Highly stable $CsPbBr_3@SiO_2$ nanocomposites prepared via confined condensation for use as a luminescent ink, *Chem. Commun.*, 2018, **54**(58), 8064–8067.

68 B. Wang, S. Zhang, B. Liu, J. Li, B. Cao and Z. Liu, Stable $CsPbBr_3$:Sn@SiO_2 and Cs_4PbBr_6:Sn@SiO_2 Core–Shell Quantum Dots with Tunable Color Emission for Light-Emitting Diodes, *ACS Appl. Nano Mater.*, 2020, **3**(3), 3019–3027.

69 Q. Zhong, M. Cao, H. Hu, D. Yang, M. Chen, P. Li, L. Wu and Q. Zhang, One-Pot Synthesis of Highly Stable $CsPbBr_3@SiO_2$ Core–Shell Nanoparticles, *ACS Nano*, 2018, **12**(8), 8579–8587.

70 X. Tang, W. Chen, Z. Liu, J. Du, Z. Yao, Y. Huang, C. Chen, Z. Yang, T. Shi, W. Hu, Z. Zang, Y. Chen and Y. Leng, Ultrathin, Core–Shell Structured SiO_2 Coated Mn(2+)-Doped Perovskite Quantum Dots for Bright White Light-Emitting Diodes, *Small*, 2019, **15**(19), 1900484.

71 Z. Li, L. Kong, S. Huang and L. Li, Highly Luminescent and Ultrastable $CsPbBr_3$ Perovskite Quantum Dots Incorporated into a Silica/Alumina Monolith, *Angew. Chem., Int. Ed.*, 2017, **56**(28), 8134–8138.

72 Z. J. Li, E. Hofman, J. Li, A. H. Davis, C. H. Tung, L. Z. Wu and W. Zheng, Photoelectrochemically Active and Environmentally Stable $CsPbBr_3/TiO_2$ Core/Shell Nanocrystals, *Adv. Funct. Mater.*, 2017, **28**(1), 1704288.

73 H. Liu, Y. Tan, M. Cao, H. Hu, L. Wu, X. Yu, L. Wang, B. Sun and Q. Zhang, Fabricating $CsPbX_3$-Based Type I and Type II Heterostructures by Tuning the Halide Composition of Janus $CsPbX_3/ZrO_2$ Nanocrystals, *ACS Nano*, 2019, **13**(5), 5366–5374.

74 Y. Wei, X. Deng, Z. Xie, X. Cai, S. Liang, P. Ma, Z. Hou, Z. Cheng and J. Lin, Enhancing the Stability of Perovskite Quantum Dots by Encapsulation in Crosslinked Polystyrene Beads via a Swelling-Shrinking Strategy toward Superior Water Resistance, *Adv. Funct. Mater.*, 2017, **27**(39), 1703535.

75 Y. Wang, J. He, H. Chen, J. Chen, R. Zhu, P. Ma, A. Towers, Y. Lin, A. J. Gesquiere, S. T. Wu and Y. Dong, Ultrastable, Highly Luminescent Organic–Inorganic Perovskite-Polymer Composite Films, *Adv. Mater.*, 2016, **28**(48), 10710–10717.

76 H. Yu, Y. Lu, Z. Feng, Y. Wu, Z. Liu, P. Xia, J. Qian, Y. Chen, L. Liu, K. Cao, S. Chen and W. Huang, A $MAPbBr_3$:poly(ethylene oxide) composite perovskite quantum dot emission layer: enhanced film stability, coverage and device performance, *Nanoscale*, 2019, **11**(18), 9103–9114.

77 J. Ren, X. Dong, G. Zhang, T. Li and Y. Wang, Air-stable and water-resistant all-inorganic perovskite quantum dot films for white-light-emitting applications, *New J. Chem.*, 2017, **41**(22), 13961–13967.

78 S. Pathak, N. Sakai, F. Wisnivesky Rocca Rivarola, S. D. Stranks, J. Liu, G. E. Eperon, C. Ducati, K. Wojciechowski, J. T. Griffiths, A. A. Haghighirad, A. Pellaroque, R. H. Friend and H. J. Snaith, Perovskite Crystals for Tunable White Light Emission, *Chem. Mater.*, 2015, **27**(23), 8066–8075.

79 K. Ma, X. Du, Y. Zhang and S. Chen, In situ fabrication of halide perovskite nanocrystals embedded in polymer composites via microfluidic spinning microreactors, *J. Mater. Chem. C*, 2017, **5**(36), 9398–9404.

80 J. Hai, H. Li, Y. Zhao, F. Chen, Y. Peng and B. Wang, Designing of blue, green, and red $CsPbX_3$ perovskite-codoped flexible films with water resistant property and elimination of anion-exchange for tunable white light emission, *Chem. Commun.*, 2017, **53**(39), 5400–5403.

81 A. Loiudice, S. Saris, E. Oveisi, D. T. L. Alexander and R. Buonsanti, $CsPbBr_3$ QD/AlO_x Inorganic Nanocomposites with Exceptional Stability in Water, Light, and Heat, *Angew. Chem., Int. Ed.*, 2017, **56**(36), 10696–10701.

82 B. Wang, C. Zhang, W. Zheng, Q. Zhang, Z. Bao, L. Kong and L. Li, Large-Scale Synthesis of Highly Luminescent Perovskite Nanocrystals by Template-Assisted Solid-State Reaction at 800 °C, *Chem. Mater.*, 2019, **32**(1), 308–314.

83 Y. Duan, C. Ezquerro, E. Serrano, E. Lalinde, J. García-Martínez, J. R. Berenguer and R. D. Costa, Meeting High Stability and Efficiency in Hybrid Light-Emitting Diodes Based on SiO_2/ZrO_2 Coated $CsPbBr_3$ Perovskite Nanocrystals, *Adv. Funct. Mater.*, 2020, **30**(40), 2005401.

84 C. Guhrenz, A. Benad, C. Ziegler, D. Haubold, N. Gaponik and A. Eychmüller, Solid-State Anion Exchange Reactions for Color Tuning of $CsPbX_3$ Perovskite Nanocrystals, *Chem. Mater.*, 2016, **28**(24), 9033–9040.

85 G. Yang, Q. Fan, B. Chen, Q. Zhou and H. Zhong, Reprecipitation synthesis of luminescent $CH_3NH_3PbBr_3/NaNO_3$ nanocomposites with enhanced stability, *J. Mater. Chem. C*, 2016, **4**(48), 11387–11391.

86 S. Lou, T. Xuan, C. Yu, M. Cao, C. Xia, J. Wang and H. Li, Nanocomposites of $CsPbBr_3$ perovskite nanocrystals in an ammonium bromide framework with enhanced stability, *J. Mater. Chem. C*, 2017, **5**(30), 7431–7435.

87 H. C. Yoon, S. Lee, J. K. Song, H. Yang and Y. R. Do, Efficient and Stable $CsPbBr_3$ Quantum-Dot Powders Passivated and Encapsulated with a Mixed Silicon Nitride and Silicon Oxide Inorganic Polymer Matrix, *ACS Appl. Mater. Interfaces*, 2018, **10**(14), 11756–11767.

88 P. Li, C. Hu, L. Zhou, J. Jiang, Y. Cheng, M. He, X. Liang and W. Xiang, Novel synthesis and optical characterization of $CsPb_2Br_5$ quantum dots in borosilicate glasses, *Mater. Lett.*, 2017, **209**, 483–485.

89 X. Di, Z. Hu, J. Jiang, M. He, L. Zhou, W. Xiang and X. Liang, Use of long-term stable $CsPbBr_3$ perovskite quantum dots in phospho-silicate glass for highly efficient white LEDs, *Chem. Commun.*, 2017, **53**(80), 11068–11071.

90 X. Xiang, H. Lin, J. Xu, Y. Cheng, C. Wang, L. Zhang and Y. Wang, $CsPb(Br,I)_3$ embedded glass: fabrication, tunable luminescence, improved stability and wide-color gamut LCD application, *Chem. Eng. J.*, 2019, **378**, 122255.

91 X. Pang, S. Si, L. Xie, X. Zhang, H. Huang, S. Liu, W. Xiao, S. Wang, T. Xuan, J. Zhuang, C. Hu, Y. Liu, B. Lei and H. Zhang, Regulating the morphology and luminescence properties of $CsPbBr_3$ perovskite quantum dots through the rigidity of glass network structure, *J. Mater. Chem. C*, 2020, **8**(48), 17374–17382.

92 Y. Su, Q. Jing, Y. Xu, X. Xing and Z. Lu, Preventing Anion Exchange between Perovskite Nanocrystals by Confinement in Porous SiO_2 Nanobeads, *ACS Omega*, 2019, **4**(26), 22209–22213.

93 D. H. Park, J. S. Han, W. Kim and H. S. Jang, Facile synthesis of thermally stable $CsPbBr_3$ perovskite quantum dot-inorganic SiO_2 composites and their application to white light-emitting diodes with wide color gamut, *Dyes Pigm.*, 2018, **149**, 246–252.

94 Y. Q. Hu, L. J. Fan, H. Y. Hui, H. Q. Wen, D. S. Yang and G. D. Feng, Monodisperse Bismuth-Halide Double Perovskite Nanocrystals Confined in Mesoporous Silica Templates, *Inorg. Chem.*, 2019, **58**(13), 8500–8505.

95 D. N. Dirin, L. Protesescu, D. Trummer, I. V. Kochetygov, S. Yakunin, F. Krumeich, N. P. Stadie and M. V. Kovalenko, Harnessing Defect-Tolerance at the Nanoscale: Highly Luminescent Lead Halide Perovskite Nanocrystals in Mesoporous Silica Matrixes, *Nano Lett.*, 2016, **16**(9), 5866–5874.

96 Z. Chen, Q. Wang, Z. He, J. Li, E. Mei, X. Liang and W. Xiang, Controlling and optimizing amplified

spontaneous emission based on $CsPbBr_3$@MCM-41 molecular sieve composite, *J. Lumin.*, 2023, **253**, 119411.

97 Z. Li, L. Li, H. Liu, F. Li, J. Zhao and Y. Wang, Strongly quantum-confined Mn^{2+}-doped $CsPbBr_3$ nanocrystals in MCM-41 with pure blue emission, *New J. Chem.*, 2020, **44**(7), 2980–2985.

98 X. Li, Y. Wei, P. Dang, X. Xiao, H. Xiao, G. Zhang, G. Li and J. Lin, Enhancing the stability of perovskite quantum dots $CsPbX_3$ (X = Cl, Br, I) by encapsulation in porous Y2O3 nanoparticles for WLED applications, *Mater. Res. Bull.*, 2022, **146**, 111592.

99 Y. Wei, H. Xiao, Z. Xie, S. Liang, S. Liang, X. Cai, S. Huang, A. A. Al Kheraif, H. S. Jang, Z. Cheng and J. Lin, Highly Luminescent Lead Halide Perovskite Quantum Dots in Hierarchical CaF_2 Matrices with Enhanced Stability as Phosphors for White Light-Emitting Diodes, *Adv. Opt. Mater.*, 2018, **6**(11), 1701343.

100 W. Zhou, Y. Zhao, E. Wang, Q. Li, S. Lou, J. Wang, X. Li, Q. Lian, Q. Xie, R. Q. Zhang and H. Zeng, Charge Transfer Boosting Moisture Resistance of Seminude Perovskite Nanocrystals via Hierarchical Alumina Modulation, *J. Phys. Chem. Lett.*, 2020, **11**(8), 3159–3165.

101 P. Ma, Y. Hou, Z. Chen, J. Su, L. Li, N. Liu, Z. Zhang, X. Jiang, F. Long, Y. Ma and Y. Gao, Enhanced stability of $CsPbBr_3$ Quantum Dots by anchoring on the hierarchical three-dimensional layered double hydroxide, *Chem. Eng. J.*, 2021, **425**, 130471.

102 J. Hao, X. Qu, L. Qiu, G. Li, Y. Wei, G. Xing, H. Wang, C. Yan, H. S. Jang, Z. Cheng and J. Lin, One-Step Loading on Natural Mineral Halloysite Nanotube: An Effective Way to Enhance the Stability of Perovskite $CsPbX_3$ (X = Cl, Br, I) Quantum Dots, *Adv. Opt. Mater.*, 2018, **7**(4), 1801323.

103 Z. Wu, B. Du, G. Tong, H. Zhang, Y. Zhang, J. Xia and Z. Zhao, Highly luminescent and stable inorganic perovskite micro-nanocomposites for crucial information encryption and decryption, *Chem. Eng. J.*, 2022, **428**, 131016.

104 G. Wang, S. Yu, B. Liu, Z. Liu and J. Li, Nanocomposites of $CsPbBr_3$ perovskite quantum dots embedded in Gd_2O_3:Eu^{3+} hollow spheres for LEDs application, *J. Rare Earth*, 2022, **40**(10), 1509–1518.

105 X. Zhou, J. Ren, X. Dong, X. Wang, T. Seto and Y. Wang, Controlling the nucleation process of InP/ZnS quantum dots using zeolite as a nucleation site, *CrystEngComm*, 2020, **22**(20), 3474–3481.

106 J. Sun, F. T. Rabouw, X. Yang, X. Huang, X. Jing, S. Ye and Q. Zhang, Facile Two-Step Synthesis of All-Inorganic Perovskite $CsPbX_3$ (X = Cl, Br, and I) Zeolite-Y Composite Phosphors for Potential Backlight Display Application, *Adv. Funct. Mater.*, 2017, **27**(45), 1704371.

107 S. Ye, J. Y. Sun, Y. H. Han, Y. Y. Zhou and Q. Y. Zhang, Confining Mn(2+)-Doped Lead Halide Perovskite in Zeolite-Y as Ultrastable Orange-Red Phosphor Composites for White Light-Emitting Diodes, *ACS Appl. Mater. Interfaces*, 2018, **10**(29), 24656–24664.

108 D. Huang, Y. Liu, Q. Ouyang, H. Lian and J. Lin, Enhancing the stability of $CsPbX_3$ (X = Br, I) through combination with Y-zeolites for WLED application, *Dalton Trans.*, 2021, **50**(46), 17281–17289.

109 P. Wang, B. Wang, Y. Liu, L. Li, H. Zhao, Y. Chen, J. Li, S. F. Liu and K. Zhao, Ultrastable Perovskite-Zeolite Composite Enabled by Encapsulation and In Situ Passivation, *Angew. Chem., Int. Ed.*, 2020, **59**(51), 23100–23106.

110 B. Li, Y. Zhang, Y. Xu and Z. Xia, Design optimization of $CsPbBr_3$ nanocrystals into zeolite Beta composites as ultrastable green emitters for backlight display applications, *J. Mater. Chem. C*, 2021, **9**(36), 12118–12123.

111 R. Li, J. Yu, S. Wang, Y. Shi, Z. Wang, K. Wang, Z. Ni, X. Yang, Z. Wei and R. Chen, Surface modification of all-inorganic halide perovskite nanorods by a microscale hydrophobic zeolite for stable and sensitive laser humidity sensing, *Nanoscale*, 2020, **12**(25), 13360–13367.

112 Y. Zhang, L. Han, B. Li and Y. Xu, Improved stability of all-inorganic perovskite nanocrystals in hierarchical ZSM-5 zeolites for multimodal applications, *Chem. Eng. J.*, 2022, **437**, 135290.

113 Y. Tong, Q. Wang, E. Mei, X. Liang, W. Gao and W. Xiang, One-Pot Synthesis of $CsPbX_3$ (X = Cl, Br, I)@Zeolite: A Potential Material for Wide-Color-Gamut Backlit Displays and Upconversion Emission, *Adv. Opt. Mater.*, 2021, **9**(11), 2100012.

114 Y. Tong, M. Jin, Y. Chen, Y. Zhao, H. Yang, Q. Wang, L. Zhai, X. Liang and W. Xiang, Ultrastable and high colour rendering index WLEDs based on $CsPbBrI_2$ nanocrystals prepared by a two-step facile encapsulation method, *J. Mater. Chem. C*, 2021, **9**(7), 2530–2538.

115 O. M. Yaghi and H. Li, Hydrothermal Synthesis of a Metal–Organic Framework Containing Large Rectangular Channels, *J. Am. Chem. Soc.*, 1995, **117**, 10401–10402.

116 O. M. Yaghi, G. Li and H. Li, Selective binding and removal of guests in a microporous metal–organic framework, *Nature*, 1995, **378**, 703–706.

117 Z. Mai and D. Liu, Synthesis and Applications of Isoreticular Metal–Organic Frameworks IRMOFs-*n* (*n* = 1, 3, 6, 8), *Cryst. Growth Des.*, 2019, **19**(12), 7439–7462.

118 M. Eddaoudi, J. K. Kim, N. Rosi, D. Vodak, J. Wachter, M. O'Keeffe and O. M. Yaghi, Systematic Design of Pore Size and Functionality in Isoreticular MOFs and Their Application in Methane Storage, *Science*, 2002, **295**(5544), 469–472.

119 S. S. Y. Chui, S. M. F. Lo, J. P. H. Charmant, A. G. Orpen and I. D. Williams, A Chemically Functionalizable Nanoporous Material $[Cu_3(TMA)_2(H_2O)_3]_n$, *Science*, 1999, **283**(5405), 1148–1150.

120 C. Serre, F. Millange, C. Thouvenot, M. Nogues, G. R. Marsolier, D. Louer and G. R. Ferey, Very Large Breathing Effect in the First Nanoporous Chromium(III)-Based Solids: MIL-53 or CrIII(OH),{O_2C-C_6H_4-CO_2},{HO_2C-C_6H_4-CO_2H}$_x$,H_2O_y, *J. Am. Chem. Soc.*, 2002, **124**, 13519–13526.

121 B. Wang, A. P. Cote, H. Furukawa, M. O'Keeffe and O. M. Yaghi, Colossal cages in zeolitic imidazolate frameworks as selective carbon dioxide reservoirs, *Nature*, 2008, **453**(7192), 207–211.

122 S.-i Noro, S. Kitagawa, M. Kondo, K. Seki and A. New, Methane Adsorbent, Porous Coordination Polymer [{$CuSiF_6$(4,4′-bipyridine)$_2$}$_n$], *Angew. Chem., Int. Ed.*, 2000, **39**(12), 2081–2084.

123 S. Ma, H. Zhou and A. Metal−Organic, Framework with Entatic Metal Centers Exhibiting High Gas Adsorption Affinity, *J. Am. Chem. Soc.*, 2006, **128**(36), 11734–11735.

124 D. Tanaka, K. Nakagawa, M. Higuchi, S. Horike, Y. Kubota, T. C. Kobayashi, M. Takata and S. Kitagawa, Kinetic gate-opening process in a flexible porous coordination polymer, *Angew. Chem., Int. Ed.*, 2008, **47**(21), 3914–3918.

125 J. H. Cavka, S. Jakobsen, U. Olsbye, N. Guillou, C. Lamberti, S. Bordiga, K. P. Lillerud and A. New, Zirconium Inorganic Building Brick Forming Metal Organic Frameworks with Exceptional Stability, *J. Am. Chem. Soc.*, 2008, **130**(42), 13850–13851.

126 Z. Chen, Z. G. Gu, W. Q. Fu, F. Wang and J. Zhang, A Confined Fabrication of Perovskite Quantum Dots in Oriented MOF Thin Film, *ACS Appl. Mater. Interfaces*, 2016, **8**(42), 28737–28742.

127 D. Zhang, Y. Xu, Q. Liu and Z. Xia, Encapsulation of $CH_3NH_3PbBr_3$ Perovskite Quantum Dots in MOF-5 Microcrystals as a Stable Platform for Temperature and Aqueous Heavy Metal Ion Detection, *Inorg. Chem.*, 2018, **57**(8), 4613–4619.

128 C. Zhang, B. Wang, W. Li, S. Huang, L. Kong, Z. Li and L. Li, Conversion of invisible metal–organic frameworks to luminescent perovskite nanocrystals for confidential information encryption and decryption, *Nat. Commun.*, 2017, **8**(1), 1138.

129 J. Ren, T. Li, X. Zhou, X. Dong, A. V. Shorokhov, M. B. Semenov, V. D. Krevchik and Y. Wang, Encapsulating all-inorganic perovskite quantum dots into mesoporous metal organic frameworks with significantly enhanced stability for optoelectronic applications, *Chem. Eng. J.*, 2019, **358**, 30–39.

130 Z. Xie, X. Li, R. Li, S. Lu, W. Zheng, D. Tu, Y. Feng and X. Chen, In situ confined growth of ultrasmall perovskite quantum dots in metal–organic frameworks and their quantum confinement effect, *Nanoscale*, 2020, **12**(32), 17113–17120.

131 J. Cuan, D. Zhang, W. Xing, J. Han, H. Zhou and Y. Zhou, Confining $CsPbX_3$ perovskites in a hierarchically porous MOF as efficient and stable phosphors for white LED, *Chem. Eng. J.*, 2021, **425**, 131556.

132 D. Zhang, J. Zhao, Q. Liu and Z. Xia, Synthesis and Luminescence Properties of $CsPbX_3$@Uio-67 Composites toward Stable Photoluminescence Convertors, *Inorg. Chem.*, 2019, **58**(2), 1690–1696.

133 J. Liu, Y. Zhao, X. Li, J. Wu, Y. Han, X. Zhang and Y. Xu, Dual-Emissive $CsPbBr_3$@Eu-BTC Composite for Self-Calibrating Temperature Sensing Application, *Cryst. Growth Des.*, 2019, **20**(1), 454–459.

134 S. Mollick, T. N. Mandal, A. Jana, S. Fajal, A. V. Desai and S. K. Ghosh, Ultrastable Luminescent Hybrid Bromide Perovskite@MOF Nanocomposites for the Degradation of Organic Pollutants in Water, *ACS Appl. Nano Mater.*, 2019, **2**(3), 1333–1340.

135 J. H. Cha, K. Noh, W. Yin, Y. Lee, Y. Park, T. K. Ahn, A. Mayoral, J. Kim, D. Y. Jung and O. Terasaki, Formation and Encapsulation of All-Inorganic Lead Halide Perovskites at Room Temperature in Metal-Organic Frameworks, *J. Phys. Chem. Lett.*, 2019, **10**(9), 2270–2277.

136 H. He, Y. Cui, B. Li, B. Wang, C. Jin, J. Yu, L. Yao, Y. Yang, B. Chen and G. Qian, Confinement of Perovskite-QDs within a Single MOF Crystal for Significantly Enhanced Multiphoton Excited Luminescence, *Adv. Mater.*, 2019, **31**(6), 1806897.

137 H. Wu, L. Yao, W. Cao, Y. Yang, Y. Cui, D. Yang and G. Qian, Stable and wide-wavelength tunable luminescence of $CsPbX_3$ nanocrystals encapsulated in metal–organic frameworks, *J. Mater. Chem. C*, 2022, **10**(14), 5550–5558.

138 A. I. B. Adrien, P. Côté, N. W. Ockwig, M. O'Keeffe, A. J. Matzger and O. M. Yaghi, Porous, crystalline, covalent organic frameworks, *Science*, 2005, **310**, 1166–1170.

139 C. Li, Z. Qiu, H. Sun, Y. Yang and C.-P. Li, Recent Progress in Covalent Organic Frameworks (COFs) for Electrocatalysis, *Chin. J. Struct. Chem.*, 2022, **41**, 2211084–2211099.

140 P. Kour and S. P. Mukherjee, $CsPbBr_3$/Cs_4PbBr_6 perovskite@COF nanocomposites for visible-light-driven photocatalytic applications in water, *J. Mater. Chem. A*, 2021, **9**(11), 6819–6826.

141 Y. Liu, Y. Zhu, S. B. Alahakoon and E. Egap, Synthesis of Imine-Based Covalent Organic Frameworks Catalyzed by Metal Halides and in Situ Growth of Perovskite@COF Composites, *ACS Mater. Lett.*, 2020, **2**(12), 1561–1566.

142 Y. Zhu, Y. Liu, Q. Ai, G. Gao, L. Yuan, Q. Fang, X. Tian, X. Zhang, E. Egap, P. M. Ajayan and J. Lou, In Situ Synthesis of Lead-Free Halide Perovskite–COF Nanocomposites as Photocatalysts for Photoinduced Polymerization in Both Organic and Aqueous Phases, *ACS Mater. Lett.*, 2022, **4**(3), 464–471.

143 G. Meng, L. Zhen, S. Sun, J. Hai, Z. Zhang, D. Sun, Q. Liu and B. Wang, Confining perovskite quantum dots in the pores of a covalent-organic framework: quantum confinement- and passivation-enhanced light-harvesting and photocatalysis, *J. Mater. Chem. A*, 2021, **9**(43), 24365–24373.

144 J. Ren, X. Zhou and Y. Wang, In situ passivation and thiol-mediated anchoring of perovskite quantum dots in mesoporous covalent-organic frameworks, *Chem. Eng. J.*, 2023, **454**, 140285.

145 X. Yu, L. Wu, D. Yang, M. Cao, X. Fan, H. Lin, Q. Zhong, Y. Xu and Q. Zhang, Hydrochromic $CsPbBr_3$ Nanocrystals for Anti-Counterfeiting, *Angew. Chem., Int. Ed.*, 2020, **59**(34), 14527–14532.

146 Z. Kong, J. Liao, Y. Dong, Y. Xu, H. Chen, D. Kuang and C. Su, Core@Shell $CsPbBr_3$@Zeolitic Imidazolate Framework Nanocomposite for Efficient Photocatalytic CO_2 Reduction, *ACS Energy Lett.*, 2018, **3**(11), 2656–2662.

147 S. Mollick, T. N. Mandal, A. Jana, S. Fajal and S. K. Ghosh, A hybrid blue perovskite@metal–organic gel (MOG) nanocomposite: simultaneous improvement of luminescence and stability, *Chem. Sci.*, 2019, **10**(45), 10524–10530.

148 J. Ren, A. Meijerink, X. Zhou, J. Wu, G. Zhang and Y. Wang, In Situ Embedding Synthesis of $CsPbBr_3$@Ce-MOF@SiO_2 Nanocomposites for High Efficiency Light-Emitting Diodes: Suppressing Reabsorption Losses through the Waveguiding Effect, *ACS Appl. Mater. Interfaces*, 2022, **14**(2), 3176–3188.

149 J. Ren, X. Zhou and Y. Wang, Dual-emitting $CsPbX_3$@ZJU-28 (X = Cl, Br, I) composites with enhanced stability and unique optical properties for multifunctional applications, *Chem. Eng. J.*, 2020, **391**, 123622.

150 T. Xuan, J. Huang, H. Liu, S. Lou, L. Cao, W. Gan, R.-S. Liu and J. Wang, Super-Hydrophobic Cesium Lead Halide Perovskite Quantum Dot-Polymer Composites with High Stability and Luminescent Efficiency for Wide Color Gamut White Light-Emitting Diodes, *Chem. Mater.*, 2019, **31**(3), 1042–1047.

151 D. Shen, A. Pang, Y. Li, J. Dou and M. Wei, Metal-organic frameworks at interfaces of hybrid perovskite solar cells for enhanced photovoltaic properties, *Chem. Commun.*, 2018, **54**(10), 1253–1256.

152 D. Zhang, W. Zhou, Q. Liu and Z. Xia, $CH_3NH_3PbBr_3$ Perovskite Nanocrystals Encapsulated in Lanthanide Metal-Organic Frameworks as a Photoluminescence Converter for Anti-Counterfeiting, *ACS Appl. Mater. Interfaces*, 2018, **10**(33), 27875–27884.

153 J. Li, Y. Tang, Z. Li, X. Ding, B. Yu and L. Lin, Largely Enhancing Luminous Efficacy, Color Conversion Efficiency, and Stability for Quantum-Dot White LEDs Using the Two-Dimensional Hexagonal Pore Structure of SBA-15 Mesoporous Particles, *ACS Appl. Mater. Interfaces*, 2019, **11**(20), 18808–18816.

154 J. S. Li, Y. Tang, Z. T. Li, J. X. Li, X. R. Ding, B. H. Yu, S. D. Yu, J. Z. Ou and H. C. Kuo, Toward 200 Lumens per Watt of Quantum-Dot White-Light-Emitting Diodes by Reducing Reabsorption Loss, *ACS Nano*, 2021, **15**(1), 550–562.

155 M. D. Allendorf, C. A. Bauer, R. K. Bhakta and R. J. Houk, Luminescent metal–organic frameworks, *Chem. Soc. Rev.*, 2009, **38**(5), 1330–1352.

156 C. Zhang, Z. S. Li, X. Y. Dong, Y. Y. Niu and S. Q. Zang, Multiple Responsive CPL Switches in an Enantiomeric Pair of Perovskite Confined in Lanthanide MOFs, *Adv. Mater.*, 2022, **34**(11), 2109496.

157 H. Tsai, S. Shrestha, R. A. Vilá, W. Huang, C. Liu, C. Hou, H. Huang, X. Wen, M. Li, G. Wiederrecht, Y. Cui, M. Cotlet, X. Zhang, X. Ma and W. Nie, Bright and stable light-emitting diodes made with perovskite nanocrystals stabilized in metal–organic frameworks, *Nat. Photonics*, 2021, **15**(11), 843–849.

158 H. Tsai, H. H. Huang, J. Watt, C. H. Hou, J. Strzalka, J. J. Shyue, L. Wang and W. Nie, Cesium Lead Halide Perovskite Nanocrystals Assembled in Metal-Organic Frameworks for Stable Blue Light Emitting Diodes, *Adv. Sci.*, 2022, **9**(14), 2105850.